

Reversing the tides:

Experiments on tidal bars and ebb- and flood-dominated channels in tidal systems

MSc thesis Earth Sciences



Tessa van Rosmalen BSc. 3349438

Utrecht University

Faculty of Geosciences. Department of Physical Geography,

Earth Science graduate schools: track Coastal morphodynamics and fluvial systems

May 2013

Final version

1st Supervisor: dr. M.G. Kleinhans

2nd supervisor: dr. Maarten van der Vegt

Abstract

Tidal bars and ebb- and flood-dominated channels are characteristic for tidal inlet systems and estuaries. The dynamics of tidal bars are poorly understood whereas fluvial bars are well understood due to linear stability analyses, numerical modelling and field observations. Ebb- and flood-dominated tidal channels flank tidal bars. For both tidal bars and ebb- and flood-dominated channels theory is hardly theory available and scale experiments on bars and tidal channels have not yet been performed. Main objective of this thesis is to ascertain whether tidal bars and channels form in physical scale experiments, investigate characteristics of tidal bars and channels and compare with previous literature. The experimental setup consisted of a tilting basin that was 3.2 meters long and 1 meter wide. Tides were created by tilting the basin over the diagonal. In addition braided rivers bars were investigated by unidirectional flow for comparison with the formation of tidal bars under reversing flow conditions. The results show that both tidal bars and ebb- and flood-dominated channels initiated spontaneously due to small perturbations in the sediment bed and led to the formation of bar-channel couples. These bar-channel systems were only morphological active during one phase of the tides. Two types of bars emerged in the system: either large round/diamond shaped bars or elongated sharper-edged bars. Tidal excursion length was the main forcing that determined the shape and size of bars and channels. The length of the bars is significantly correlated to tidal excursion length, which is in agreement with previous modelling studies. Unlike fluvial bars, tidal bars exhibited no net migration and moved back and forth symmetrically. The formed ebb- and flood-tidal channels were similar to observations in nature. The braided river formed in the experimental setting was characterized by multiple channel systems, irregular bar patterns and bars that varied in shape and size.

Keywords: tidal bars, ebb- and flood-dominated channels, tidal excursion length, fluvial bars, experiment.

Contents

	Page number
Abstract	2
List of figures	5
List of tables	9
1. Introduction	10
2. Theoretical framework	12
2.1 Tidal systems: tidal inlets and estuaries	12
2.1.1 Tidal inlet systems	12
2.1.2 Tide-dominated estuaries	14
2.1.3 Sediment transport	15
2.2 Ebb- and flood-dominated channels	16
2.3 The role of bars	19
2.3.1 Bars in fluvial systems	19
2.3.2 Bars in tidal systems	24
2.4 Previous tidal experimental and scaling issues	28
2.4.1 Previous tidal experiments	28
2.4.2 Scaling problems	28
2.5 Research questions and hypothesis	31
2.5.1 Research questions	31
2.5.3 Hypotheses	32
2.6 Thesis outline	34
3. Methods	35
3.1 Experimental set-up	35
3.1.1 Tilting basin	35
3.1.2 Flume set-up	36
3.1.3 Cameras and Z-snapper camera	37
3.1.3 Sediment characteristics	37
3.2 Experimental scenarios	38
3.2.1 Tidal experiments	38
3.2.2 Braiding river experiments	39
3.3 Data collection	40
3.3.1 Photographs and movies	40
3.3.2 DEM calculations	40

4. Results	42
4.1 Evolution of experimental tidal bars and channels	43
4.4.1 Basic high-amplitude case	43
4.4.2 Basic low-amplitude case	47
4.2 Dependence of tidal bars on imposed tidal conditions	53
4.2.1 Overall trends	53
4.2.2 Effect of conditions	56
4.2.3 Visual analyses of bar and channel shapes	62
4.2.4 Tidal symmetry versus tidal asymmetry	67
4.2.5 Braided river bars	72
5. Discussion	76
5.1 Experimental tidal bars and channels	76
5.1.1 Bar and channel initiation	76
5.1.2 Development of the system	77
5.1.3 Bar migration	79
5.1.4 Ebb- and flood-dominated channels and recirculating sediment transport	79
5.2 Dominant forcing parameter: tidal excursion length	80
5.2.1 Tidal excursion length and bar length	80
5.2.2 Tidal excursion length and bar shape	81
5.3 Braided rivers bars	82
5.3.1 Experimental braided bars	82
5.3.2 Braided rivers bars versus tidal bars	83
5.4 Recommendations	84
6. Conclusions	85
7. Acknowledgements	87
8. References	88

List of figures

Figure 1.1: Single row bars in the Westerschelde estuary in the Netherlands (**left**) and multiple row bars in the Waimak River in New Zealand (**right**) (Bing maps, assessed on April 2013; Google, assessed on April 2013).

Figure 2.1: Tidal bars and ebb- and flood-dominated channels in the outer zone of (A) Afon Maddwach estuary, England. (B) Zoom of yellow box in Afon Maddwach estuary. (C) Aberdovey estuary, England. (D) Tidal bars and ebb- and flood-dominated channels in the backbarrier basin in the Wadden Sea, the Netherlands (Bing maps, assessed on April 2013).

Figure 2.2: (A) Schematic representation of a funnel-shaped tide-dominated estuary (Dalrymple and Choi., 2007). Note the changes in channel geometry (straight and meandering), presence of elongate tidal bars at the seaward end of the system and tidal flats and salt marshes. (B) Variation in intensity of energy of waves and river- and tidal currents.

Figure 2.3: Multichannel system that consists of ebb- and flood-dominated channels that recombine around tidal bars (**left**) (Van Veen, 1950) and circulating sand currents in tidal system (**right**). Sand moves upstream in the flood-tidal channel and downstream in the ebb-tidal channel (Van Veen, 1950). E= ebb dominated channel, F= flood-dominated channel.

Figure 2.4: (A) Ebb- and flood-tidal channels and bar areas in the Western Scheldt (bathymetry, 2002) (Swinkels et al. 2009). (B) View of Westerschelde from Bing maps, ebb- and flood-dominated channels in yellow with bars inbetween (assessed on April 2013).

Figure 2.5: Marginal stability curves predicted by 2D and 3D models (Seminara and Tubino, 2001; Tubino et al, 2013). When wavenumber (λ) falls in the unstable range the perturbation leads to amplification of the bars (free bar range). Otherwise the perturbation dampens out and the bed returns to its original flat bed state (plane bed range).

Figure 2.6: Three bar regimes and bar mode (Kleinhans and Van den Berg, 2010). Note the overdamped, underdamped and unstable growing regime (excitation regime).

Figure 2.7: Different bar regimes for mode 1 bars that are generated by perturbations for (A) sand-bed rivers and (B) gravel bed rivers. Width-to-depth ratio is indicated on top. Further explanation on other parameters of these graphs is present in Kleinhans and van den Berg (2011).

Figure 2.8: Braided channels and mid-channel bars in (**Left**): South Saskatchewan River, Canada and (**Right**): Brahmaputra, India. Photos obtained from Schuurmans et al, (in press).

Figure 2.9: Bottom pattern of series of alternating bars and pools (de Swart and Zimmerman, 1999). The black line indicates tidal residual circulation.

Figure 2.10: Bottom pattern modeled with a numerical model that shows bottom profile after an initial state (Hibma et al., 2003 in Schuttelaars and de Swart, 1999). Upper panel: Seaward end with main meandering ebb-tidal channel and straight flood-tidal channels at the bends of the meandering ebb channel. Lower panel: Meandering of ebb and flood-dominated channels, also observed by Ahnert (1960) in Hibma et al., (2004).

Figure 2.11: Growth or decay of perturbation for different values of r (friction parameter). When the friction values remain below zero, the perturbation decays. If the friction parameters exceeds zero the perturbation can start to grow due to positive feedback between the bed and flow (Schuttelaars and de Swart, 1999). When friction is not included, no positive feedback arises and perturbations always decay.

Figure 2.12: Recirculating sediment transport pattern observed in the Cobequid Bay, Fundy by Dalrymple et al (1977).

Figure 3.1: Initial situation when the tilting basing is at equilibrium. Red arrows indicate one half of a tidal cycle where the right-hand side of the tilting basin moves up and reaches low water (ebb) and the left-hand side of the tilting basin moves down and reaches high water (flood). Vice versa for the green arrows.

Figure 3.2: Sieve curve of the lightweight plastic grains. $D_{10}=0.42\text{mm}$, $D_{50}=0.62\text{mm}$ and $D_{90}=1.1\text{mm}$ and the density equals $1150\text{-}1250\text{ kg/m}^3$.

Figure 3.3: Definitions of bars and channels for the calculations. Bar height is calculated by the height of the bar minus the average heightFigure 4.1: Evolution of tidal bars and channels for the basic high-amplitude case. Yellow arrows indicate dominant flow pattern of the tidal currents. Dark-blue colors indicate deeper tidal channels and light areas represent tidal bars.

Figure 4.2: Separate ebb- and flood-dominated channels. Ebb-dominated channels are indicated in red and flood-dominated channels (reversed flow) are indicated in yellow. Smaller arrows at the bar indicate flow divergence and green arrows indicate recirculating sediment transport.

Figure 4.3: Bifurcations indicated in yellow and connecting channels in red.

Figure 4.4: Erosion and deposition pattern of the basic high-amplitude case for three timesteps. Negative values indicate erosion and positive values indicate deposition. Black ellipses indicate connecting channels (connecting ebb-and flood-tidal channels).

Figure 4.5: Evolution of tidal bars and channels for the basic low-amplitude case. Yellow arrows indicate dominant flow pattern of the tidal currents.

Figure 4.6: Characteristic bar pattern for the low-amplitude case that consists of multiple elongated bars below each other.

Figure 4.7: Erosion and deposition pattern of the basic low-amplitude case for three timesteps. Negative values indicate erosion and positive values indicate deposition. Note the characteristic pattern of bars in the system (see fig 4.6).

Figure 4.8: Evolution of bar width and height for both HA-case and LA-case.

Figure 4.9: Evolution of number of bars for both HA-case and LA-case.

Figure 4.10: The 25th, 50th and 75th percentiles for bar width and height for both basic HA- and LA-case. The blue and red box indicates the 50th percentile. The upper limit of the dotted-black line represents the 75th percentile and the lower limit indicates the 25th percentile.

Figure 4.11: Bar width (mm) versus bar height (mm).

Figure 4.12: Number of bars versus bar width (mm), height (mm) and width/height.

Figure 4.13: Bar length versus bar width (mm), height (mm) and width/height.

Figure 4.14: Tilting speed (mm/min) versus bar width (mm) and height (mm).

Figure 4.15: Tilting speed (mm/min) versus bar length (mm).

Figure 4.16: Amplitude versus bar width (mm), height (mm) and width/height

Figure 4.17: Amplitude (mm) versus bar length (mm).

Figure 4.18: Tidal delay (s) versus bar length (mm).

Figure 4.19: Tidal excursion length (mm) versus bar length (mm) and number of bars.

Figure 4.20: Sketch of different bar shapes: elongated sharp-edged bars (LA-case / Low tidal excursion length) and round/diamond shaped bars (HA-case / High tidal excursion length). E=ebb-dominated channel with a bar at the end and F=flood-dominated channel with a bar at the end.

Figure 4.21: Along profile for the basic case. Bars are present above the average height line and channels are present below the average height line. Black arrows indicate up-slope bars and green arrow indicate steep down-slope (higher angle of repose).

Figure 4.22: (**Top**) Narrow, long and intermediate/deep channels in experiment T2, (**Middle**) Wide, long and deep channels in experiment T7, (**Bottom**) Intermediate in width, small in length and shallow in depth in experiment T9. Experiment T2 and T7 are high-amplitude cases and T9 is a low-amplitude case (table 4A).

Figure 4.23: Morphological evolution of the tidal system in the symmetrical experiment T10 (Table 4A). Yellow arrows indicate dominant flow direction. Green arrow indicates disappearance of the bar.

Figure 4.24: Morphological evolution of the asymmetrical experiment T11 (Table 4A). Orange box indicates dominant system.

Figure 4.25: Evolution of bar width and height through time for the asymmetrical and symmetrical tide case.

Figure 4.26: Evolution of number of bars through time for the asymmetrical and symmetrical tide case.

Figure 4.27: Digital elevation maps for symmetrical tide case (top) and asymmetrical tide case (bottom) after 96 hours. The DEM demonstrates the difference in bar and channel development under symmetrical or asymmetrical currents.

Figure 4.28: Bars and channels in braiding river experimental setting. Black arrows indicate flow pattern and the orange arrow indicates unidirectional flow.

Figure 4.29: Relation between bar width (mm) and bar length (mm) and height (mm).

Figure 4.30: Relation between number of bars and bar width (mm) and length (mm) and bar height (mm).

Figure 4.31: Digital elevation maps of the braiding experiments. High values indicate deposition (red) and low values indicate erosion (dark blue).

List of tables

Table 3.1

Flow conditions in experimental design in order to prevent scaling issues (Kleinhans et al. 2010b; Van Dijk et al. 2012). Design scale rules were calculated for the experiments (value experimental design).

Table 3.2

Free-setting scenarios with cases for the tilting basin, where basin length equalled 3.2 meters and basin width equalled 1 meter. Red-colored numbers indicate cases used in chapter 4.

Table 3.3

Overview of braiding river experiments.

Table 4A: Description of tidal cases. Bold red numbers indicates used cases in chapter 4.1. Initial waterdepth was equal for all tidal experiments (5 mm). TEL= tidal excursion length (m), TWL=tidal wavelength (m). For calculations tidal excursion length see chapter 4.2 and tidal wavelength see chapter 5.

Table 4B: Description of braiding cases. Bold red number indicates used case in chapter 4.2

Table 4.1: Mean bar height, width, number of bars and bar length for all experiments. Red bold numbers indicates cases used in chapter 4.1 and chapter 4.2

Table 4.2: Correlation factor is given to indicate the strength of the relationship between the two parameters (x and y). Strong and significant correlation factors are indicated in green. The relation, either positive or negative is given (P/N) in the correlation column.

Table 4.3: Relative shape of tidal bars in experimental setting with tidal excursion length. Initiation indicates either few bars (one or two) or multiple bars (more bars below each other). Arrows → or ← a very specific dominant grow direction in the system.

Table 4.4: Relative shape of tidal channels (either flood-or ebb-dominated) in the experiments.

Table 4.5: Mean values for width, height and width/height-ratio and mean number of bars for the braiding cases. Tides represent the mean average values for the tidal experiments with tidal amplitude of 8 mm. Braiding represents the mean average values for braiding case 1 and 2. Braiding case 3 is not taken into account due to the fact that no initial DEM was made.

1. Introduction

Bars are found in both fluvial and tidal systems. In fluvial systems, bars are solitary repeated patterns that occur in a river channel, and control the altimetric and planimetric evolution of rivers (Seminara et al., 2012). The current knowledge on fluvial bars is that they are considered to be the key factor controlling important fluvial processes, such as meandering and braiding river patterns (Seminara et al., 2012). From a mechanistic point of view, bars can be distinguished into free and forced bars, whereas their classification is based on the mechanism that underlies their formation (Seminara et al., 2012). Forced bars are stationary and initiated and forced by channel curvature, variations in channel width or flow convergence (Tubino et al., 2013; Kleinhans and van den Berg, 2010). On the other hand, free bars are unstable features and migrate downstream (Seminara et al., 2012; Seminara and Tubino, 2001). This thesis focuses on free bars. The celerity and size of fluvial bars is determined by the width/depth ratio of the river channel (Tubino et al., 2013; Kleinhans, 2010; Garotta et al., 2006). Depending on the width/depth ratio being small or large, bars may occur in single row bars or in multiple rows in rivers (fig 1.1). Width/depth ratio also influences bar shape. In relative wide rivers, fast migrating and small bars occur, whereas slowly migrating and large bars may occur in narrow rivers (fig 1.1).

Bars are also typically observed in tidal systems, referred as tidal bars, where they are affected by reversing flow during ebb and flood (Kleinhans, 2012). Tidal bars are defined as sediment waves with their wavelengths scaling width channel width (Garotta et al., 2006). Tidal bars may occur in tidal inlet systems such as the Dutch Wadden Sea or tide-dominated estuaries, such as the Aberdovey and Westerschelde estuary. In tidal systems, tidal bars differ also in shape and size (fig 2.1). Unlike fluvial bars, little is known about initiation of tidal bars and development in tidal scale experiments. The current state of knowledge for tidal bars is based on modelling studies (Schramkowski et al., 2002; Seminara and Tubino, 2001; Schuttelaars and de Swart, 1999; Schramkowski et al., 2004, Garotta et al., 2006) and from observational studies (Dalrymple, 1977; Dalrymple et al., 1975; de Vries-Klein, 1970). No significant experiment data on tidal bars is currently available that could show significant insights in the characteristics of tidal bars.

Ebb- and flood-dominated channels flank tidal bars (fig 2.1) (Van Veen, 1950). Van Veen (1950) investigated these ebb- and flood-dominated tidal channels in the Netherlands tidal waters. Swinkels et al., (2009) extended the research of van Veen (1950) in the Westerschelde. Although some efforts were made to understand ebb- and flood-dominated channels (Van Veen, 1950; Swinkels et al., 2009), there is still hardly any theory and experiments on ebb- and flood dominated channels are rare. The objective of this thesis is to ascertain whether tidal bars and ebb- and flood tidal channels may form in experimental setting, investigate characteristics of tidal bars and channels, and if results are in agreement with previous literature.



*Figure 1.1: Single row bars in the Westerschelde estuary in the Netherlands (**left**) and multiple row bars in the Waimakariri River in New Zealand (**right**) (Bing maps, assessed on April 2013; Google, assessed on April 2013).*

2. Theoretical framework

The morphology of tidal systems results from the nonlinear interaction between water and sediment motion and the bed topography (Hibma et al., 2004). The smallest morphological phenomena in tidal systems are characterized as ripples and dunes that have formed on the sediment bed and are referred as microscale features. Interacting ebb- and flood-dominated channels and bars are referred as mesoscale features. When looking at an aggregated scale, both features belong to macroscale elements of tidal systems such as the tidal inlet and ebb-tidal delta (Hibma et al., 2004). This thesis focuses on the mesoscale features in tidal systems, such as tidal inlets and estuaries, where the principal forcing of those features is tidal motion.

2.1 Tidal systems: tidal inlets and estuaries

Tidal systems are defined as systems where the influence of the energy of the waves is relatively low compared to the influence of the tidal currents (Masselink and Hughes, 2003). Examples of such tidal systems are tidal inlet systems and estuaries. However, only tide-dominated estuaries are referred as tidal systems, as estuaries can also be mixed-energy estuaries or completely wave-dominated (Masselink and Hughes, 2003; Dalrymple and Choi, 2007; Todeschini, 2006). This chapter will explain dynamics and sediment transport processes in tidal inlet systems and tide-dominated estuaries.

2.1.1 Tidal inlet system

A tidal inlet system is defined as a system that consists of a barrier island, tidal inlet and deltas and a backbarrier basin (fig 2.1E). Tidal inlets separate barrier islands, defined as elongated offshore ridges or bodies of sandy/gravelly sediments, running parallel with the mainland coast. The islands lie above high-tide level and are separated by the mainland coast by a backbarrier basin or salt marsh. A typical backbarrier basin system is composed of several morphological units (de Swart and Zimmerman, 2009): ebb- and flood-dominated channels, ebb-tidal delta and tidal bars. Tidal bars are present in the main channels, which undergo a sequence of bifurcations when moving further into the tidal basin. This results in a complex pattern of tidal bars and channels (fig 2.1E).

Tidal flow asymmetry is the main factor for net sediment transport in tidal systems (Dronkers, 1986; Todeschini, 2006). However, not only tidal flow influences sediment transport, also wave-driven processes affect sediment transport in tidal systems. The presence of waves can lead to reduction of the ebb-current and enhancement of the flood current. During ebb, the ebb-tidal currents and waves are in opposite direction and this result in a reduction in magnitude of the ebb current. During flood, the flood-tidal currents and waves are both flowing in the same direction. The tidal inlet however, is an obstacle for the approaching waves. A small fraction of the incoming waves is able to pass through the tidal inlet and propagates into the tidal basin (Hayes, 1980; Sha, 1989).

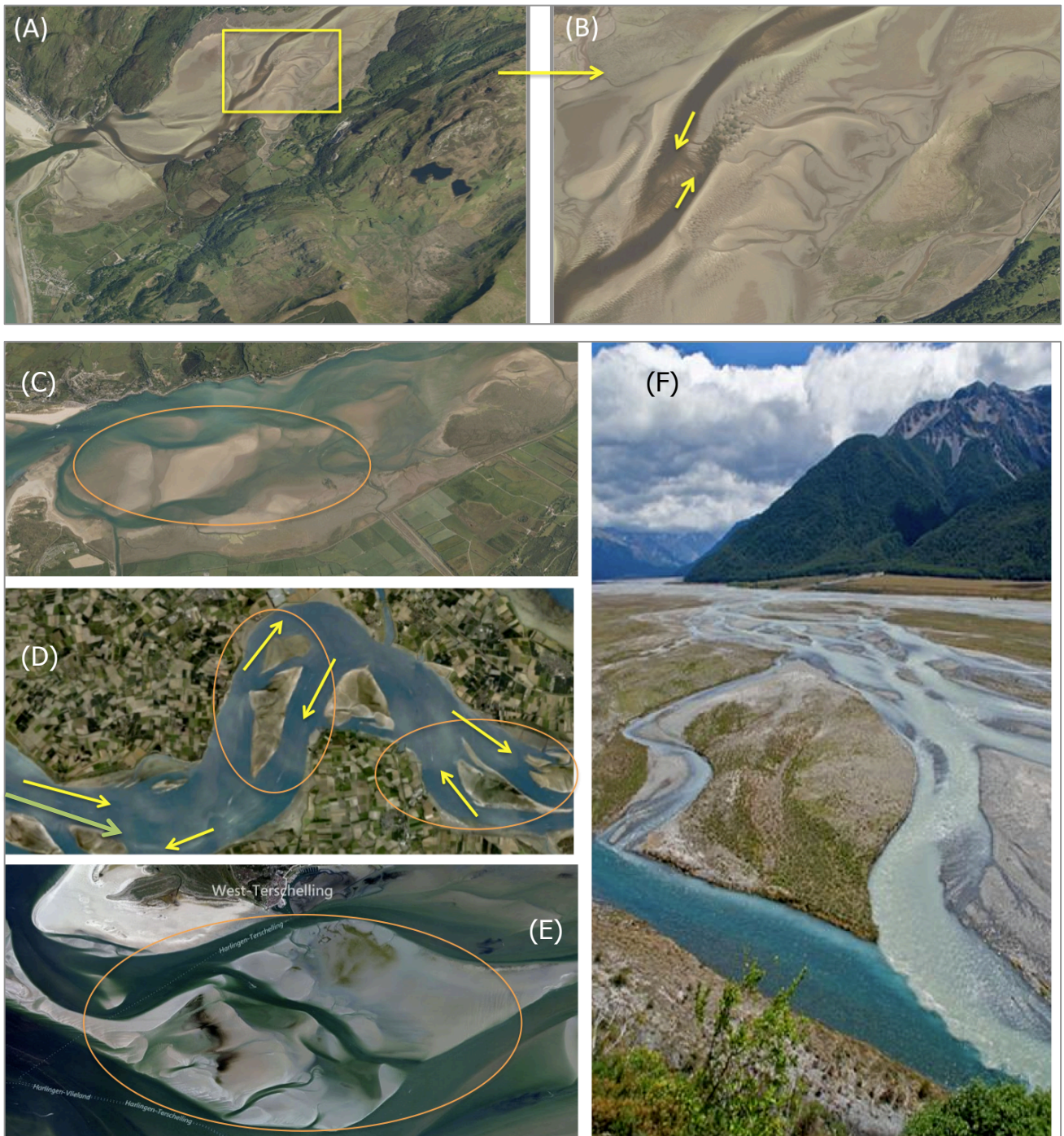


Figure 2.1: Tidal bars and ebb- and flood-dominated channels in the outer zone of (A) Afon Maddwach estuary, England. (B) Zoom of yellow box (in A) in Afon Maddwach estuary. (C) Round-shaped tidal bars in Aberdovey estuary, England. (D) Sharper-shaped single row tidal bars in Westerschelde estuary in the Netherlands. Yellow arrows indicate ebb or flood channel and orange ellipse represents tidal bars. (E) Tidal bars and ebb- and flood-dominated channels in the backbarrier basin in the Wadden Sea, the Netherlands. Green arrow indicates tidal inlet between Vlieland and Terschelling. (F) Multiple channel system and bars in Waimakariri River, New Zealand (Bing maps, assessed on April 2013; Google assessed on April 2013).

2.1.2 Tide-dominated estuaries

Pritchard (1967) defines an estuary as a semi-enclosed coastal body of water, which has a free connection with the open sea and where the seawater mixes with freshwater derived from land drainage. The seaward part of the estuary is subjected to the tidal motion that produces landward-directed currents (flood) and seaward-directed currents (ebb). The magnitude of the tidal currents is weakest at the mouth and head of the estuary (Dalrymple and Choi, 2007) (fig 2.2). The strongest tidal currents are present in the middle of the estuary, close near the place where the distributary channels bifurcate around tidal bars (fig 2.2). Ahner (1960) in Hibma et al. (2004) observed this pattern of bifurcating channels around bars in the middle of estuaries in the USA and the Westerschelde Estuary in the Netherlands. Ahner (1960) attributed this pattern to modification of the tidal wave that propagates through the estuary. The tidal wave has the character of a progressive wave when the tidal wave enters the estuary (Hibma et al., 2004). Maximum ebb currents occur around minimum waterlevel and maximum flood currents around maximum waterlevel. However, when the tidal wave propagates further into the estuary, an increasing phase shift develops between maximum waterlevel and currents.

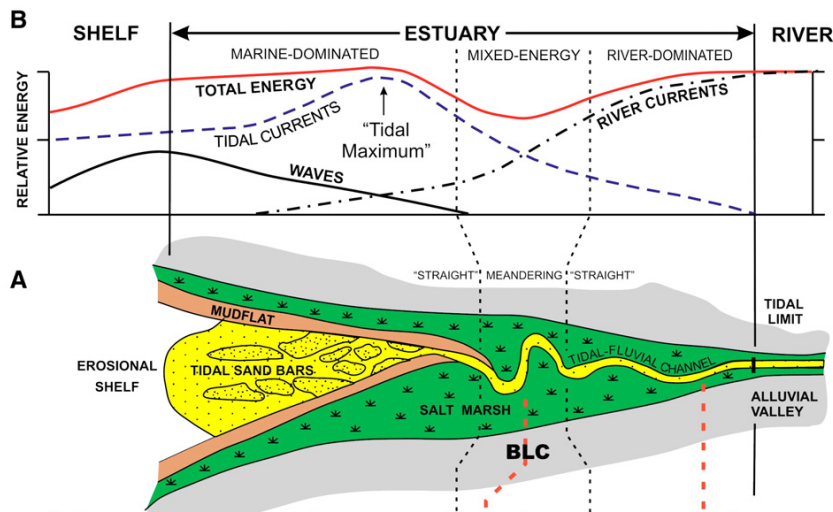


Figure 2.2: **(A)** Schematic representation of a funnel-shaped tide-dominated estuary (Dalrymple and Choi, 2007). Note the presence of elongate tidal bars at the seaward end of the system and tidal flats and salt marshes. **(B)** Variation in intensity of energy of waves and river- and tidal currents.

The inland parts of tidal systems are narrow and more sinuous channels are present with bars (Dalrymple and Choi, 2007). Here bars are often bank-attached point bars or alternating bars and no flow separation occurs of the flow into mutually evasive ebb- and flood-dominated channels (Van den Berg et al. *in press* in Dalrymple and Choi, 2007). Tidal channels are wide and straight at the seaward part of the estuaries (outer zone). Here, elongate tidal bars are present that delineate usually multiple tidal channels, which become longer when moving seaward (Masselink and Hughes, 2003). The elongate tidal bars in tidal channels may become dissected by smaller channels, which have cut oblique across the tidal bar. Those smaller channels are called swatchways (Robinson, 1960 in Dalrymple and Choi, 2007) or connecting channels (Swinkels et al., 2009). Further landwards the tidal inlet is present.

Examples of tide-dominated estuaries are the *Aberdovey* estuary and *Afon Mawddach* estuary. The estuaries exhibit a well-developed system of multiple ebb- and flood-dominated channels separated by tidal bars in the outer zone of the estuary (fig 2.1).

2.1.3 Sediment transport

In general two types of sediment transport can be distinguished (Van Rijn, 1993; van Leeuwen, 2002): bedload transport and suspended load transport. When the bed-shear stress velocity exceeds the critical value for initiation of motion (θ_{cr} , eq. 3), bed material particles will move by rolling and/or sliding when being in continuous contact with the bed surface. When the bed-shear velocity increases, particles move by saltation, which is referred as the particles moving by regular jumps across the bed. When the bed-shear velocity starts to exceed the fall-velocity of particles, sediment can be lifted up from the bed to a level where upwards-turbulent forces are higher than then the submerged weight of the particle, which causes the particles to go into suspension. The process whereby particles are rolling, sliding and saltation is called bedload transport, while the movement of suspended particles is referred as suspended-load transport (Van Rijn, 1993). Suspended load is for considerable period of time without contact with the bed. The combination of bedload and suspended load transport is defined as total load transport (Van Leeuwen, 2002). An important characteristic of suspended load particles is that the particles in the water column need time to reach the bed. This time span is defined as settling lag and is an important difference between bedload and suspended load (van Leeuwen, 2002). Net sediment transport in tide-dominated environments during one tidal cycle is important for the development of morphodynamic units.

Sediment particles will start to move when the bed shear-stress acting on the particles starts to exceed a certain threshold value, referred as critical bed-shear stress (Van Rijn, 1993; van Leeuwen, 2002). The bed-shear stress [N/m^2] can be defined as follows:

$$\tau_b = \rho g (u^2/C^2) = \rho U_*^2 \quad (1)$$

Wherein ρ represents the density of water [kg/m^3], g the gravitational acceleration [m/s^2], u the depth-averaged flow velocity [m/s], C being the Chezy coefficient [$m^{0.5}/s$] and U_* being the friction velocity (Van Rijn, 1993). From equation (1) it follows that the bed-shear stress is related to the flow velocity above the bed. In order for particles to start moving the flow velocity must exceed a critical value (van Leeuwen, 2002). Shields (1965) studied initiation of motion and related the bed-shear stress (τ) to the dimensionless sediment mobility parameter (θ). The dimensionless shields parameter is given by (Van Rijn, 1993):

$$\theta = \tau_b / ((\rho_s - \rho_w) g d_{50}) \quad (2)$$

Wherein τ_b is the bed-shear stress [N/m^2], ρ_s represents the density of sediment [kg/m^3], ρ_w the water density [kg/m^3], g the gravitational acceleration [m/s^2] and d_{50} being the median grain size [m] (Van Rijn, 1993).

In order for particles to start moving, the dimensionless sediment mobility parameter (θ) has to exceed the critical sediment mobility parameter (θ_{cr}), given by (Van Rijn, 1993):

$$\theta_{cr} = \tau_{b,cr} / ((\rho_s - \rho_w) g d_{50}) \quad (3)$$

where $\tau_{b,cr}$ represents the critical bed-shear stress [N/m^2]. The dimensionless sediment mobility parameter (θ) and the critical sediment mobility parameter (θ_{cr}) are important parameters when using (scale) experiments (Van Dijk et al., 2012). The experiment conditions must be designed such that the flow is able to rework the sediment and is able to transport the sediment due to both bedload and suspended load transport processes ($\theta > \theta_{cr}$) (Kleinhans and van den Berg, 2010).

The main factor for net sediment transport in tidal systems is a result of tidal flow asymmetry (Dronkers, 1986). Two types of asymmetry in relation to tidal systems are present. This first asymmetry can be described as the difference in magnitude between maximum flood and ebb currents. The second asymmetry is defined as time-flow asymmetry, which is caused by the difference in variation of the current velocity around high water slack (HWS) and low water slack (LWS). The slack water period is defined as the period when flow starts to reverse, while flow velocities are still low and particles start to settle down (Leeuwen, 2002). The time-flow asymmetry type is responsible for the development of asymmetry in sedimentation processes, erosion and resuspension of sediment, and consequently responsible for the tidal displacement of sediment in tidal inlet systems.

2.2 Ebb- and flood-dominated channels

Tide-dominated systems are often characterized by a pattern of multiple channels that divide and recombine around tidal bars (fig 2.3, *left*) (Dalrymple and Choi, 2007; Hibma et al., 2004; Swinkels et al., 2009). This channel pattern changes every tidal cycle and results in an ebb- and flood-dominated channel system (Van Veen, 1950). The resulting pattern develops during the ebb- and flood cycle is referred as a multichannel system (Swinkels et al., 2009). So far only Van Veen investigated in some extent the pattern of ebb- and flood-dominated channels in the 1950s for the Westerschelde estuary and the Dutch Wadden Sea. In Van Veen (1950) definitions, the flood-tidal channel (ebb-tidal channel) is open to the flood current (ebb current) and exhibits a sill at the landward end (seaward end). The curved ebb-channel is often deeper than the flood-channel. The ebb-tidal channel starts to meander in cases where the width between the banks of the channel is not too large (three to five times larger than the width of the main ebb channel). The flood-channel is relatively straight and forms a shortcut through the inner bend of the meandering ebb-channel (fig 2.3, *right*) (Van Veen, 1950; Swinkels et al., 2009). In the beginning the flood channels transport little sediment and only start to transport sediment as it propagates more landwards (Van Veen, 1950).

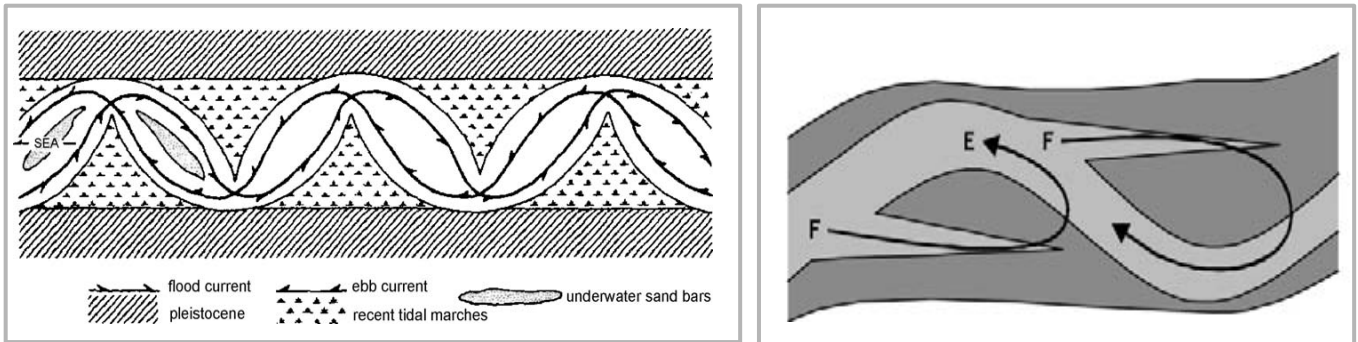


Figure 2.3: Multichannel system that consists of ebb- and flood-dominated channels that recombine around tidal bars (**left**) (Van Veen, 1950) and circulating sand currents in tidal system (**right**). Sand moves upstream in the flood-tidal channel and downstream in the ebb-tidal channel (Van Veen, 1950). E= ebb dominated channel, F= flood-dominated channel.

An important feature of ebb and flood channels is that they often seem to evade another. Sometimes an ebb-or flood-channel splits into two branches and embraces the other opposing channel. In some cases the two opposing channels move sideways and approach each other in a flank attack. These features develop due to opposing sand transport during ebb and flood and due to meandering. Flood-driven sediment transport is dominant in flood-channels during flood and vice versa. The opposing sediment fluxes form a sill when the flood and ebb-tidal channel meet. However, tidal motion oscillates the sediment, which results in a residual sediment transport (fig 2.3, *right*). Near flood and ebb channels sand eddies develop where sand moves downstream in ebb channels and upstream in flood channels. However, sand in the sill at the upstream and downstream end in flood and ebb channel does not cease there. Where the sand is deposited differs from deposition on tidal flats or it may return by the sides of the flood and ebb channel (van Veen, 1950).

The characteristic behavior of ebb- and flood-tidal channels is also observed in the Westerschelde (Swinkels et al., 2009; Hibma et al., 2004; Van Veen, 1950). This multichannel system can be schematized as a series of repetitive units that consists of a curved main ebb-channel and a straight flood-tidal channel that is separated by subtidal shoals or tidal bars (fig 2.4 & 2.4B) (Swinkels et al., 2009; Van Veen, 1950). These units are distinct morphological cells and can be defined on such as the basis of the residual sediment circulation. This circulation pattern arises due to the asymmetric water motion during flood and ebb (several studies in Swinkels et al., 2009; Van Veen, 1950). These so-called macrocells are present in the Westerschelde (fig 2.4A). The main ebb- and flood-channel are connected by connecting channels that intersect the bars inbetween the two channels. The connecting channels are unique morphological features of the multichannel system and induce exchange of water between the two main channels and distribute tidal flow in the channel system (Jeuken, 2000 in Swinkels et al., 2009). The connecting channels are maintained by the difference in waterlevels between the two main channels. Swinkels et al.. 2009 investigated three hydrodynamic mechanisms that are responsible for the difference in waterlevels: (1) differences in tidal wave propagation, (2) centrifugal forces and (3) Coriolis forces.

Tidal channel systems are controlled by three main factors: tidal prism, meandering and sediment transport according to van Veen (1950). Changes that occur in tidal channel systems can for a large extent be explained by meandering. On tidal flats natural processes can cut off meanders. Without any bank or protection of the bank of the meander, a bend can become so large that meander cutoff occurs. However, important to note is that the sill of a flood channel does not easily breach. Therefore in tidal basins or estuaries it is very scarce for meanders to be cut off, due to the fact that the sill of a flood channel is seldom breached. When breaching of the sill does occur, it is mostly of short duration. The elevation of a sill upstream of a flood channel maintains its elevation. The sill maintains its elevation even though the location of the flood channel is at the position where one would expect the cutoff. Though large currents and waterlevel gradients occur on the sill, the elevation is maintained due to the relative large sediment transport on the sill according to Van Veen (1950).

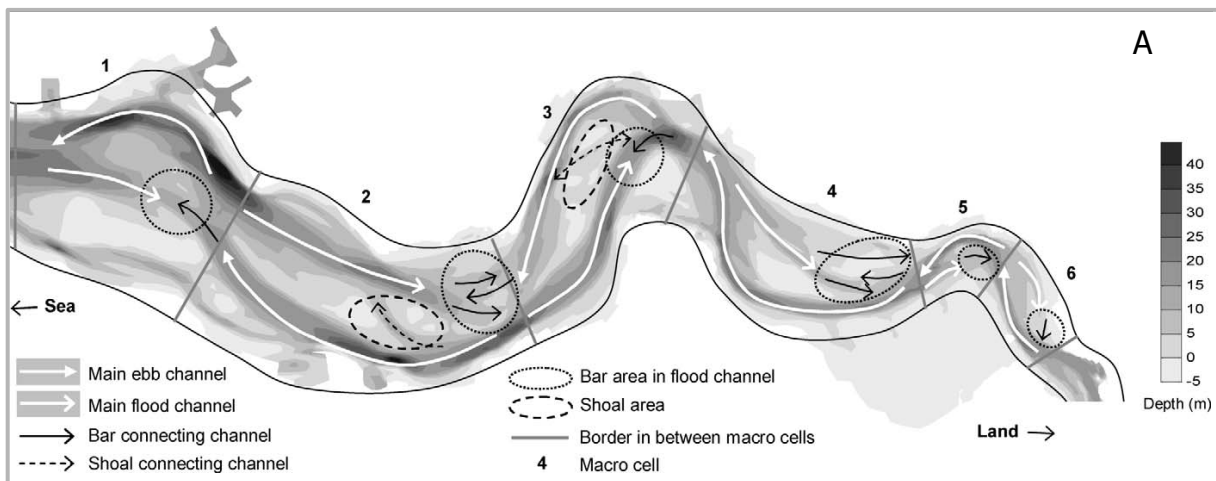


Figure 2.4: (A) Ebb- and flood-tidal channels and bar areas in the Western Scheldt (bathymetry, 2002) (Swinkels et al. 2009). (B) View of Westerschelde with ebb- and flood-dominated channels in yellow with bars inbetween (Bing maps, assessed on April 2013).

2.3 The role of bars

Fluvial bar theory explains how small perturbations may lead to the formation of regular patterns in channels, such as bars (Kleinhans and van den Berg, 2010). Bar theory also predicts whether bars focus bank erosion for the development of meandering rivers or when braid bars develop that erode the riverbank more uniformly for the development of braiding rivers (Tubino et al, 2013). First free bars in fluvial systems (meandering and braiding) will be discussed together with fluvial bar theory. Hereafter the presence of free tidal bars in tidal systems will be discussed.

2.3.1 Bars in fluvial systems

Bar theory

It is well known from fluvial literature that free fluvial bars form due to irregularities in the sediment bed (Kleinhans, 2010; Tubino et al., 2013, Seminara et al., 2012). Bed surface patterns emerge at many scales in fluvial rivers due to the fact that sediment transport rate depends upon the flow shear stress to the power 3-5 (Kleinhans and Van den Berg, 2010). Therefore, a slight irregularity on the sediment bed causes the flow to decelerate, which leads to a large local sediment transport gradient that may result in essential large scale-features of fluvial rivers, such as rivers bars (Tubino et al., 2013; Kleinhans, 2010; Kleinhans and van den Berg, 2010). The crucial parameter that controls the formation of free fluvial bars is the width/depth ratio β of the channel (Tubino et al., 2013; Kleinhans, 2010; Kleinhans and van den Berg, 2010). When the β ratio is larger than a certain critical value β_c , the bar perturbation may be enhanced as when their wavenumber falls in the unstable range where bed perturbations lead to the development of free bars in fluvial rivers (fig 2.5) (Tubino et al., 2013).

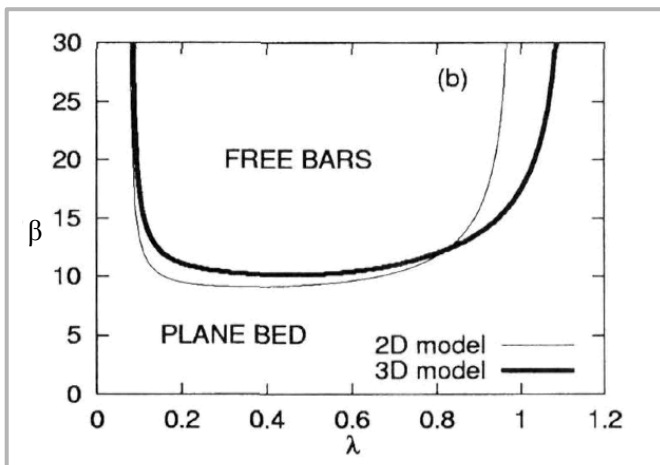


Figure 2.5: Marginal stability curves predicted by 2D and 3D models (Seminara and Tubino, 2001; Tubino et al, 2013). When wavenumber (λ) falls in the unstable range the perturbation leads to amplification of the bars (free bar range). Otherwise the perturbation dampens out and the bed returns to its original flat bed state (plane bed range).

The development of the sediment bed suggests that spatial variation in both flow and sediment transport is present (Tubino et al, 2013). Development of the bars in fluvial rivers occurs when the longitudinal transport at the bar crests decreases and deposition occurs. Experimental observations in fluvial systems suggested that the selection process of bar length when starting from an initial flat bed is relatively fast (Tubino et al, 2013).

Then bars develop slower until they reach a quasi-steady equilibrium. The wavelengths of free fluvial river bars fall in the range of 5-12 times channel width according to observations (Tubino et al, 2013; Seminara and Tubino, 2001).

Bar regime

The existence of bars in straight channels and bar type for specific flow conditions is predicted by the equations of Struiksma et al., (1986). His theory is valid for alternate bars, where development of alternating bars depends upon the width/depth ratio. When the width/depth ratio is below 20, no bars develop. When the width/depth ratio lies between 20 and 30 stable alternating bars develop and when the ratio exceeds 30 dynamic alternating bars develop (Kleinhans and Van den Berg, 2010). The theory by Struiksma et al., (1985) is summarized by Kleinhans and Van den Berg (2010).

Initiation of bars in straight fluvial channels is predicted with the use of the Interaction Parameters (*IP*, eq. 4).

$$IP = \frac{\lambda_s}{\lambda_w} \quad (4)$$

It shows from equation 4 that the interaction parameter equals the ratio between the adaptation length of the sediment (λ_s) and of the water (λ_w), which in turn depends strong on the width/depth ratio (eq. 5):

$$\frac{\lambda_s}{\lambda_w} = 2\pi^2 f(\theta) \frac{g}{C^2} \left(\frac{W}{h} \right)^2 \quad (5)$$

In where, h equals water depth [m], w equals width [m], θ represents the non-dimensional shear-stress (also referred as Shields number) and C represents Chezy friction coefficient [$\sqrt{m} s^{-1}$].

The ratio between the adaptation length of the sediment and water can be explained by using a straight river channel with an upstream perturbation (Kleinhans and Van den Berg, 2010). This perturbation in the flow arises when uniform steady flow in a straight channel suddenly enters a river bend. The waterlevel is forced to rise at the opposite bank, as the flow is directed towards the outer bank of the channel due to conservation of momentum. This results in a pressure gradient were spiral flow is directed towards the inner bend. The spiral flow transport sediment towards the inner bend of the channel. The sediment bed responses due to the change in flow pattern in the channel. While the flow is slightly directed towards the inner bend, also sediment transport is directed towards the inner bend and hence a bar is build in the inner bend of the channel.

Already state in equation 4, the characteristic of bars depends on both adaption length of the flow and the bed, which in turn depends strongly on the width/depth ratio in the river (eq. 5). The width of the river depends on bank strength, whereas the depth of the river depends in turn on the width of the river and roughness (due to cohesion and vegetation).

Therefore, depending upon the ratio (eq. 4), three specific morphological regimes are present. When channels are deep and relatively narrow (low width/depth ratio), bars dampen out in less than one bar length or over longer distance (fig 2.6) ($IP < 1$) (Kleinhans and Van den Berg, 2010). This results in a plane bed. When channels are less deep and narrow (intermediate channels) bars are underdamped (fig 2.6) ($IP > 1$). This regime leads to overdeepening of the pool in the outer-bend and enhancement of the bar in the inner bend of the channel just downstream of the entrance of the bend or other perturbations, such as a sudden widening of narrowing of the channel. However, the resulting bed deformation dampens out downstream of the local perturbation (Mosselman et al., 2006 in Kleinhans and van den Berg, 2010). When the channel is relatively shallow and wide (large width/depth ratio) bars become unstable and can theoretically grow in height downstream of the local perturbation, defined as the exciting regime ($IP > 1$) (fig 2.6). Growth of bars can be related to a positive feedback between the deforming bed and the flow. Both bed and flow adapt to the local perturbation but both have different adaption lengths. When the flow has already adapted to the perturbation, but the bed has not yet adapted to the same perturbation, the flow will adapt again to the changing bed and so on. Now the perturbation can grow in downstream direction. In this stage, higher-mode bars can appear, which appear as multiple bars present within the channel (fig 2.6 & fig 2.2) (Kleinhans and Van den Berg, 2010).

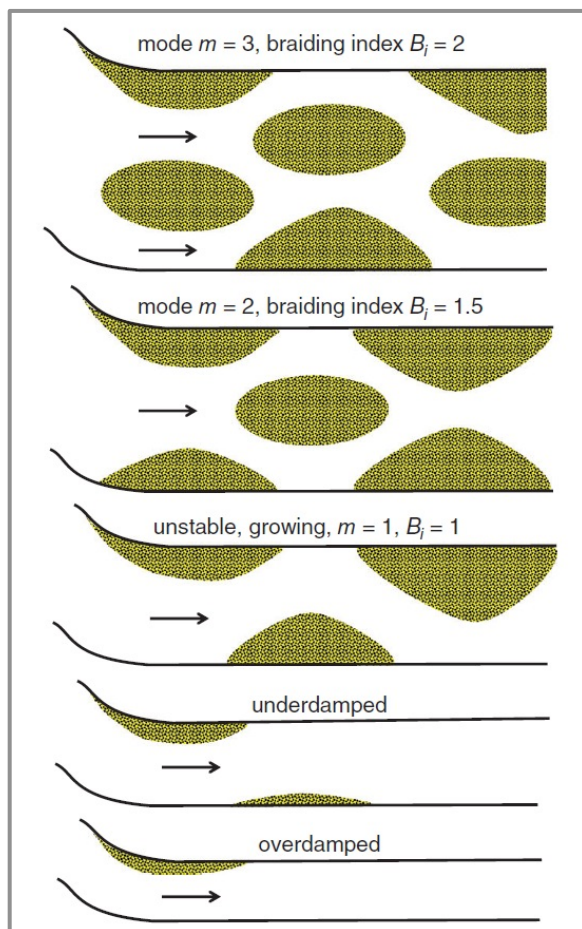


Figure 2.6: Three bar regimes and bar mode (Kleinhans and Van den Berg, 2010). Note the overdamped, underdamped and unstable growing regime (excitation regime).

Topography of the changed bed can vary from pronounced alternate bars to braided channel patterns. The overdamped, underdamped or excitation regimes differ for sand-bed rivers or gravel-bed rivers (Kleinhans and van den Berg, 2010). Excitation bars develop in sand-bed rivers when width-to-depth ratio exceeds approximately 70, while excitation bars develop in gravel-bed rivers when width-to-depth ratio is 30 (fig 2.7).

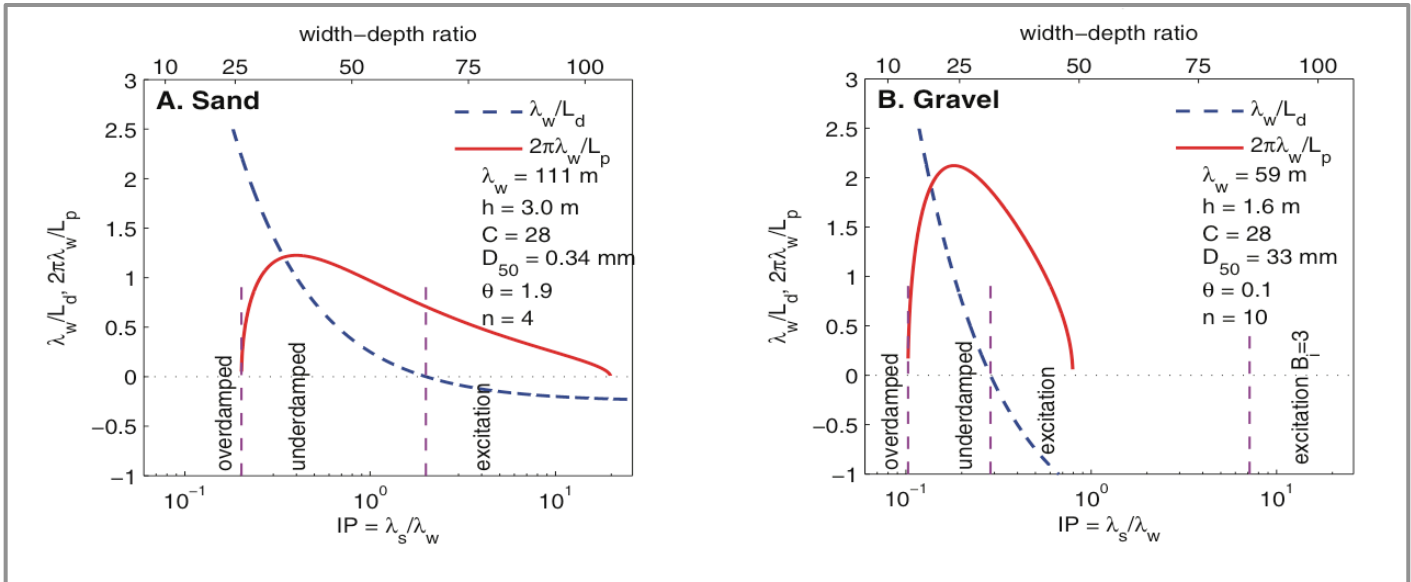


Figure 2.7: Different bar regimes for mode 1 bars that are generated by perturbations for (A) sand-bed rivers and (B) gravel bed rivers. Width-to-depth ratio is indicated on top. Further explanation on other parameters of these graphs is present in Kleinhans and van den Berg (2011).

Meandering river bars

Bars are important in meandering rivers as they provide an explanation for the development of a meandering river pattern. Meandering rivers are possibly explained by two theories. The first is that of bar instability that states that instable bars grow in vertical direction. The second theory is that of bend instability (Kleinhans, 2012). Bars are forced to their position in meandering channel bends. One might suggest that the alternating bars will always result in alternating bank erosion such that meandering channels develop (Kleinhans, 2010). However, Seminara and Tubino (1989) in Kleinhans (2010) showed that alternating bars in an initially straight channel can migrate so fast that the banks will be eroded everywhere and not only in the bends of the channel. When the banks erode everywhere, the channel widens such that the channel pattern can evolve towards braiding.

Several studies in Kleinhans (2010) showed that both natural and experimental channels with weak banks often evolve into wide and shallow rivers. Irregular bars develop in the channel and form a braiding river pattern. However, rivers become narrow and steep when they have strong banks and bars at the surface, and as a result alternating bars develop in the stream (several studies in Kleinhans, 2010). Meander bend growth, cutoff and meander migration are the result of strong flow present in pools between the alternating bars. This can lead to local bank undercutting and mass wasting during flooding (several studies in Kleinhans, 2010).

Balance between erosion of the bank and floodplain formation determines channel width, whereas channel width determines bar pattern. This developed bar pattern determines where erosion of the bank occurs, while bar migration is reduced by floodplain formation, armouring of bars or presence of resistance material in the floodplain (Kleinhans, 2010). Channel banks are eroded on either side when bars and floodplain form (Kleinhans and van den Berg, 2010). Therefore the width of the channels is determined by the balance between floodplain destruction and formation, and hence width determines the presence of bars in river channels.

Braided rivers bars

Braided rivers are characterized by their multiple channel systems, irregular bar pattern, variability in bar shape and size and due to their morphodynamics (Schuurman et al., *in prep*). Important feature of braiding bars is the interaction between their bars and channels, as bar erosion is induced by channel migration and bar itself induce channel avulsion within the river system. Large braided rivers bars can be stable, as is the case in the Brahmaputra where their bars are stable due to vegetation or topographic forcings or resistant rivers banks. Braided rivers bars are found in rivers with relatively large width/depth ratio (fig 2.2), as been explained by linear stability analyses (several studies in Schuurman et al, *in prep*). River pattern can be predicted by the use of potential specific stream power, as a function of valley slope, channel width and mean annual discharge, as was illustrated by Kleinhans and Van den Berg (2010). For a braiding pattern do develop a high potential specific stream power and a large enough width-to-depth ratio are necessary (Schuurman et al, *in prep*).

Different processes may be responsible for the formation of braided rivers bars according to Ashmore (1991) in Schuurman et al., (*in press*). Initiation of braided rivers bars in experimental settings are often the result of chute cutoffs in meandering channels, due to the non-cohesive sediment bed material and narrow initial channels (several studies in Schuurman et al., *in press*). When starting with a relatively wide channel in experimental settings central bars could initiate (Fujita, 1989 in Schuurman et al., *in prep*). Field observations have showed that braided bars have different sizes and shapes and can be classified into three types of bars: unit bars, compound bars and islands (several studies in Schuurman et al., *in press*) (fig 2.8). The unit bars are the key element in braiding rivers as they migrate fast through the river. When unit bars merge together, they form large, irregular compound bars. Those bars can be either mid-channel bars or bank-attached bars. Islands are often covered by vegetation and are more stable.



Figure 2.8: Braided channels and mid-channel bars in **(Left)**: South Saskatchewan River, Canada and **(Right)**: Brahmaputra, India. Photos obtained from Schuurmans et al, (*in press*).

Schuurman et al., (*in prep*) modelled self-formed braided rivers with a physics-based model to quantify bar pattern dynamics that are compared with field observations, flume experiments and linear stability analyses. Their model results reveal two types of bar formation. Either bars formed due to a response to the initial bedlevel perturbation or bars formed as a response of continuous upstream inflow perturbation. Bars that formed as a response of upstream inflow perturbation were high bars. A front of these bars migrated downstream, whereas the upstream bars hardly migrated and therefore influenced the bars downstream. In the first stage of bar evolution, the small bars grew rapidly in horizontal direction. Further growth of bars was not by expansion of individual bars but due to bar merging (Schuurman et al., *in prep*). Later on, bars grew more in their height and channels deepened further. Sediment transport and flow concentrated in the channels. The total braiding index decreased and this indicates that more channels were closed off and became inactive, but still were present in the system. Bars still increased in their length until they reached the water surface. The modelled bars reached a steady equilibrium. The braided rivers bars were immobile when they were surrounded by deep channels and grew in height towards the water surface. This increase in height resulted in a significant reduced of sediment transport over the bars. The final height of the bars was therefore reached when they grew towards the water surface.

2.3.2 Bars in tidal systems

Fluvial bar theory states that fluvial bars strongly depend on width/depth ratio of the tidal channel, but such extensive formulations are not yet given for bars in tidal systems. The current knowledge on tidal bars is based on modelling studies (Schramkowski et al., 2002; Seminara and Tubino, 2001; Schuttelaars and de Swart, 1999; Schramkowski et al., 2004, Garotta et al., 2006) and from observations (Dalrymple, 1977; Dalrymple et al., 1970). Different types of modelling methods are used to study channel-bar dynamics in tidal embayments (Schramkowski et al., 2004). Tidal bars were recently investigated with the use of a three-dimensional model used by Seminara and Tubino (2001). They modelled the basic mechanism whereby tidal bars form in tidal channels. Seminara and Tubino (2001) stated in their formulations that tidal bars do depend on width/depth ratio of the tidal channel (their equations 2.1a,b in Seminara and Tubino, (2001)). Their results revealed that if the width/depth ratio of the tidal channel exceeds a critical value positive growth rates for bars are obtained. If this condition is achieved, tidal bars grew spontaneously due to feedback mechanism between the tidal flow and sediment bed. The growth of bars is resembled by a series of alternating bars and pools (fig 2.9) and wavelength is in the order of 10 times channel width. It also turned out from their results that bars exhibit no net migration over a tidal cycle.

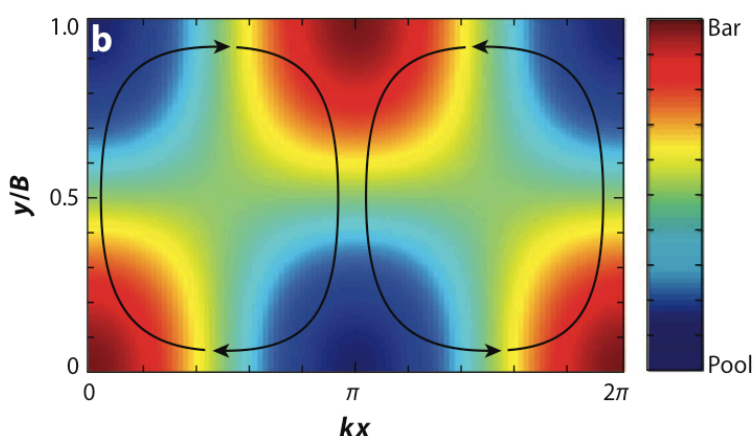


Figure 2.9: Bottom pattern of series of alternating bars and pools (de Swart and Zimmerman, 1999). The black line indicates tidal residual circulation.

Both Schramkowski et al. (2002) and Garotta et al. (2006) also captured the excitation of tidal bars in their model study. Schramkowski et al., (2002) extended the model of Seminara and Tubino (1998). The model of Seminara and Tubino (1998) is a three-dimensional model that can only be applied to narrow channels (when width is small compared to tidal excursion length) and when tidal flow is frictional dominated. The extended model of Schramkowski et al., (2002) is applicable for both wider tidal basins and flow conditions do not need to be completely friction dominated. Schramkowski et al., (2002) used a 2DH morphodynamic model that also included local inertial terms in their momentum equations when defining the model. The use of inertial terms is important if flow is not frictionally dominant and the width of the tidal channel is in the order of tidal excursion length. Therefore, their results showed that the dimensional growth rates of tidal bars were not only depended on channel wave number but also on the tidal excursion length. They demonstrated that estuarine bars formed with length scales in the order of tidal excursion length can initiate due to a positive feedback between the sediment bed, water motion and sediment transport. The modelling study of Garotta et al., (2006) showed that when used an external tidal forcing (primary tide and first overtide), bars showed a net migration in the direction of the peak current due to the fact that the forcing allows peak ebb and flood flow do differ (Garotta et al., 2006).

The modelling studies discussed above all use a linear stability analyses in order to investigate dynamics of the perturbations that evolves on a basic state. This basic state is characterized by tidal flow over horizontal sediment bed. This results in the fact that the validity of their model is limited to the initial growth stage of the perturbation (when their bar amplitudes are small). The linear stability analyses can be extended to non-linear effects in order to determine the finite-amplitude of tidal bars. Schramkowski et al., (2004) developed such non-linear model. Their model describes the long-term behaviour of bedforms in tidal channels and is used to study the finite-amplitude of tidal bars. Their results also revealed that finite-amplitude bars initiated when they scaled with tidal excursion length. They also aimed at analyzing the dependence of finite-amplitude bar solutions on the width of the tidal channel and bottom friction parameter (Schramkowski et al., 2004). Their results showed that solutions were found for a significant range of values for the width of the channel and bottom friction parameter. Different types of finite-amplitude bars were found, such as time-independent bar types and stable time-dependent bar types. The latter being non-migrating features.

Hibma et al., (2004) modelled finite-amplitude tidal bars in long embayments in tidal systems. They used a numerical model that simulates the interaction between the sandy bed and tidal flow in a rectangular embayment of 80km in length. At the seaward boundary tidal motion is forced by the sea-surface elevations. Their results start with a randomly perturbed initial state. After a while, ebb and flood-tidal channels and tidal bars emerged (Hibma et al., 2004). Figure 2.10 shows the modelled bottom patterns for $t=120$ years. Their model results show strong similarities with the observed patterns in the Westerschelde according to van Veen (1950). The flood-tidal channels are straight and exhibit at the seaward end a bar, while ebb-tidal channels meander (length scale is about 10km). When moving further inland, both ebb- and flood-tidal channels start to meander.

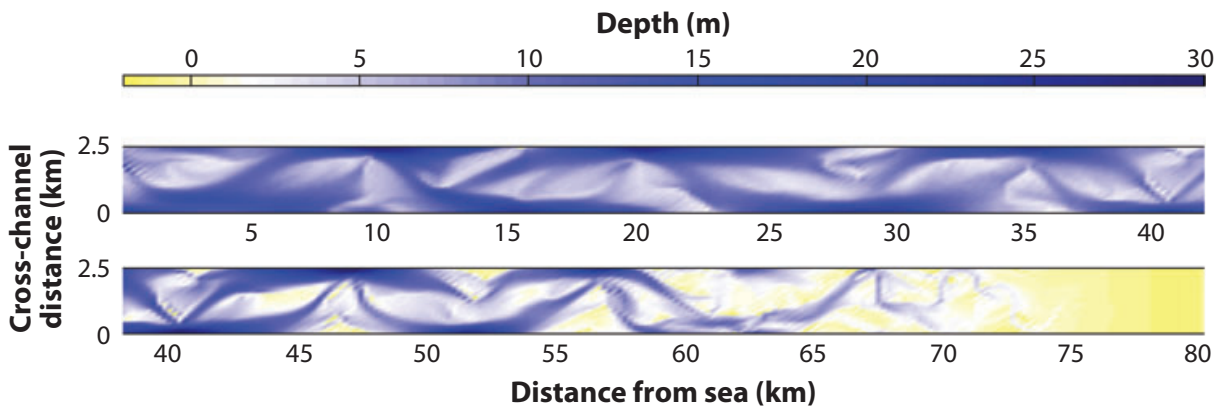


Figure 2.10 Bottom pattern modeled with a numerical model that shows bottom profile after an initial state (Hibma et al., 2003 in Schuttelaars and de Swart, 1999). Upper panel: Seaward end with main meandering ebb-tidal channel and straight flood-tidal channels at the bends of the meandering ebb channel. Lower panel: Meandering of ebb and flood-dominated channels, also observed by Ahnert (1960) in Hibma et al., (2004).

A necessary condition for instability in the system is the presence of frictional forces in the tidal channel and on the shoals (Schuttelaars and de Swart, 1999). The frictional forces cause a reduction of the flow velocity above the shoals (due to small waterdepth) and to increase in the tidal channels. Sediment concentration increases therefore in the channel and is lower on the shoals. Therefore sediment flux is from the channel towards the shoals and hence shoals height increases and flow velocity reduces further (positive feedback). However, flow continuity results in slowing down of flow velocity in the tidal channel and increasing flow velocities on the shoals. If the frictional forces are larger than the continuity forces, the perturbation on the bottom can grow (Schuttelaars and de Swart, 1999; Seminara and Tubino, 2001) (fig 2.11).

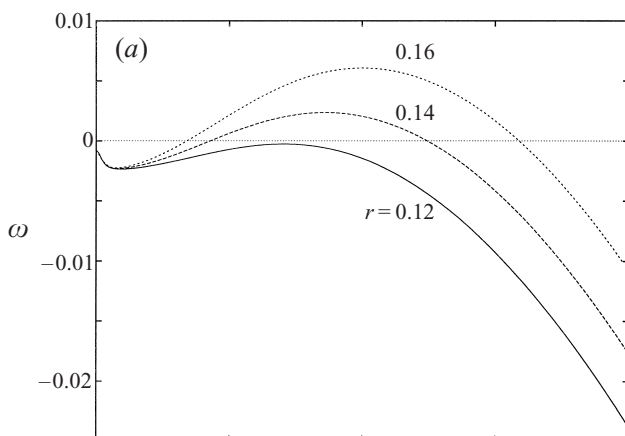


Figure 2.11: Growth or decay of perturbation for different values of r (friction parameter). When the friction values remain below zero, the perturbation decays. If the friction parameters exceeds zero the perturbation can start to grow due to positive feedback between the bed and flow (Schuttelaars and de Swart, 1999). When friction is not included, no positive feedback arises and perturbations always decay.

On the other hand, observational studies showed insight in the shape and size of tidal bars. Dalrymple (1977), Dalrymple et al. (1975) and de Vries-Klein (1970) studied numerous large sand bars present in the Minas Basin and Cobequid Bay in Fundy. Tidal bars are in general asymmetric with their gentle side facing the shoreline and where bar length is being longer than bar width. The dominant process operating on the tidal sand bars are reversing tidal currents (Dalrymple, 1977; Dalrymple et al., 1975). Observation by Dalrymple (1977) also indicated a recirculating sediment transport pattern in the Cobequid Bay, Fundy (fig 2.12). There deep major channels located at the north and south shores of the bay are flood dominated as was shown from their data. Channels in the middle of the bay are shallower and ebb-dominated (Dalrymple, 1977). This result eventually in two large-scale flow and sediment transport cells in the bay. Also smaller-scale circulation patterns were visible in the system. Bottom tidal currents are segregated into flood-and ebb-dominated channels over the sand bars (de Vries-Klein, 1970; Dalrymple, 1977). Here, flood currents are dominant over the steep side of the bars, while ebb currents are dominant over the gentle sloping bar surfaces.

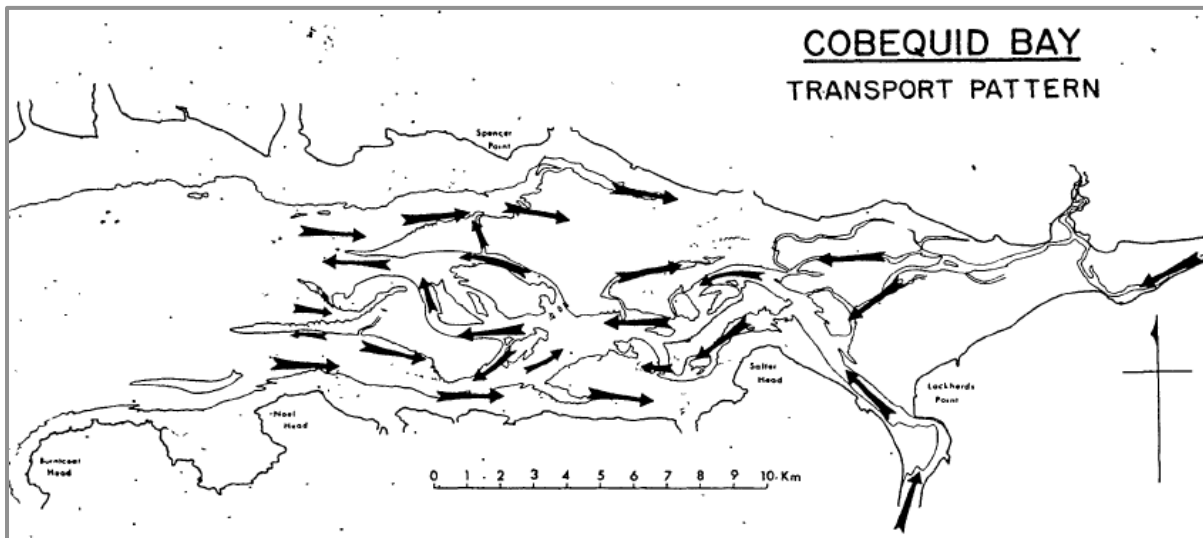


Figure 2.12: Recirculating sediment transport pattern observed in the Cobequid Bay, Fundy by Dalrymple et al (1977).

2.4 Previous tidal experiments and scaling issues

This chapter will start with a brief review on experiments that have already been done in order to understand more about tidal channels and bars. Then scaling issues in experimental settings will be discussed.

2.4.1 Previous tidal experiments

Experiments with tides are very rare (Kleinhans, 2012). Only five publications reports on experiments with tides are available (Tambroni et al., 2005; Garotta et al., 2008; Kleinhans et al., 2009; Stefanon et al., 2010 and Vlaswinkel and Cantelli, 2011). Kleinhans et al., (2012b) have been the first to create tidal basins in experimental settings by tilting of the entire basin instead of creating tides by varying the waterlevel. Terwisscha van Scheltinga (2012) performed those experiments. The main objective of her research was to create a tidal inlet system in dynamic equilibrium state in an experimental scale model. In the experiments tidal channels, ebb-tidal deltas and tidal bars were successfully created. Earlier experiments produced also tidal channel networks, tidal deltas and bars. Stefanon et al., (2010) aimed in their study at reproducing a tidal lagoonal environment subjected by tidal forcing. They simulated tidal channel network in four experiments where tides were created by fluctuating waterlevels in a basins with a narrow inlet and non-cohesive sand. Tidal channel network evolution is also investigated by Vlaswinkel and Cantelli (2011) and Tambroni et al., (2005). Vlaswinkel and Cantelli (2011) did experiments on tidal channel network in a filled basin (3 m by 2.5 m) filled with sediment. The experimental system of Tambroni et al. (2005) consisted of an erodible channel connected through an inlet to a tidal sea. They created successfully small- and large-scale bedforms in the tidal channel and basin. Garotta et al., (2008) have experimented on long-term morphodynamics of a tidal meandering channel connected to a tidal basin. Their results included the evolution of a bar-pool pattern driven by curvature of the channel.

2.4.2 Scaling problems

Experiments can create natural phenomena at smaller scale and can lead to new hypotheses that are able to explain natural phenomena (Kleinhans et al., 2010b). With the use of experiments scale problems arise, unless the system in nature is so small that it will fit exactly in the experiment (Kleinhans et al., 2010b). However, that is almost never the case. The experiment will be designed such that the experimental conditions will be compromise between important scaling problems in experimental setting. Typical scaling problems in experiments are that of low sediment mobility, prevention of scour holes and sediment cohesion (van Dijk et al. 2012). Another problem is that surface flow in experimental setting is very thin and therefore has relatively low Reynolds numbers and high Froude numbers (several studies in Kleinhans et al., 2010b).

It is important to discuss the scale effects of the Froude number and typical shallow flow in laboratory experiments. Scaling of the Froude number is well known (several studies in Kleinhans, 2010a). Both Reynolds number (eq. 7) and Froude number (eq.6) should be equal in the prototype system and in the scale experiment.

In order to have such similar flow conditions in the experimental setting and the prototype the flow length in the scale experiment L_s has to be equal to the flow length in reality L_r . The Froude number is defined as follows:

$$Fr = \frac{u}{\sqrt{gh}} \quad (6)$$

In where the g represents the gravitational acceleration [m/s^2], h equals water depth [m] (or hydraulic radius) and u is velocity [m/s].

$$Re = \frac{\rho hu}{\mu} \quad (7)$$

Where ρ represents the density of water [kg/m^3] and μ represents dynamic viscosity [$kg/m*s$]. When looking at both the Froude number and Reynolds number equations it seems that the Froude number depends on \sqrt{h} whereas the Reynolds number depends on waterdepth itself. It is therefore impossible to satisfy both conditions in order to obtain the same velocity scale (Kleinhans et al., 2010b). The Froude number is often relaxed as when the flow condition remains subcritical, while the Reynolds number is usually relaxed under the assumption that inertia dominates viscosity. However, this assumption is problematic when shallow flow occurs on small-scale floodplains.

In order to experiment with mobile bed settings, the mobility of sediment in experimental setting has to be similar with sediment in reality. The mobility of sediment is expressed as the Shields number (eq. 2). Here, the particle size D has to be scaled with the L_s/L_r . However, the use of silt and fine sediment is not usable in experimental settings due to the cohesiveness of fine sediments. Therefore, coarse sediment has to be chosen. Ripples and large scour holes can develop in experimental settings when the flow conditions are hydraulic smooth. The hydraulic resistance scales with particle size and waterdepth. Hydraulic smooth flow conditions cannot be scaled with water depth and results in unrealistic morphology (Kleinhans et al., 2010b). In order to prevent hydraulic smooth conditions, the particle Reynolds number has to be larger than the transition from hydraulic smooth conditions to rough conditions:

$$Re^* = \frac{\rho u^* D}{\mu} > 11.63 \quad (8)$$

In where u^* represents the shear velocity [m/s] and D is defined as the particle size [m] that represents the roughness (Kleinhans et al., 2010a). However, the particle size is often unknown in realistic systems and often the D_{50} is used.

Bar regime depends on the ratio of adaption length of the flow and adaption length of the sediment after a perturbation (such as a bend) (Struiksma et al., 1985) and the ratio is described as the interaction parameter IP (see chapter 2.3). The balance between bank erosion and floodplain formation determines channel width and depth. In turn, the width/depth ratio determines the bar pattern. Banks are eroded fastest at the pools between the bars. Then, alternating bars can lead to meandering, but bars can migrate fast so that erosion is not focused long enough at the specific bank location to create meandering river patterns. Bar migration can be reduced by vegetation, cohesive sediment or armouring of the bars. Without any cohesion of the banks, the banks erode until a braided river channel develops. To have strong banks that can be eroded the bank strength τ_f has to be higher than the critical shear stress for sediment motion τ_c , but the bank strength τ_f has to be smaller than the actual shear stress τ_b :

$$\tau_c < \tau_f < \tau_b \quad [13]$$

In order to increase bank strength, seeding vegetation, silica flour and clay can be added to the banks. Also vegetation can add strength to the banks, which depends upon depth of the roots, vegetation density and production of organic material (Tal and Paola, 2007 in Kleinhans et al. 2010b). However, too dense or fast-growing sediment prevents channel migration. In experimental settings is mixture of sediment essential for the parameters in the relaxed scaling approach. This is due to the fact that the sediment mixture determines in the strength of the banks, variation in roughness and in turn determines river pattern and bar dynamics (Kleinhans et al. 2010b).

2.5 Research questions and hypothesis

Here the literature review is synthesized by combining the knowledge of tidal bars and channels with the current lack of knowledge. This results in a set of research questions with their aim at investigating characteristics of tidal bars and channels in experimental setting. As already mentioned, scale experiments with tides are extremely rare (Kleinhans, 2012).

2.5.1 Research questions

The current state of knowledge is based on modelling studies or observations in nature. Tidal bars are mainly investigated with the use of models. Seminara and Tubino (2001) were the first that modelled the mechanism that controls the initial formation of tidal bars. They hypothesized that tidal bars spontaneously emerge due to feedback between the tidal flow and sediment bed. Recent studies have also showed an important characteristic of tidal bars. It showed from their modelling studies that tidal bars scale with tidal excursion length (Schramkowski et al., 2002; Schramkowski et al., 2004). The model study of Seminara and Tubino (2001) have showed that tidal bars exhibit no net migration under tidal forcing, but this has not yet been performed in experimental settings. Observational studies (de Vries-Klein 1970; Dalrymple, 1977; Dalrymple et al., 1975) have proven insight in the sediment circulation patterns and about shapes and sizes of tidal bars in the Cobequid Bay of Fundy.

Several aspects of tidal bars remain unanswered, as no link is present between modelling studies and tidal bars being observed in nature. Data of scale experiments on tidal bars and tidal channels are currently unavailable. It is general known that width/depth controls the formation of fluvial bars in channels, but it remains unclear what triggers the initial formation of tidal bars and what determines the shape and size of tidal bars.

In order to understand whether tidal bars can form in experimental setting, how they are characterized, and agree with observations in nature and previous literature, several research questions (1,2) will be addressed:

- Do tidal bars develop spontaneously in tidal experiments or only results from forcings?
- How are tidal bars characterized in experimental setting?

As already mentioned, tidal bars are flanked by ebb- and flood-dominated channels. From observations it showed that natural ebb- and flood-dominated channels exhibit a recirculating sediment transport pattern (Dalrymple et al, 1975; Dalrymple, 1977), but this has not yet been observed in experimental data. The following question is (3):

- Is tidal channel network created in experimental setting similar to nature (i.e. ebb- and flood-tidal channels according to van Veen (1950)) and how do the ebb- and flood-tidal channels evolve over time?

In addition also braided river bars are investigated that form under unidirectional flow, and otherwise same conditions, to compare between tidal bars that form under reversing flow. This allows looking at differences between fluvial and tidal bars. The final questions (4,5) are:

- How is the braiding pattern characterized?
- How do tidal bars differ from (experimental) fluvial bars?

2.5.2 Hypotheses

Based on the literature review hypotheses are formulated. The hypotheses are tested in the experiments.

Hypothesis question 1:

Do tidal bars develop spontaneously in tidal experiments or only results from forcings?

Several modelling studies have demonstrated the fact that bars grow spontaneously due to feedback between the tidal flow and the sediment bed (Seminara and Tubino, 2001; Schramkowski et al., 2002; Schramkowski et al., 2004; Schuttelaars and de Swart, 1999; Hibma et al., 2004), both with linear stability analyses and stability analyses extended with non-linear effects. However, this is only simulated with modelling. According to Schuttelaars and de Swart (1999) are frictional forces responsible for the development of positive feedback between the bed and flow. Therefore, in order for tidal bars to develop spontaneously there has to be enough friction of the flow in the experiment to create the positive feedback between flow and sediment and the perturbation at the bottom can start to grow. This will eventually lead to the development of tidal bars in the experimental system.

Hypothesis question 2:

How are tidal bars characterized in experimental setting?

Several modelling studies have already shown insight in some characteristics of tidal bars, but then again this is only observed in modelling studies and not yet in experimental data. The most important finding of the modelling studies is that of bar length scales with tidal excursion length (Schramkowski et al., 2002; Schramkowski et al., 2004). This important finding will then also be visible in the experiments. The results of Seminara and Tubino (2001) also revealed that unlike fluvial free bars, tidal bars exhibit no net migration during a tidal cycle.

Observational studies have showed that tidal bars in nature show variation in size and shape (Dalrymple, 1977; Dalrymple et al, 1975). The large sand bars in their observations were asymmetric in shape and the zones of ebb- and flood-dominated channels distribute sediment. The bars formed in the experiments will probably differ also in shape and size and will expand if the system evolves through time. The variables of the tilting basin will probably affect the shape and size of the formed bars (*variables of tilting basin*, see chapter 3).

Hypothesis question 3:

Is tidal channel network created in experimental setting similar to nature (i.e. ebb- and flood-tidal channels according to van Veen (1950)) and how do the ebb- and flood-tidal channels evolve over time?

The pattern in the experiment probably has the same configuration as described by van Veen (1950). Tide-dominated systems are often characterized by a pattern of multiple channels that divide and recombine around tidal bars (Dalrymple and Choi, 2007; Hibma et al, 2004; Swinkels et al, 2009). This channel pattern changes every tidal cycle and results in an ebb- and flood-dominated channel system (Van Veen, 1950). Over time, the tidal channels will probably increase in depth and more channels will develop. Also recirculating sediment transport patterns were visible in the tidal systems (Van Veen, 1950; Swinkels et al, 2009). Another important feature is that of connecting channels being observed in the Westerschelde by Swinkels et al (2009) that induce exchange of water between the two main channels. Both recirculating sediment transport patterns and connecting channels may be visible in the experiments.

Hypothesis question 4:

How is the braiding pattern characterized in experimental setting?

In nature braiding river systems are characterized by multiple channel systems, irregular bar pattern and bars vary in their shape and size due to their morphodynamics (Schuurman et al, *in prep*). This will also be visible in the experiments if the braiding pattern develops, as bars will probably differ much in their shape and size. Bars will migrate downstream and the braiding pattern will expand. In natural systems bars may be stable due to due to vegetation or topographic forcings or resistant rivers banks and hence do not migrate (Schuurman et al, *in prep*). However, no vegetation or strong resisting riverbanks are present in the experiments so therefore bars will not be stable.

Hypothesis question 5:

How do experimental tidal bars differ from fluvial bars?

Unstable fluvial bars show a net migration downstream (Seminara et al., 2012; Tubino et al., 2013), whereas tidal bars show no net migration under tidal forcings (Seminara and Tubino, 2001). It also stated from literature that fluvial bars develop fast in length until they reach equilibrium. Experiments will show if tidal bars will also reach equilibrium. If the experimental tidal bars will be compared with the experimental braided river bars it will probably results in different shapes and sized for the bars.

2.6 Thesis outline

In order to answer the research questions of this thesis, chapter 3 will first explain how the experiments were performed. Here the experimental set-up will be described, and experimental scenarios and data collection. Chapter 4 described the results of the laboratory experimentation with the use of two basic cases. The results are discussed in chapter 5. This thesis will end with a short conclusion provided in chapter 6.

3. Methods

This chapter will describe the experimental set-up that was used to answer the research questions. The use of the experimental basin and flume set-up are also described. Hereafter the associated photo cameras and Z-snapper apparatus and sediment characteristics will be explained. Then the experimental scenarios and data collection are explained.

3.1 Experimental set up

3.1.1 Tilting basin

The experiments were performed in an indoor apparatus, which is referred in this report as the tilting basin, located in the basement of the Van Unnik building. The tides were generated by vertically tilting the basin around its equilibrium point in the middle (fig 3.1). The tilting basin is 3.2 meters long, 1.0 meter wide and 25 centimeters deep (Terwisscha van Scheltinga, 2012). The plastic tub, designed by Chris Roosendaal of University Utrecht, is set on a metal frame where the legs of the frame are in contact with the floor at the middle and at one end of the tub. In order to set the variables of the tilting basin, the tilting basin is connected to software designed by ing. Henk Markies of Utrecht University. This software in the mechanical jack allowed the tilting basin to move up and down around its leg in the middle of the tilting basin (fig 3.1). The tilting amplitude from the horizontal level, tilting speed and tidal delay at high and low water level represented the variables of the tilting basin. Tidal delay represented the time before the tilting basin turned towards the reversed tide. Two overflow pipes were installed at the end of the basin, which are used to set the minimum waterlevel. When the tilting basin was at horizontal level, the two overflow pipes needed to be at equal heights in order to have no net flow. At the two overflows at either side of the tilting basin, the water was continuously pumped in the tilting basin, while the excess of water left the system while drained into a storage tank beneath the tilting basin. The discharge at both end of the tilting basin was set equally during all tidal experiments.

The sediment bed in the tilting basin was 2.40 meters long and 1.0 meter wide. The sediment bed was 5 centimeters deep and therefore the tilting basin contained 0.12 m^3 sediment during the experiments. At both end sides of the sediment bed, 40 cm of water was present that could either flow during the tidal cycle or leave the system as excess water. When one side of the tilting basin reached his highest point, referred as low water, the other side of the tilting basin reached high water. The period for the tilting basin to reach low water is defined as the ebb-phase and the period for the basin to reach high water is defined as the flood-phase. During the flood phase the water flowed through a change in water surface gradient towards the lower end of the tilting basin and caused increasing waterlevels (fig 3.1).

During both high and low water periods, the system induced a cycle of sediment transport, sediment deposition and erosion. This resulted in morphological changes in the system. The water was colored with a blue indigo, such that the waterdepth was better visible on the cameras. Darker blue colors indicated deeper channels.

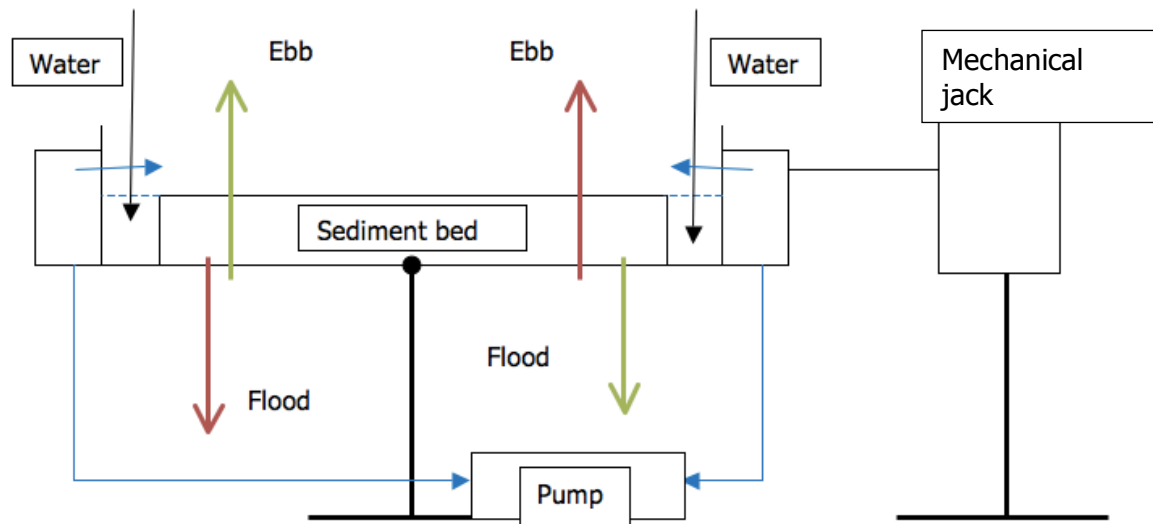


Figure 3.1. Initial situation when the tilting basing is at equilibrium. Red arrows indicate one half of a tidal cycle where the right-hand side of the tilting basin moves up and reaches low water (ebb) and the left-hand side of the tilting basin moves down and reaches high water (flood). Vice versa for the green arrows.

3.1.2 Flume set-up

In the experiments design conditions were achieved in order to compromise between important scaling issues, such as low mobility of sediment, prevention of scour holes and sediment cohesion (table 3.1) (Van Dijk et al. 2012). In the experimental system it was necessary that flow conditions were subcritical ($Fr < 1$, table 3.1). It was important that flow conditions remained subcritical during the experiment and more or less uniform, otherwise the Froude number cannot be relaxed (Kleinhans et al., 2010a). In the experiments, flow conditions need to be turbulent, in order to rework the sediment and for the transport of sediment in suspension in the tidal channels and in the basin ($Re > 2000$) (Van Dijk et al. 2012). In order for sediment to be mobile, the shields number must exceed the critical shields number ($\theta > \theta_{cr}$). The sediment in the basin had a hydraulic rough bed, to prevent large scour holes and ripples. Large particles were needed to disrupt the laminar sublayer (Reynolds particle number $Re^* > 11.6$) (table 3.1).

The calculations show that the design scale rules were achieved in the experimental setting (see *experimental design*, table 3.1). Indeed flow was subcritical and turbulent. Turbulent flow was also visible with the colored indigo-blue water. Sediment exceeded the critical mobility parameters in such way that both suspended load and bedload transport occurred.

Table 3.1 Flow conditions in experimental design in order to prevent scaling issues (Kleinhans et al. 2010b; Van Dijk et al. 2012). Design scale rules were calculated for the experiments (value experimental design). Equations are presented in chapter 2.4.

Condition	Symbol	Design scale rule	Value experimental design
Froude number	Fr (-)	< 1	0.67
Reynolds number	Re (-)	> 2000	34630
Shields critical mobility number	θ_{cr} (-)	0,04	0,04
Shields parameters	θ (-)	> 0.04	0,10
Grain Reynolds number	Re* (-)	> 11.6	51

3.1.3 Cameras and Z-snapper camera

Three overhead cameras hanged above the tilting basin followed the evolution of the experiments. The three cameras made pictures at set intervals to record time-series of the morphological evolution of the system. The three overhead cameras were connected to the mechanical jack, which was connected to the PSRemote and photobooth software at the computer. The software at the mechanical jack allowed that the photo cameras took pictures at four moments in the tidal cycle: low water, MSL during flooding stage, high water, and MSL during ebb. The overhead cameras took pictures at the start of the experiment until the end of the experiment.

The Z-snapper camera also hanged above the tilting basin and captured the tilting basin in terms of height of the sediment bed. The Z-snapper was used to create Digital Elevation Maps at several timesteps in the system, in order to evaluate the evolution of the system in terms of height and depths. The Z-snapper is connected to software at the computer and this allowed calculations of height and depths for tidal bars and channels, and erosion and deposition patterns. The DEMs were further used to calculate tidal bar and channel width and length on different locations in the sediment bed. An initial DEM was made before the experiment started and represented the flat sediment bed without any morphological changes.

3.1.4 Sediment characteristics

The sediment used for both the tidal experiments and braiding river experiments was lightweight plastic grains provided by Utrecht University. The Sieve curve is represented in figure 3.2 and shows the $D_{50}=0.62\text{mm}$, $D_{90}=1.1\text{mm}$ and $D_{10}=0.42\text{mm}$ respectively. The sediment density of the lightweight plastic grains equalled $1150\text{-}1250\text{ kg/m}^3$. The lightweight sediment was used to enhance both bedload and suspended load transport in order to have morphological changes in the system.

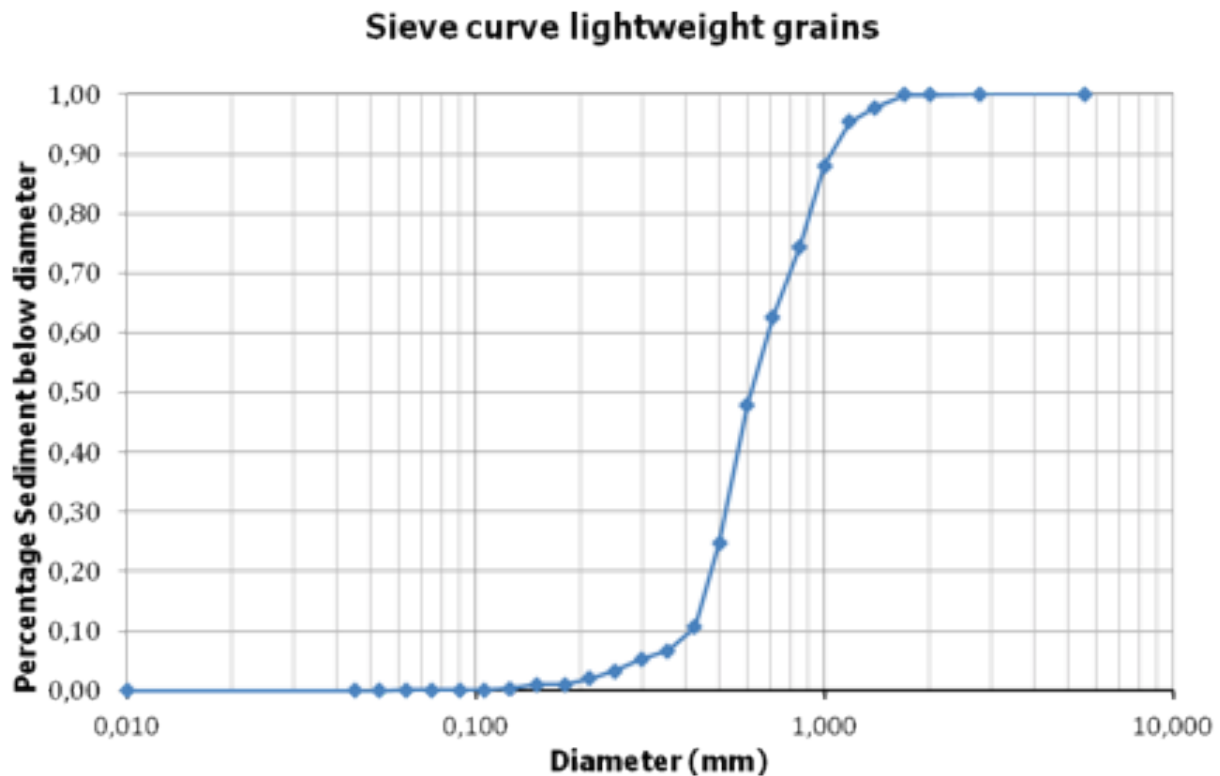


Figure 3.2: Sieve curve of the lightweight plastic grains. $D_{10}=0.42\text{mm}$, $D_{50}=0.62\text{mm}$ and $D_{90}=1.1\text{mm}$ and the density equals $1150\text{-}1250\text{ kg/m}^3$.

3.2 Experimental scenarios

The experiments performed in the tilting basin represent a small part of a tidal system (tidal inlet or estuary).

3.2.1 Tidal experiments

Tidal bars were investigated in a free-setting scenario. Here, the setup of the experiment is such that tidal bars developed autogenically in such way that no initial perturbation is made in the sediment. In other words, no forcing in topography is made (channel curvature, variation in channel width). The water forcing at both ends of the tilting basin is equal in force. This induces that at both ends the waterlevels were kept equal so no net flow of water is present. In this free-setting scenario, the development of tidal bars and channels were investigated by the variation in tilting amplitude, tilting speed and delay of the tilting basin. Also the effect of tidal symmetry and asymmetry were investigated by setting different tilting amplitudes and speed for both sides of the tilting basin (table 3.2). Waterdepth in the experiments is held constant at 5 mm in order to eliminate effects of different waterdepth on the morphological evolution of the system. Slope is calculated over the total distance of the tilting basin and is highest for the experiments with the highest amplitudes (table 3.2).

The tidal experiments were all symmetrical except for experiment number 13 (table 3.2). The experiments are divided into basic high- and low-amplitude case, high amplitude cases and low amplitude cases, and the symmetrical tide and asymmetrical tide case. The two basic cases (red in table 3.2) are used in chapter 4.

Table 3.2 Free-setting scenarios with cases for the tilting basin, were basin length equalled 3.2 meters and basin width equalled 1 meter. Red-colored numbers indicate cases used in chapter 4.

Number	Case	Tilting speed (mm/min)	Amplitude (mm)	Slope (m/m)	Delay (s)	Tilt cycles	Duration (hours)
1	High amplitude	15	10	0.0031	10	197	5 ½
2	High amplitude	12	10	0.0031	5	67	5
3	High amplitude	13	10	0.0031	4	90	5 ¼
4	High amplitude	14	10	0.0031	2	285	8 ½
5	Low amplitude	14	8	0.0025	2	174	5 ¼
7	High amplitude	16	9	0.0028	2	806	7
8	Basic low-amplitude	16	8	0.0025	2	999	68
9	Low amplitude	18	8	0.0025	2	837	46
10	Low amplitude / symmetrical tide	17	8	0.0025	2	2492	94
11	Asymmetrical tide	17	Up 8 down 9	0.0025 0.0028	2	2502	95
13	Basic high-amplitude	14	10	0.0031	2	1134	75

3.2.2. Braiding river experiments

Bars in braided river systems were also investigated with the use of the tilting basin (table 3.3). The braiding experiments are used as control experiments, as here tidal bars were expected to form under unidirectional flow by tilting the basin to one side only, instead of reversing flow for the tidal experiments. The slope of the tilting basin was equal during all experiments and equalled 0.0025 m/m (amplitude of 8 mm and total basin length of 3.2 meters). The braided river bars were compared with tidal bars.

To ensure that the upstream boundary of the river received enough sediment for the braiding pattern to develop, a sediment feeder was placed in front of the tilting basin. The sediment from the sediment feeder was mixed with water before entering the system, to prevent floating of the sediment and ensure bedload transport. The sediment feeder fed at constant rate sediment to the system. The sediment feeder was set in all braiding river experiments at 300 Hz and represented an average sediment transport rate of 0.11 kg/m³. The PSRemote program controlled the cameras in such way that the cameras were taking pictures at set intervals between the frames. The Z-snapper was also used for making Digital Elevation Maps of the system. An initial DEM was also made before the experiment started in order to calculate differences in height, width and length between timesteps in the experiment.

Table 3.3 Overview of braiding river experiments.

Experiment number	Setting	Slope (m/m)	Duration time (hours)
Braiding_1	Braiding river	0.0025	4
Braiding_2	Braiding river	0.0025	4,5
Braiding_3	Braiding river	0.0025	4,5

3.3 Data collection

3.3.1 Photographs and movies

The collected photographs of the experiments were first three separate photographs, which were stitched together with a Matlab script. This matlab script made eventually movies of the stitched photographs. The movies were used to follow the evolution of experimental tidal bars and channels (chapter 4.1) and for the visual analysis of bar and channel shapes (chapter 4.2). The movies were also used for the visual analysis of the differences between tidal symmetry and asymmetry (chapter 4.2.4). The resolution of the cameras is determined from a ruler on the photographs and equalled approximately 0.06 cm.

3.3.2 DEM calculations

The DEMs were used in matlab scripts to perform calculations to reveal several characteristics of bars and channels in the system (width, height, length and number of bars/channels). The horizontal resolution equalled 4 mm and vertical resolution of the DEMs equalled 1 mm. With the use of the resolutions the height, width and length of bars could be calculated.

Height and width

In almost all tidal and braiding experiments an initial DEM was made. For the calculation of bar height and width this initial DEM is subtracted from DEM files at later timesteps. In this way slope effect in the sediment bed were smoothed out, because the sediment bed was not perfectly flat. This DEM difference was used to calculate mean height and width of bars and channels in the system. Mean height and width were filtered to smooth out very high and low peaks. One must keep in mind the definition of bars and channels for this report. All values above the mean bed level elevation were referred as bars, whilst all values below the mean bed level elevation were referred as channels (fig 3.3). Bar height (or amplitude) and width are defined as the relative change in bar height and width with respect to the initial DEM. The same holds on for channel depth. This mean height and width represent an average value for height and width for bars and channels through the whole evolution of the system. The head of the bar is defined as the start of the bar just after the end of the tidal channel (fig 3.3).

Length

Bar and channel length was not calculated automatically with a matlab scripts (as was the case for calculating bar with and height), due to the fact that the method of calculating bar height and width was not suited for bar length. The calculated length of the bars and channels were not representable for what was actually present in the system. Therefore, bar and channel length was calculated by hand due to visual observation of the DEMs and photographs. Bar and channel length are averages lengths and calculated at the end stage of the system (when the experiments were finished).

Number of bars

The number of bars is also calculated in matlab with the same script used to calculate bar width and height. The number of bars is defined as the total number of bars (above the mean average bedlevel) (fig 3.3). With this method, the number of bars is calculated per timestep and finally averaged over all DEMs that represent eventually the total number of bars through the evolution of the system.

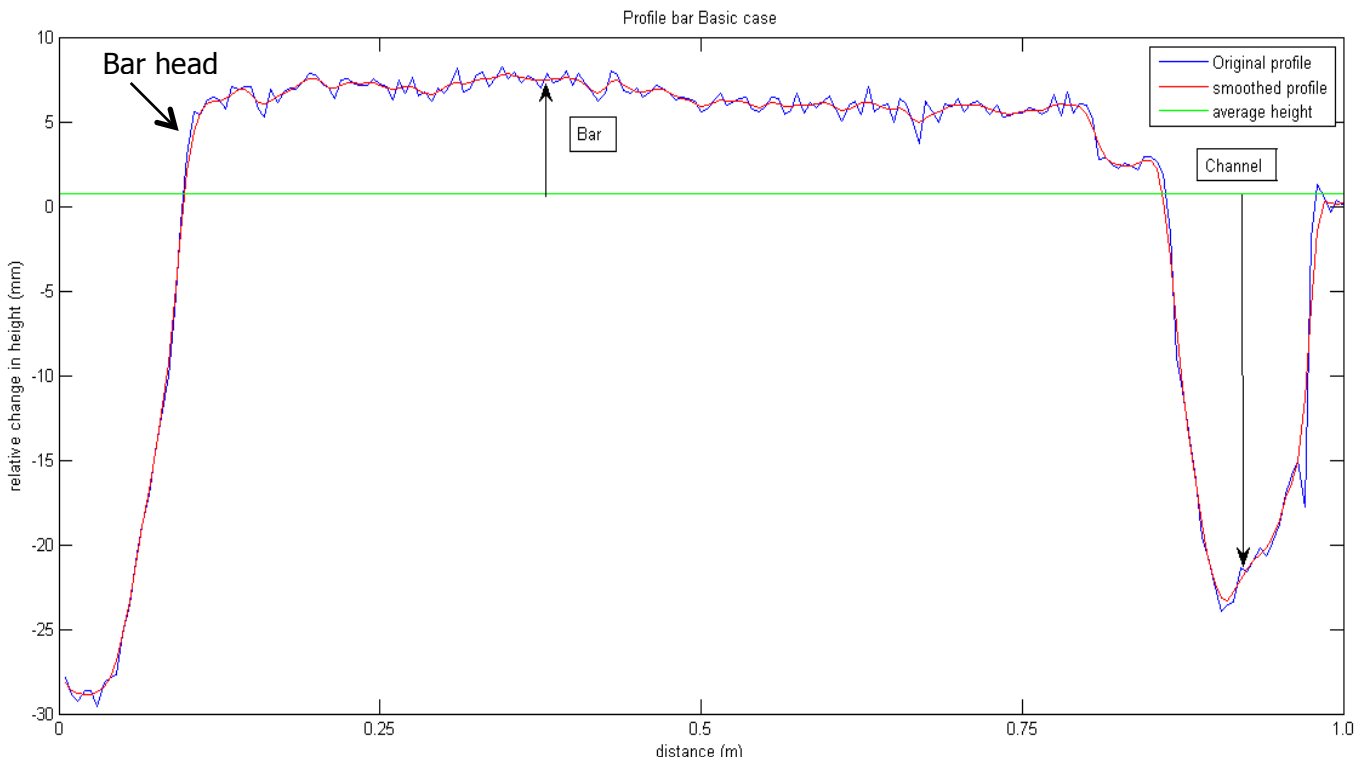


Figure 3.3: Definitions of bars and channels for the calculations. Bar height is calculated by the height of the bar minus the average height.

4. Results

The first subchapter will focus on the evolution of two morphological symmetrical tidal systems from plane bed towards a dynamical tidal system with tidal channels and bars. Describing and analyzing will be done by the use of two basic cases: basic low-amplitude case (*LA-case*) and basic high-amplitude case (*HA-case*) (table 4A). Two basic cases were chosen due to the fact that the evolution of all experiments resulted in two different end-stages, whereas the experiments could be divided into high- and low-amplitude cases. The second subchapter will focus on the dependence of tidal bars and channels on imposed tidal conditions. The main focus lies on the trends, conditions and shapes of tidal bars in the system but the tidal channels in the system will also be addressed.

Table 4A: Description of tidal cases. Bold red numbers indicates used cases in chapter 4.1. Initial waterdepth was equal for all tidal experiments (5 mm). TEL= tidal excursion length (m), TWL=tidal wavelength (m). For calculations tidal excursion length see chapter 4.2 and tidal wavelength see chapter 5.

Case	tidal	Experiment number	Tilting speed (mm/min)	Amplitude (mm)	Delay (s)	Tilt cycles	Slope (m/m)	TEL (m)	TWL (m)
Failure		-	10	8	10	-	-	-	-
Basic high-amplitude	high-	T13	14	10	2	1134	0.0031	8.6	4.8
Basic low-amplitude	low-	T8	16	8	2	999	0.0025	6	3.3
Low amplitude		T5 T9	16	8	2	174 837	0.0025	6.8 5.3	3.8 2.9
High amplitude		T1 T2 T3 T4 T7	16	9	2	197 67 90 285 806	0.0025	8 10 9.3 8.6 6.8	4.3 5.4 5.1 4.8 3.8
Asymmetrical tide		T11	17	Up/down 8/9	2	2502	0.002/ 0.0025	5.6 6.2	3.1 3.5
Symmetrical tide		T10	17	8	2	2492	0.002	5.6	3.1

Table 4B: Description of braiding cases. Bold red number indicates used case in chapter 4.2

Case	braiding	Experiment number	Slope (m/m)	Duration time (min)
Braiding 1		VI_2911	0.0025	240
Braiding 2		VI_3011	0.0025	210
Braiding 3		VI_2811	0.0025	200

4.1 Evolution of experimental tidal bars and channels

Both the experiments (*HA-case*, *LA-case*) started with an initially flat bed that was raised above mean sea level on both sides. The sediment mobility in the experiments was intermediate between suspended and bed load transport, but main transport was bedload transport. The evolution of the systems is visualized in figure 4.1 for the HA-case and in figure 4.5 for the LA-case by the use of 4 photographs. Both experiments started with a flat sediment bed with a length of 2.40 meters and approximately 1 meter wide. Two seas were present at both end sides of the sediment bed each 0.40 meters long.

4.1.1 Basic high-amplitude case

In the first 60 tilt cycles the system showed no morphological changes and the sediment bed remained flat. Hereafter the first bars started to initiate in the middle of the tilting basin due to small perturbations in the sediment bed. Few elongated tidal bars developed (fig 4.1, *tilt cycle 250*), which were observed as the first stage in the evolution of tidal bars for high-amplitude cases. At the same time small tidal channels formed. After initialization of bars they started to expand in height, width and length and occurred parallel to the direction of the tidal flow (fig 4.1, *tilt cycle 549*). Tidal channels increased in depth, width and length. A big bar-channel system was soon visible within the system (fig 4.1, *tilt cycle 549-921 at 0.40m cross-distance*).

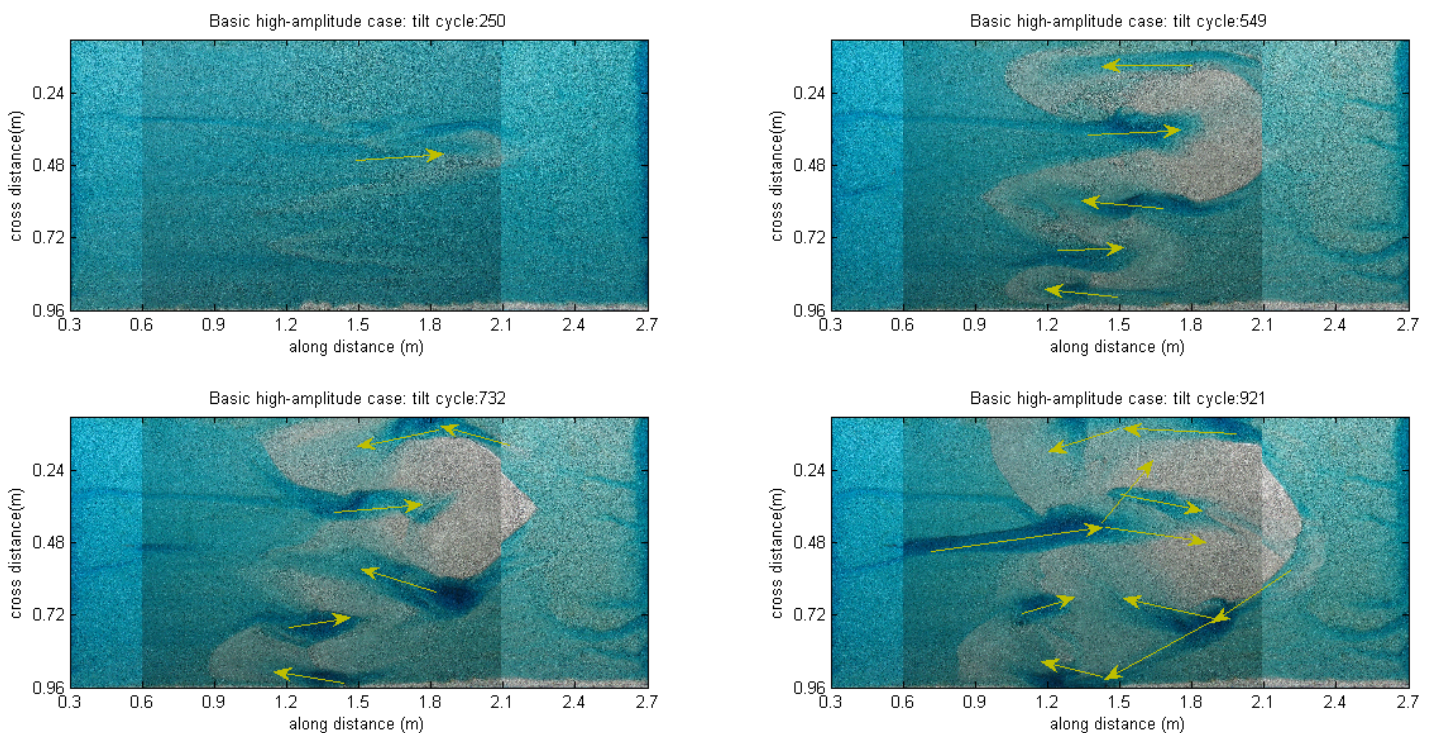


Figure 4.1: Evolution of tidal bars and channels for the basic high-amplitude case. Yellow arrows indicate dominant flow pattern of the tidal currents. Dark-blue colors indicate deeper tidal channels and light areas represent tidal bars.

An important characterization for the tidal system was that bars and tidal channels were only active during one phase of the tides. Tidal bars developed at the end of the tidal channel during one phase of the tides. Bars developed while sediment was transported in the channels to form a lobate-shaped bar on which flow diverged (fig 4.2). Bars that developed during one phase of the tides had higher resistance to the opposite flow due to the fact that reversed main flow did not flow over the bar and through the same channel. Reversed tidal currents flowed in tidal channels flanking the bars (fig 4.2) and formed tidal bars in the opposite direction. Tidal bars grew or decayed in the system due to bar merging or overtaking (fig 4.1, *tilt cycles 732-921*).

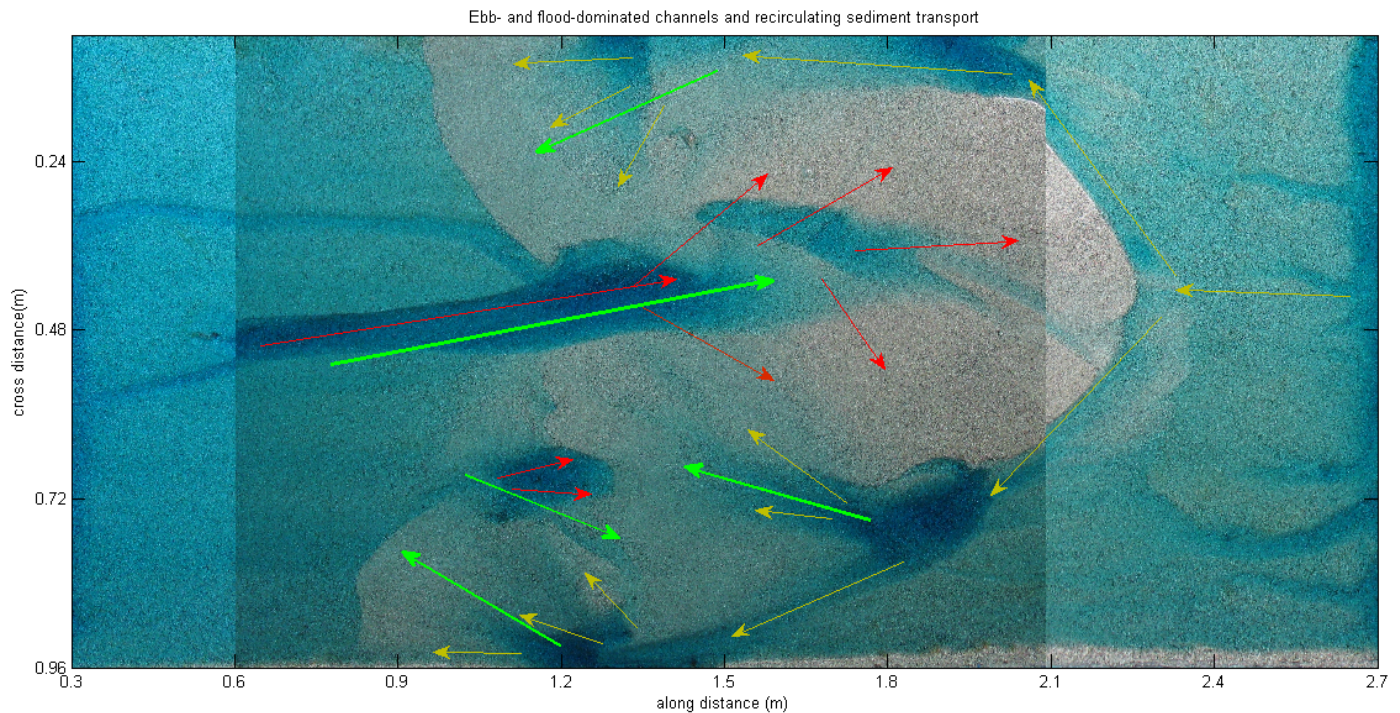


Figure 4.2: Separate ebb- and flood-dominated channels. Ebb-dominated channels are indicated in red and flood-dominated channels (reversed flow) are indicated in yellow. Smaller arrows at the bar indicate flow divergence and green arrows indicate recirculating sediment transport.

Tidal channels were very dynamic through the evolution of the system and were, just like tidal bars, only active during one phase of the tides whereas other channels were only active during the opposite tidal phase. Some channels bifurcated in the system to form new tidal channels (fig 4.3). Channel switching, deepening or shallowing characterized further channel development. Modification of tidal channels and bars occurred through the entire evolution of the system, and indicated that at the end no static equilibrium was reached. The asymmetric pattern of bar and channel development in the system during one dominant tidal phase was characterizing for these conducted experimental tidal systems. The existing tidal channels were referred as flood-dominated channels or ebb-dominated channels, as those channels were only active during one phase of the tides. This pattern of ebb-or flood-dominated channels is clearly visible in figure 4.2.

Tidal currents present in flood-dominated channels transported sediment forward in the system, while sediment was transported backwards again with the tidal currents in the ebb-dominated channels. This resulted in a recirculating pattern of sediment in the system (fig 4.2). During ebb, net sediment was transported in the ebb-dominated channels whilst during flood, net sediment was transported in the flood-dominated channels. When large round-shaped tidal bars (fig 4.1) developed further, smaller-scale channels were visible on the tidal bars. Some of those smaller channels seemed to connect the ebb- and flood-dominated tidal channels in the system (fig 4.3, fig 4.4, *black ellipses*). During ebb, tidal currents flowed in the ebb-dominated channels and flow diverged at the bars. A small amount of the main diverged tidal currents flowed over the tidal bar towards the flood-dominated channel. This small amount of flow transported sufficient sediment that channels could decrease in depth due to deposition of this sediment.

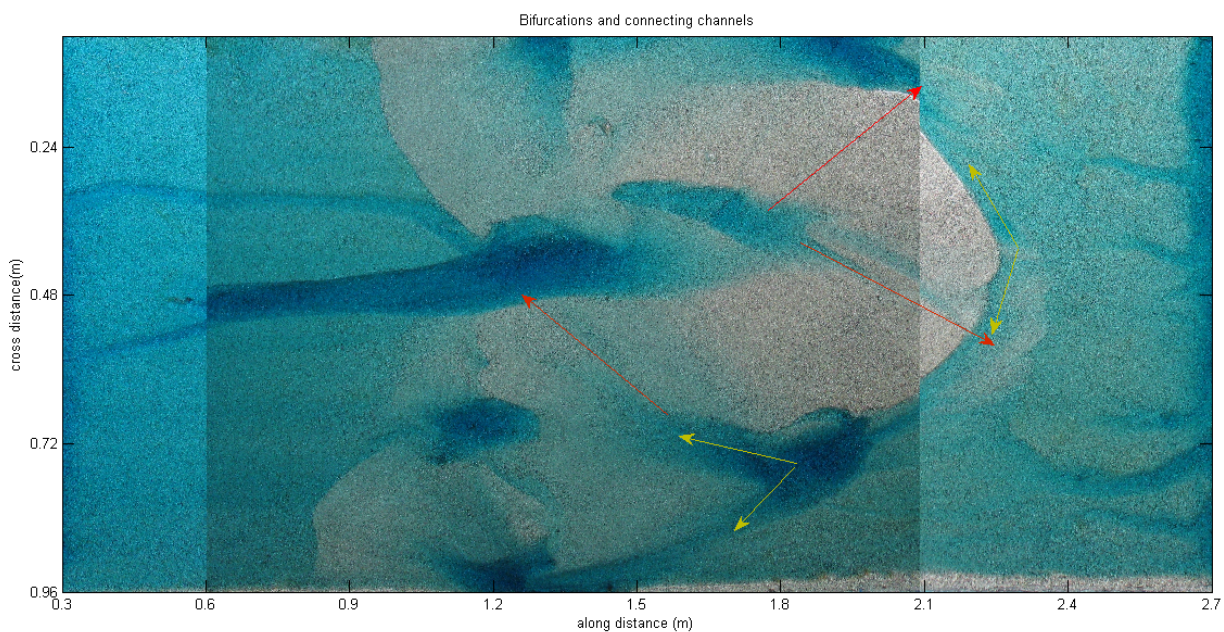


Figure 4.3: Bifurcations indicated in yellow and connecting channels in red.

About halfway the experiment (*549 tilt cycles*) a large round/diamond-shaped tidal bar developed at the end of the tidal channel (fig 4.1, *tilt cycle 549*). This bar-channel system remained the dominant bar-channel system in the experiment. From the digital elevation maps (fig 4.4) and observations it showed that one bar-channel couple expanded much in size (both height and width), while other bar-channel couples expanded less and therefore remained smaller (fig 4.1, fig 4.4). Tidal bars in the system migrated back and forth with the tidal currents during ebb and flood, but no net migration was observed. Unrealistic deep scour holes developed between bars in all tidal experiments. These scour holes often increased in depth during evolution of the system.

Evolution of initial elongated bars (fig 4.1) towards large round/diamond-shaped bars is clearly visible on the digital elevation maps (DEMs) of the tidal system (fig 4.4). The DEM shows the relative change in the system with reference to the initial flat sediment bed. The most striking observation is that bars appeared rounded with moderate elevations, while channels were relatively narrow and long with much greater depths.

The bars started as long and thin tidal bars, while these expanded towards large, round and longer bars. The large round/diamond-shaped bar that expanded towards the right-hand side of the tilting basin (*towards 2.88 meters in fig 4.4*) was most of the time the dominant bar-channel system. The channels deepened while the evolution time of the system increased. Tidal channels were deepest just before the bar started (were the sediment from the channel diverged) or at the flanks of the tidal bars. The bar crest is the highest point of the tidal bar (fig 4.4). The DEM also demonstrated the presence of connecting channels in the system (*black ellipses, fig 4.4*).

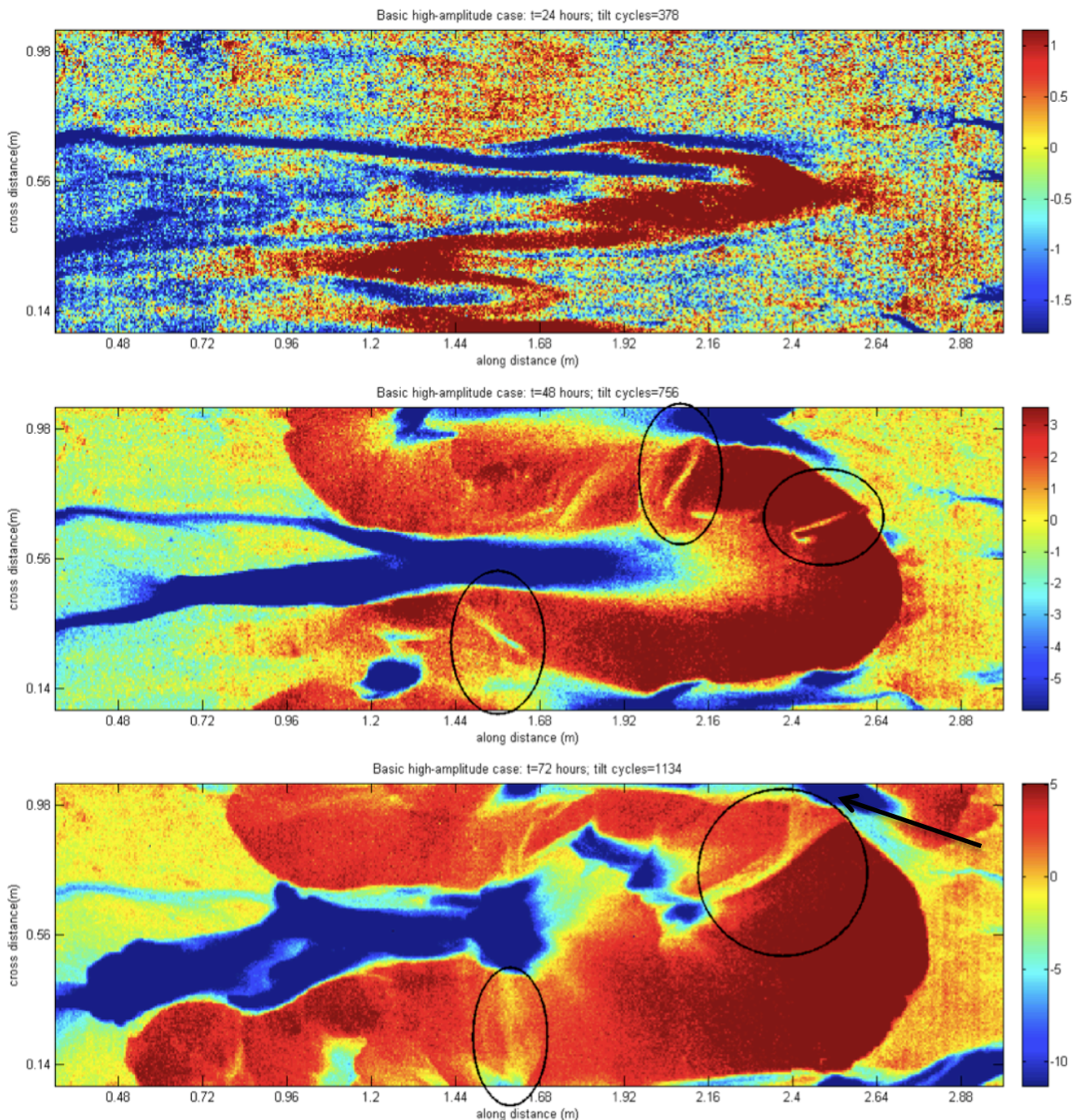


Figure 4.4: Erosion and deposition pattern of the basic high-amplitude case for three timesteps. Negative values indicate erosion and positive values indicate deposition. Black ellipses indicate connecting channels (connecting ebb-and flood-tidal channels).

4.1.2 Basic low-amplitude case

The first bars started to develop after 150 tilt cycles. Here, multiple small-elongated tidal bars developed in the middle of the tilting basin (fig 4.5). These multiple small-elongated bars formed a characteristic pattern and demonstrate the first stage in the evolution of the system for the low-amplitude cases (fig 4.6). During this first stage small tidal channels formed. These channels remained shallow and small, while bars expanded in height, width but most in length after initialization. Bars also developed parallel to the flow direction in the tidal system (fig 4.6).

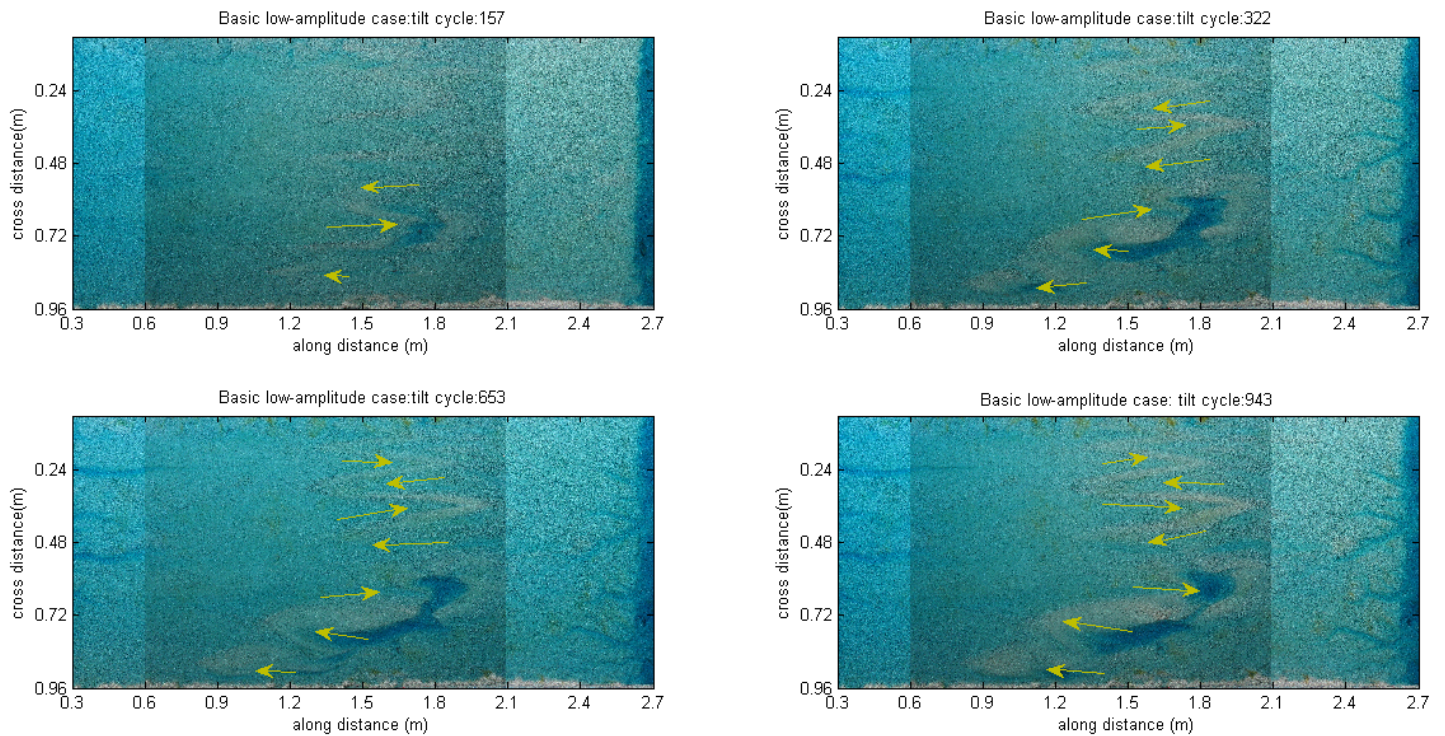


Figure 4.5: Evolution of tidal bars and channels for the basic low-amplitude case. Yellow arrows indicate dominant flow pattern of the tidal currents.

Like for the *HA-case*, tidal bars and channels were only active during one phase and ebb- and flood-dominated channels formed. These ebb- and flood-dominated channels were not as deep as was the case for the channels in the *HA-case*. Tidal channels were rather shallow. The *LA-case* experiments also exhibited scour holes, but less scour holes were present but were not that unrealistic deep as was the case for scour holes in the *HA-cases*. Tidal bars migrated back and forward with the tidal currents during ebb and flood.

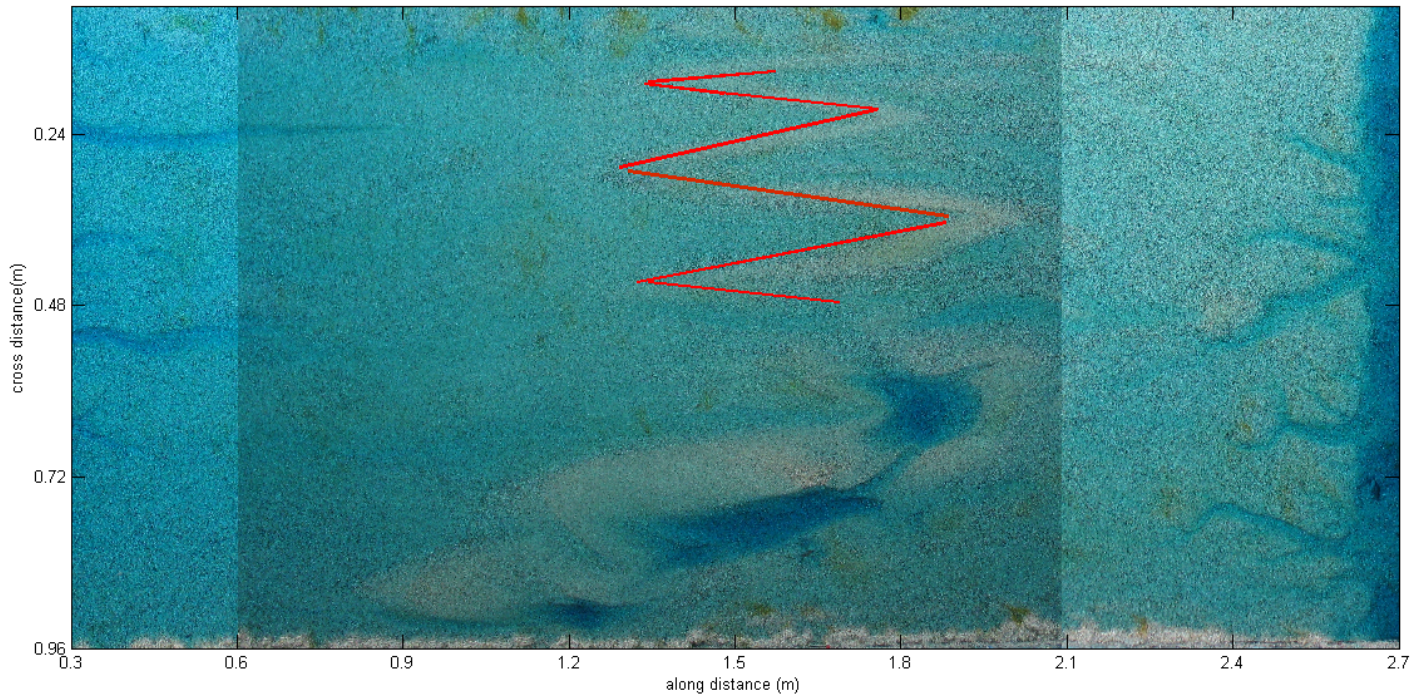


Figure 4.6: Characteristic bar pattern for the low-amplitude case that consists of multiple elongated bars below each other.

A large difference with the *HA-case* is the shape of bars during initialization and bars at the end-stage of the evolution of the tidal system (fig 4.1 & fig 4.5). Unlike the *HA-case*, were few elongate bars developed, multiple small bars developed during initialization in the *LA-case*. Large elongated (very thin bars and intermediate in length) bars characterized the end-stage of the system in the *LA-case*, whilst large round/diamond shaped tidal bars characterize the end-stage in the *HA-cases* (*HA-case*, fig 4.2). Another striking difference with the *HA-case* becomes visible in the DEM (fig 4.7). Here, no connecting channels seemed to be present and no connecting channels were visible during observations. Clearly visible on the DEM is the evolution from multiple elongate bars towards larger elongate tidal bars. The characteristic bar pattern as visible in figure 4.6 is also clearly visible in figure 4.7.

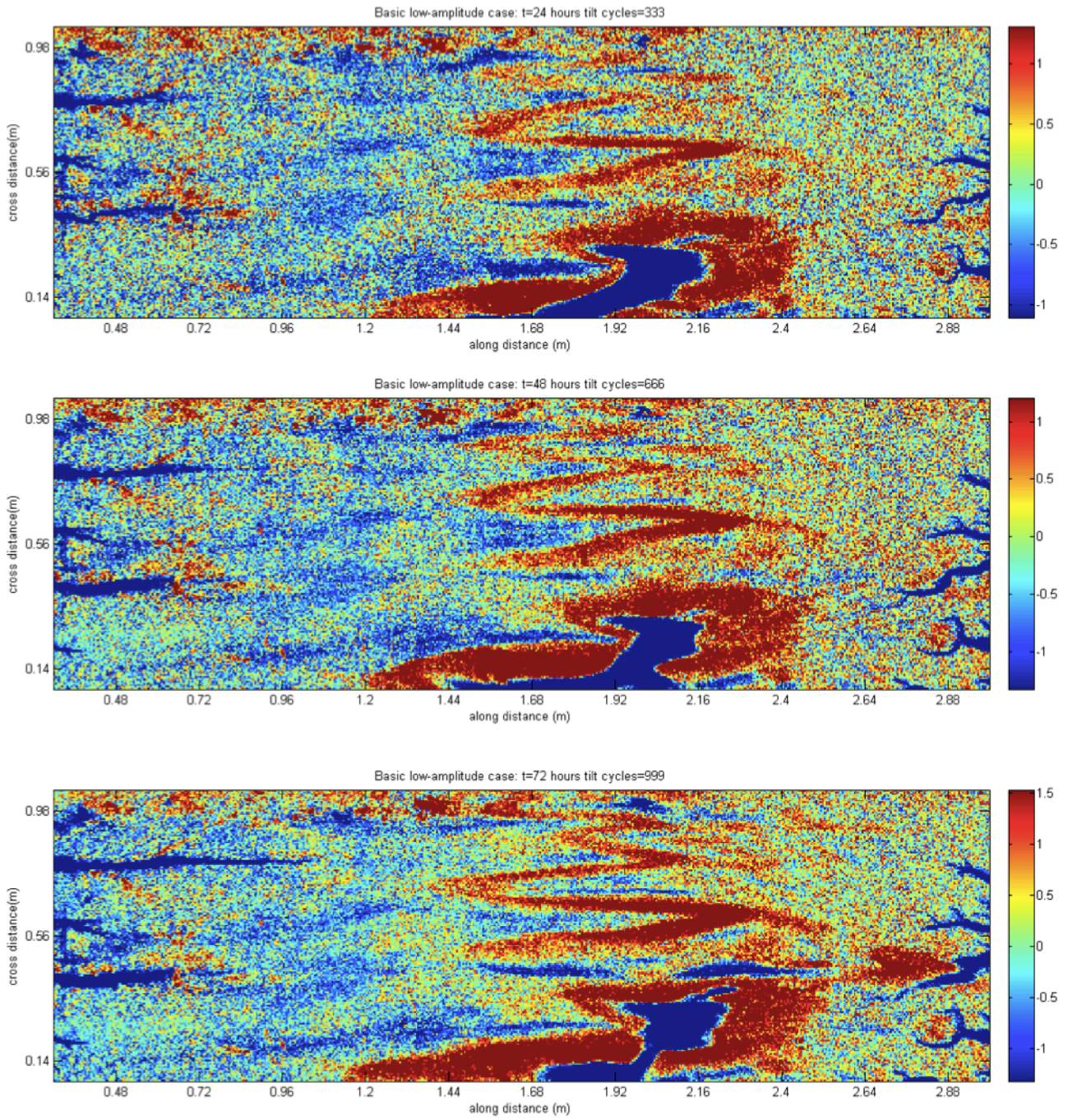


Figure 4.7: Erosion and deposition pattern of the basic low-amplitude case for three timesteps. Negative values indicate erosion and positive values indicate deposition. Note the characteristic pattern of bars in the system (see fig 4.6).

The difference in bar width and height dimensions over time is given in figure 4.8 for both *HA-case* and *LA-case*. This figure shows clearly the difference in evolution between the two cases. Bar height after 25 hours for both experiments was more or less equal. However, bars in the *HA-case* expanded fast in height and width. The reverse is the true for the *LA-case*. Here, bar height and width remained almost constant through time. It seemed that bar width and height were more or less in equilibrium in the *LA-case*. No equilibrium seemed to be reached in the *HA-case*. The number of bars for both systems is given in figure 4.9. The total number of bars is highest in the *LA-case* but these remain relatively constant. This could indicate that the *LA-case* reached equilibrium. The number of bars for the *HA-case* decreases faster. The differences in height and width dimensions and number of bars for both cases are clearly visible in the figures that show the evolution of the system (fig 4.1 & fig 4.5) and in the digital elevation maps (fig 4.4 & fig 4.7)

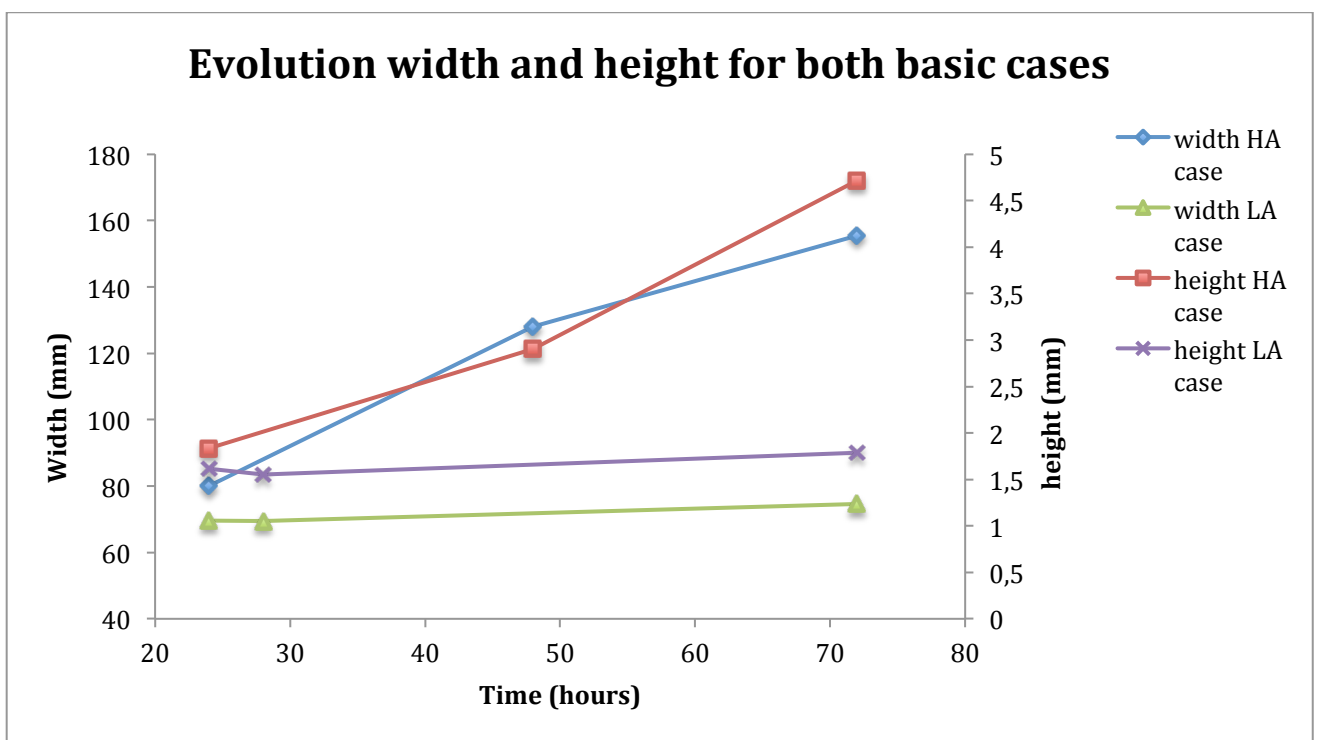


Figure 4.8: Evolution of bar width and height for both HA-case and LA-case.

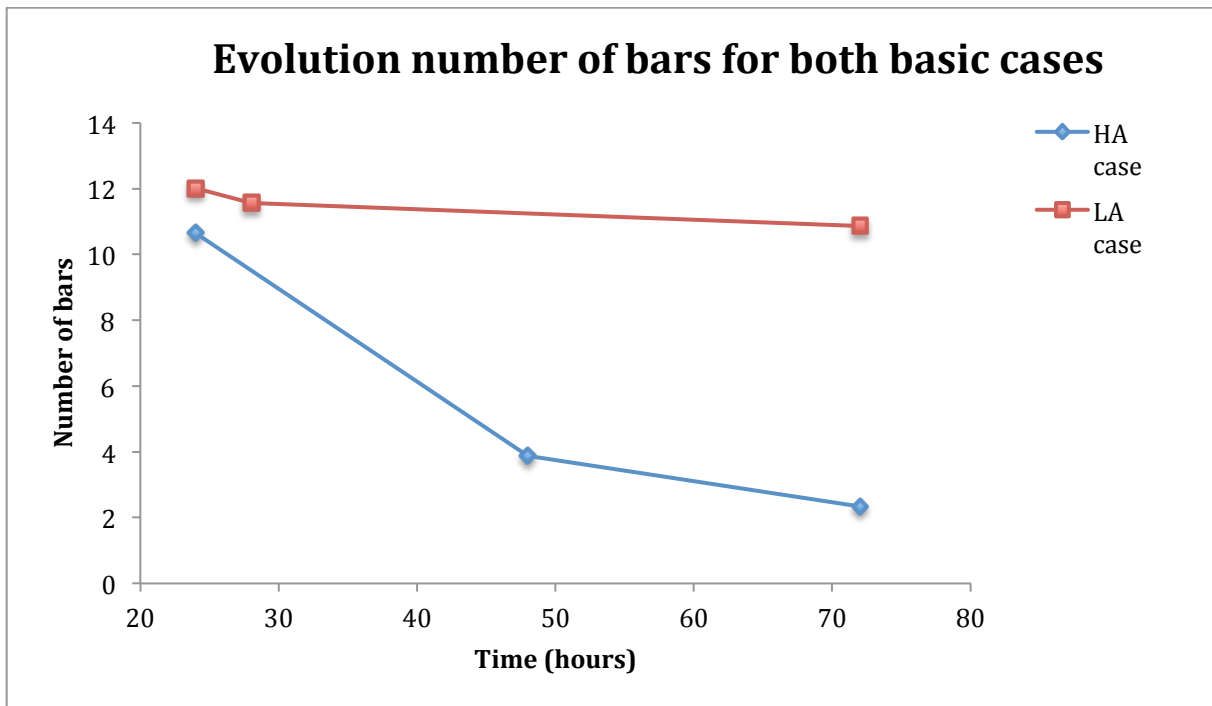


Figure 4.9: Evolution of number of bars for both HA-case and LA-case.

The fact that bar width and height expanded fast for the *HA-case* is also demonstrated with the use of the 25th, 50th (median) and 75th percentiles. Figure 4.10 shows the average values for the percentiles of the width and height for both HA-case and LA-case. The values are averaged over time. The 50th percentile is indicated in blue (width) or red (height). The 75th and 25th percentiles are indicated with the black dotted line. Figure 4.10 demonstrates that 50% of the values fall below 128 mm for the width of the bars in the HA-case; 75% falls below 142 mm for the width of the bars and 25% falls below 104 mm. This is completely different for the LA-case, whereas here the 25th and 50th percentile are equal (70 mm). 75% of the values fall below 72 mm. The figure demonstrates that bars grew extensively in width when time increased, as the percentiles differ significantly. Bar width remained more or less constant in the LA-case, and this could indicate equilibrium in the system.

The same holds on for bar height. Figure 4.10 demonstrates that 50% of the values fall below 1.6 mm for bar height in the HA-case; 75% of the values fall below 1.7 mm and 25% of the values fall below 1.5 mm. This demonstrates that bars grew in height. The 25th and 75th percentile (1.57 & 1.6 mm) are almost equal to the 50th percentile (1.6 mm). This indicates that bars height remained more or less equal during the evolution of the tidal system, which also could indicate equilibrium of the system.

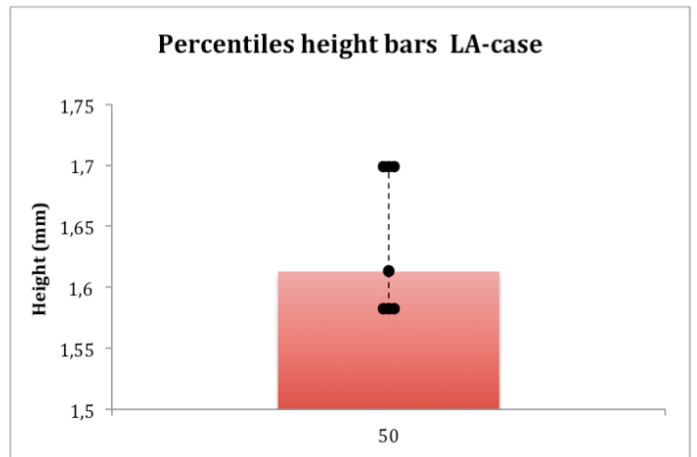
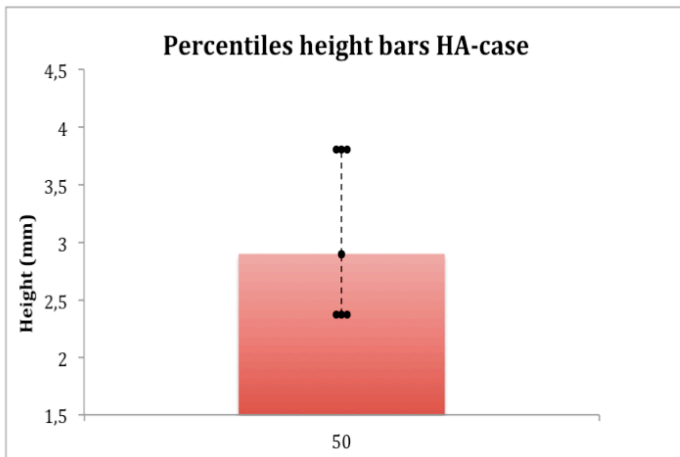
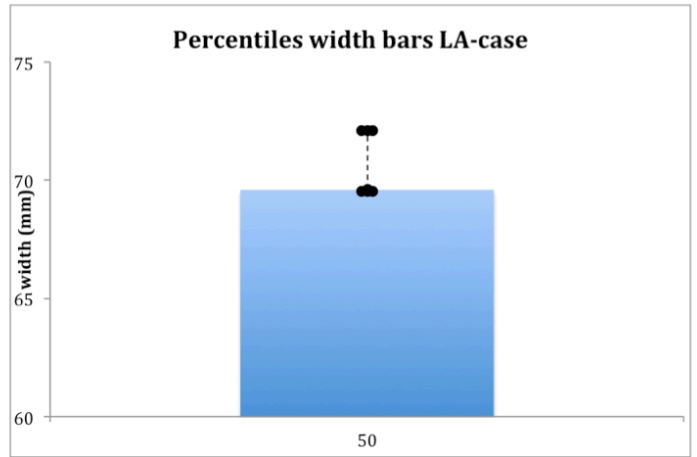
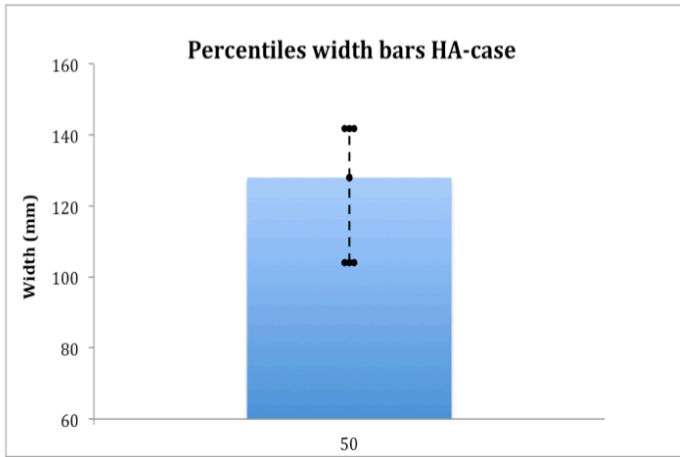


Figure 4.10: The 25th, 50th and 75th percentiles for bar width and height for both basic HA- and LA-case. The blue and red box indicates the 50th percentile. The upper limit of the dotted-black line represents the 75th percentile and the lower limit indicates the 25th percentile.

4.2 Dependence of tidal bars on imposed tidal conditions

This chapter will visualize, describe and analyze the characteristics of tidal bars in the system. Bar height, width, length and the number of bars are in this chapter compared for all tidal experiments to find possible relationships between those parameters that can define characteristics of tidal bars in the system and can be compared to characteristics of fluvial bars. The next subsection describes the effect of conditions. Thereafter the shape of tidal bars and channels will be described followed by describing the tidal asymmetrical experiment. This chapter will end by describing shortly some characteristics of experimental braiding bars.

4.2.1 Overall trends

Mean bar height, width and length per tidal experiment are presented in table 4.1. The values are averaged over the timesteps. Bar height varied between 1.3 mm (experiment 5) to 3.1 mm (experiment 13/basic HA-case). Width varied between 70 mm (experiment 9) and 121 mm (basic HA-case). The width/height ratio varied between 42 (experiment 7) and 61 (experiment 5). The mean number of bars is highest for experiment 3, 5, 8 and 9. The lowest numbers of bars were found in experiment 4, 7 and 13. Bar length varied from 700/800 mm (experiment 8,9,10 and 11) and 1000/1200 mm (experiment 1, 2, 3, 4, 7 and 13) (table 4.1).

Table 4.1: Mean bar height, width, number of bars and bar length for all experiments. Red bold numbers indicates cases used in chapter 4.1 and chapter 4.2

Case	Experiment	Bar height (mm)	Bar width (mm)	Width/height ratio	Number of bars	Length (mm)
High amplitude	1	3.36	113.58	39.89	4.22	900
	2	1.60	89.99	57.54	8.36	1500
	3	1.81	77.62	48.13	11.60	1050
	4	2.00	90.87	57.74	4.72	1200
	7	2.24	88.00	42.40	7.49	900
Basic case high-amplitude	13	3.15	121.15	45.99	5.62	1100
Low amplitude	5	1.32	78.55	61.15	12.08	900
Basic low-amplitude	8	1.65	71.23	46.25	11.48	700
Low-amplitude	9	1.52	69.54	49.92	11.78	700
Low amplitude/symmetrical	10	1.72	75.02	47.20	9.88	800
Asymmetrical	11	2.12	87.18	49.32	8.95	600

Mean bar width versus bar height is presented in figure 4.11. There is a strong correlation between bar width and bar height. When bar width increases, bars also increase in height. The coefficient of determination (R^2) represents the percentage of variation in the data that can be explained (fig 4.11) and is also listed in table 4.2 for plots that are not included. The high coefficient of determination between bar width and height implies a strong relation.

However a relationship between two variables can be strong, but yet not significant. Therefore, the significant of the correlation coefficient (R) can be tested by using the degrees of freedom and (critical) t-values (Wonnacott and Wonnacott, 1990). A two-tailed test is used. Two hypotheses are developed: a null hypothesis H_0 and an alternative hypothesis H_1 . The null hypothesis means that there is no correlation between the x and y variables. The alternative hypothesis indicates that there is a significant correlation between the variables. The distribution given by the null hypotheses is considered and a test is performed to determine whether or not the null hypotheses should be rejected in favor of the alternative hypothesis. An Alfa (α) of 0.02 is used, which implies that there is 2% change to rejecting H_0 while the H_0 is correct (Wonnacott and Wonnacott, 1990). If a significant relationship is present between the two variables is indicated in table 4.2. From table 4.2 it shows that there is indeed a significant relationship between bar width and height. Significant relations are indicated in red circles in the figures.

The relation between the number of bars and bar width, height and the width/height ratio is given in figure 4.12. It seemed that a strong relationship was present between the number of bars and bar width (fig 4.12). When the number of bars increased, bar width decreased. According to the statistics, there is a significant relation between the number of bars and bar width (table 4.2). No significant relation between the ratio of width/height and bar height and the number of bars in the experiment exists (fig 4.12). Bar length has no significant correlation with bar height, width and width/height ratio (fig 4.13 & table 4.2).

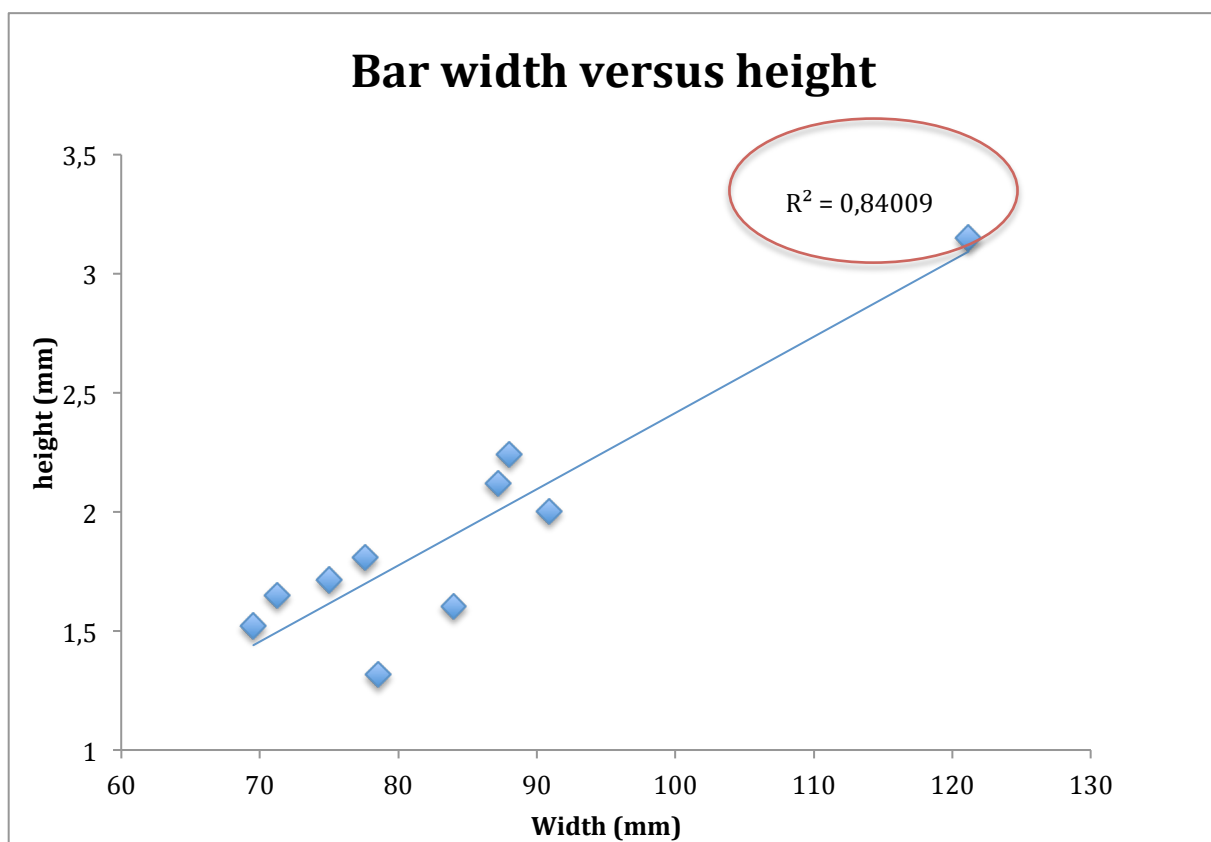


Figure 4.11: Bar width (mm) versus bar height (mm).

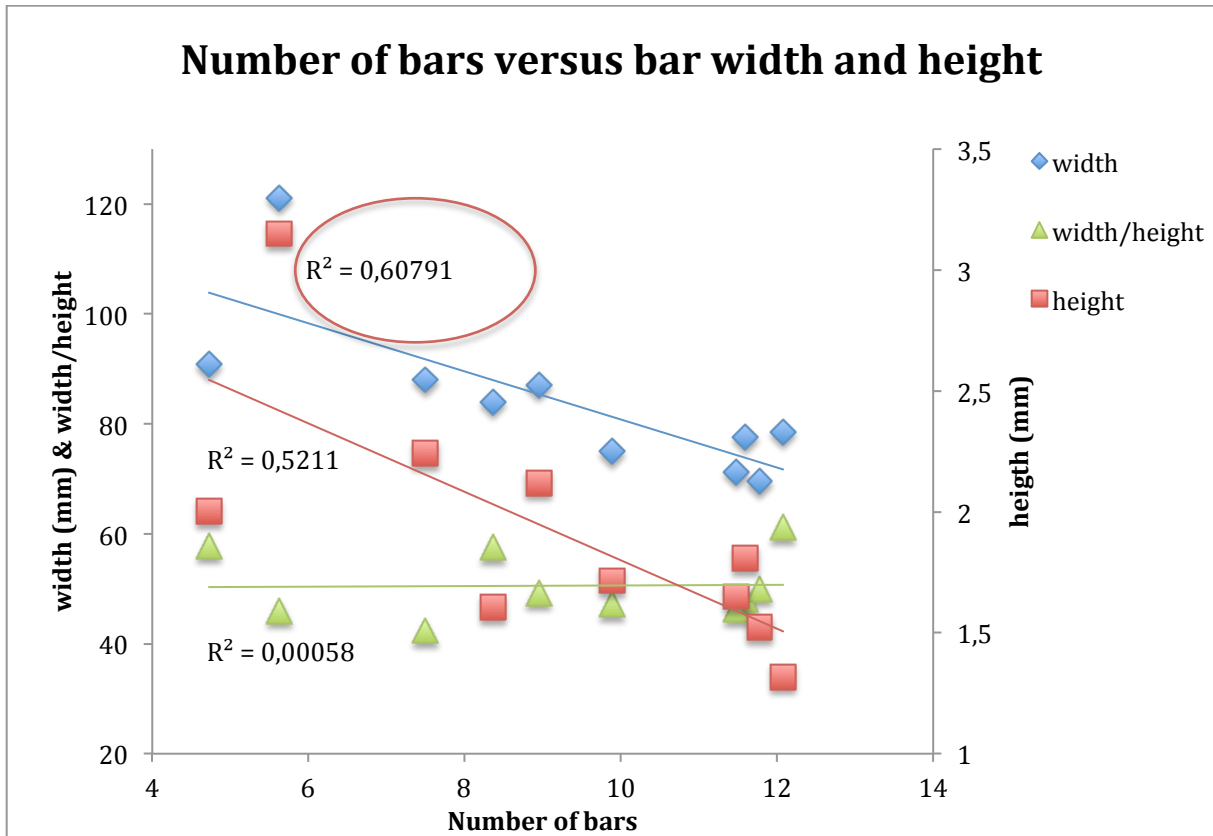


Figure 4.12: Number of bars versus bar width (mm), height (mm) and width/height.

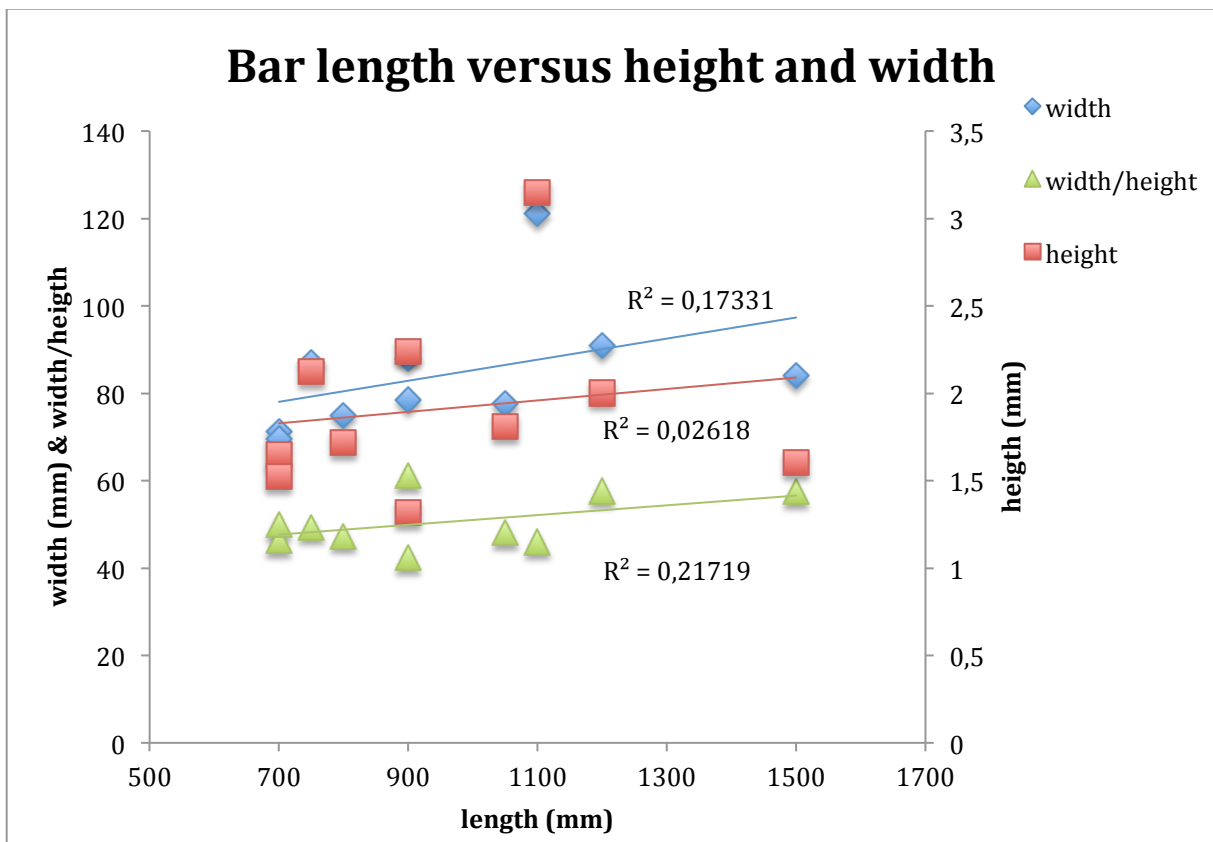


Figure 4.13: Bar length versus bar width (mm), height (mm) and width/height.

4.2.2 Effect of conditions

Three different conditions in the tilting basin were varied in the experimental setting: (1) the speed of tilting (mm/min), (2) amplitude of tilting (mm) and (3) delay (s). The condition delay corresponds to the time before the tilting basin starts to reverse (from ebb to flood or vice versa). The imposed conditions are listed in table 3.2.

Tilting speed

Tilting speed is plotted against bar height, width and width/height in figure 4.14. The coefficients of determination are low for the relations, and there is also no significant relation between tilting speed and bar height, width and width/height (table 4.2). A powerful significant relationship occurred between tilting speed and bar length (fig 4.15 & table 4.2). When tilting speed increased bars strongly decreased in their length. Tilting speed had no effect on the number of bars (table 4.2).

In order to examine the effect of the tilting speed, the other two imposed conditions must be exactly the same in order to filter out any effect of tilting amplitude or delay. Therefore, experiment 8, 9 and 10 can be compared because those have the different tilting speeds, but the same amplitude and tidal delay (table 4.1). Experiment 9 with the highest tilting speed, exhibited the lowest bar heights and bar widths in the system. The mean number of bars and channels were almost equal to experiment 8. The length of the bars fell in the same range of the other two experiments. Clearly, one can note that when tilting speed increased, bar height and width were lower.

Amplitude

Amplitude is plotted against bar height, width and width/height in figure 4.16. Although the coefficients of determination are higher here than for the tilting speed relations, still no significant correlation is present between amplitude and bar width, height and width/height. Another striking observation is that amplitude strongly affected the length of the bars (fig 4.17). The positive significant relation between the two parameters indicated that when amplitude increased, also bar length increased (table 4.2). Tilting amplitude had also no significant correlation with the number of bars in the system (table 4.2).

Experiments with different amplitude values but the same tilting speed and delay were experiment 4 and 5 and experiment 7 and 8 (table 4.1). When comparing those conducted experiments it is clear that the experiment with the lowest amplitude also exhibited the lowest bar width and heights. The highest bar width and height, was for the experiment with the highest tilting amplitude (experiment 13). The number of bars and channels were then again highest for the experiment with the lower amplitudes (experiment 5 and 8).

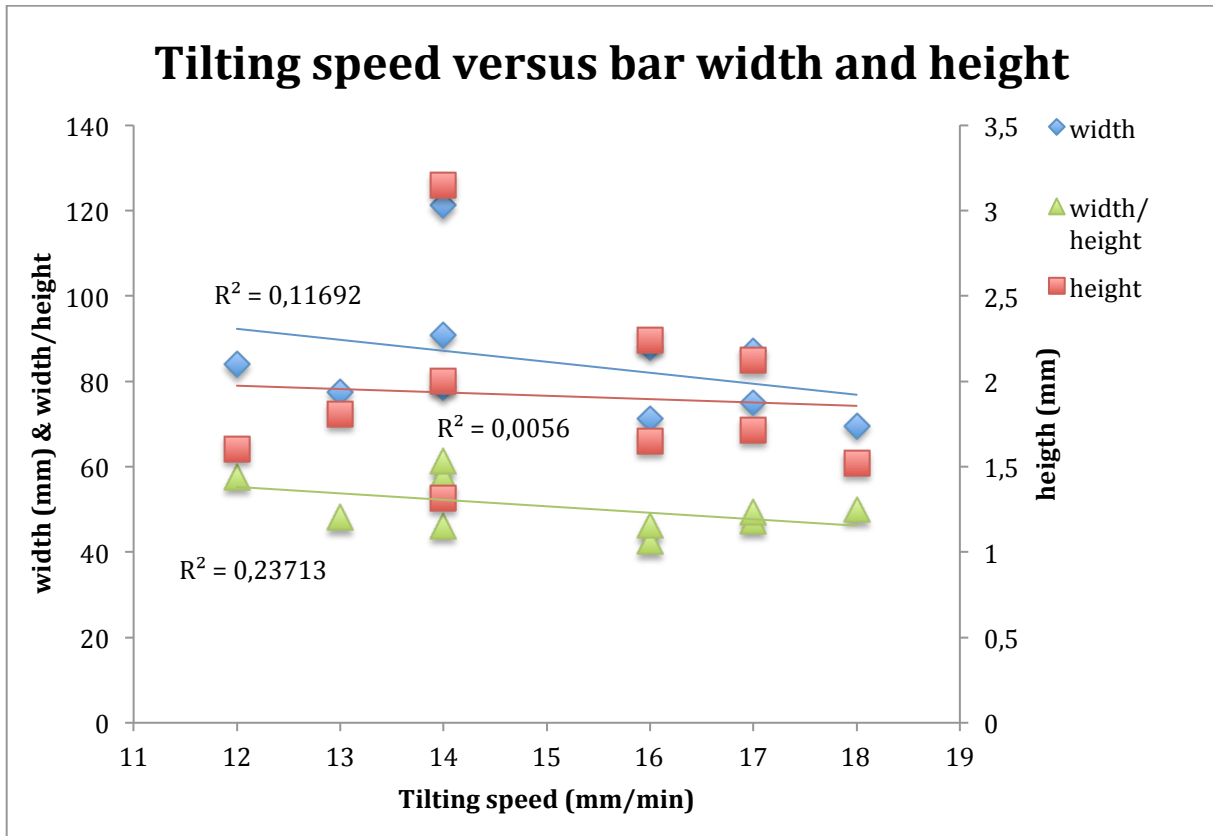


Figure 4.14: Tilting speed (mm/min) versus bar width (mm) and height (mm).

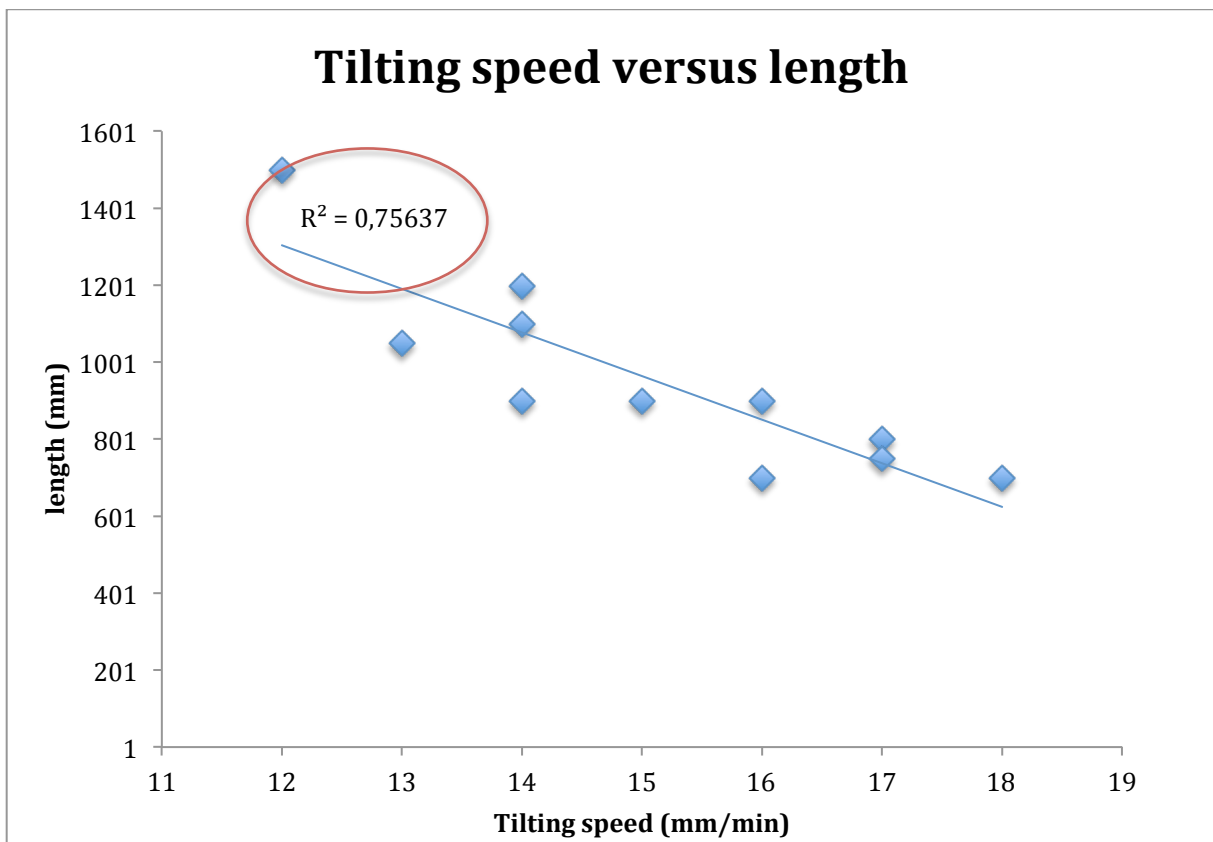


Figure 4.15: Tilting speed (mm/min) versus bar length (mm).

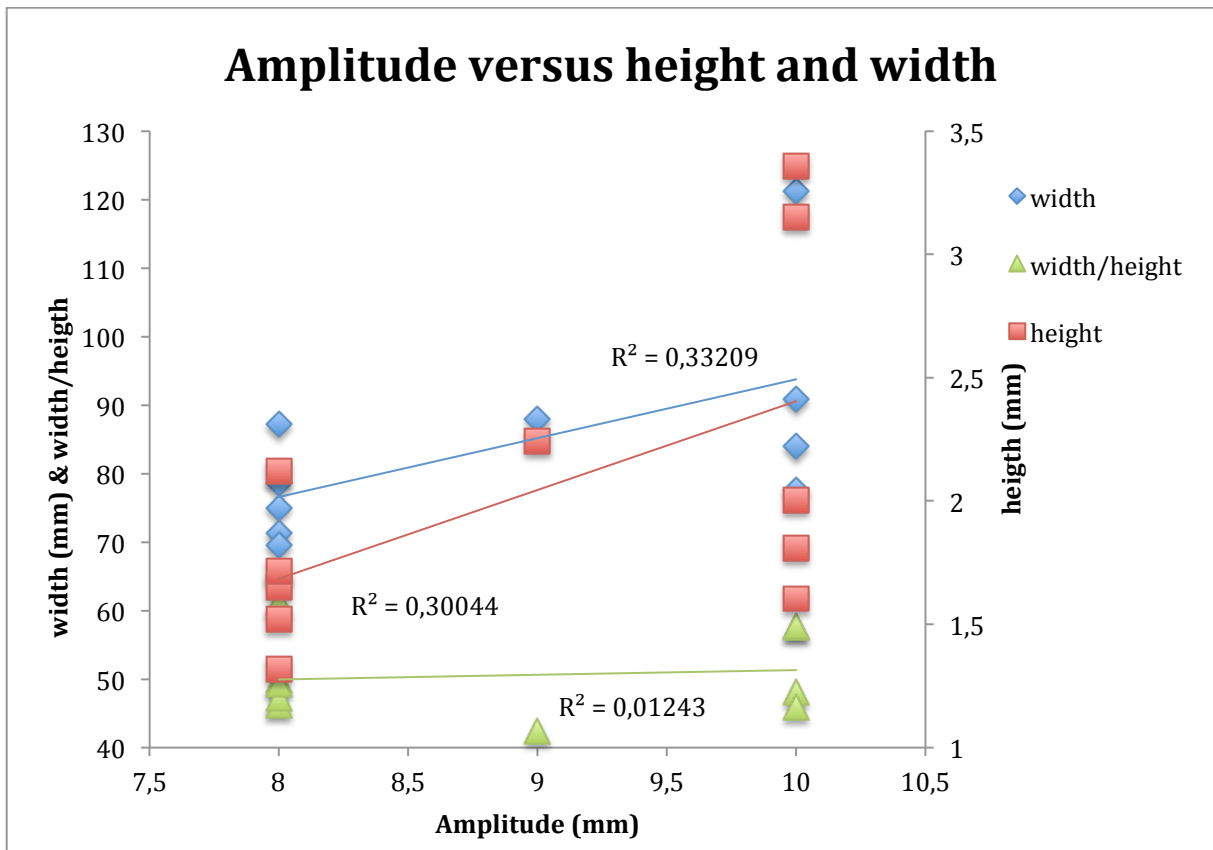


Figure 4.16: Amplitude versus bar width (mm), height (mm) and width/height.

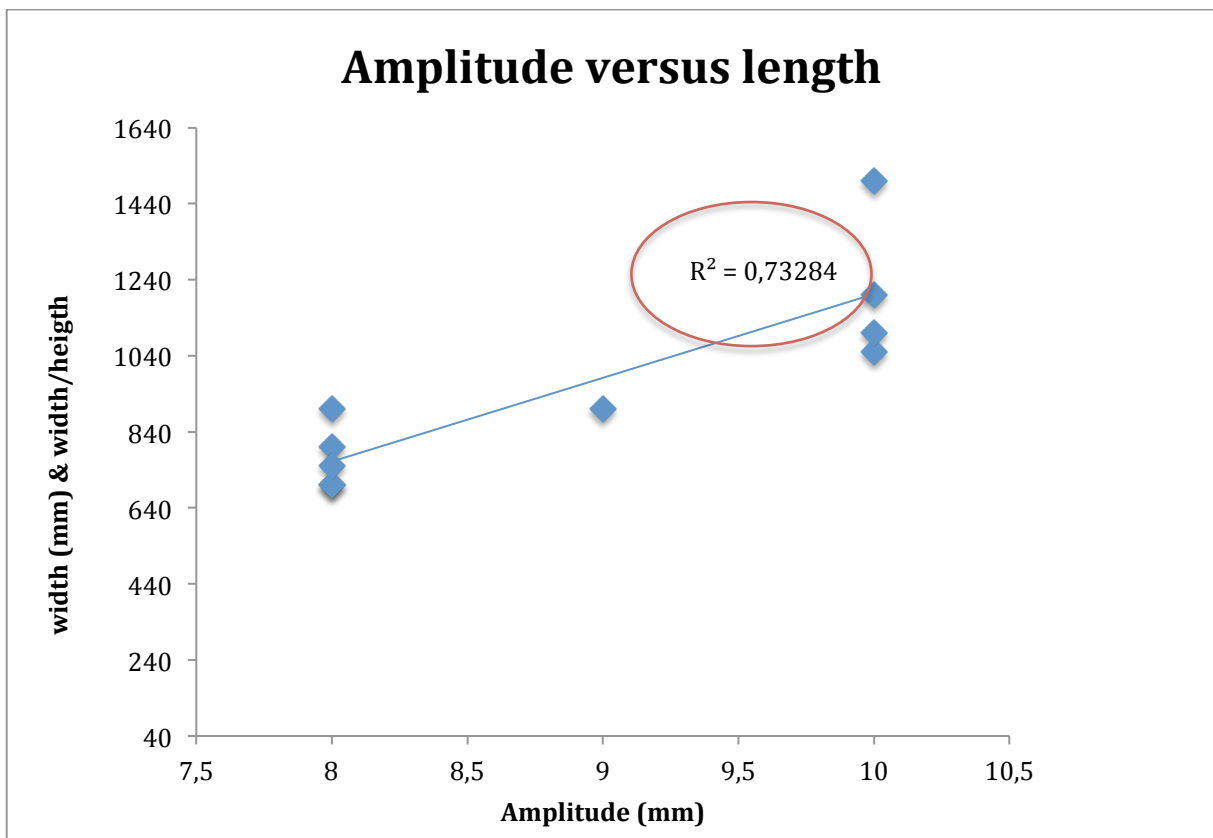


Figure 4.17: Amplitude (mm) versus bar length (mm).

Delay

Tidal delay has no effect on characteristic of tidal bars (width and height), except on the length of the bars (fig 4.18 & table 4.2). There is a significant correlation between tidal delay and bar length. Bars increased in length when tidal delay increased. However, one must note that the effect of delay was difficult to determine while almost all tidal experiments exhibited the same delay of 2 seconds. The delay of 2 seconds showed that such low delay was high enough for bars to develop.

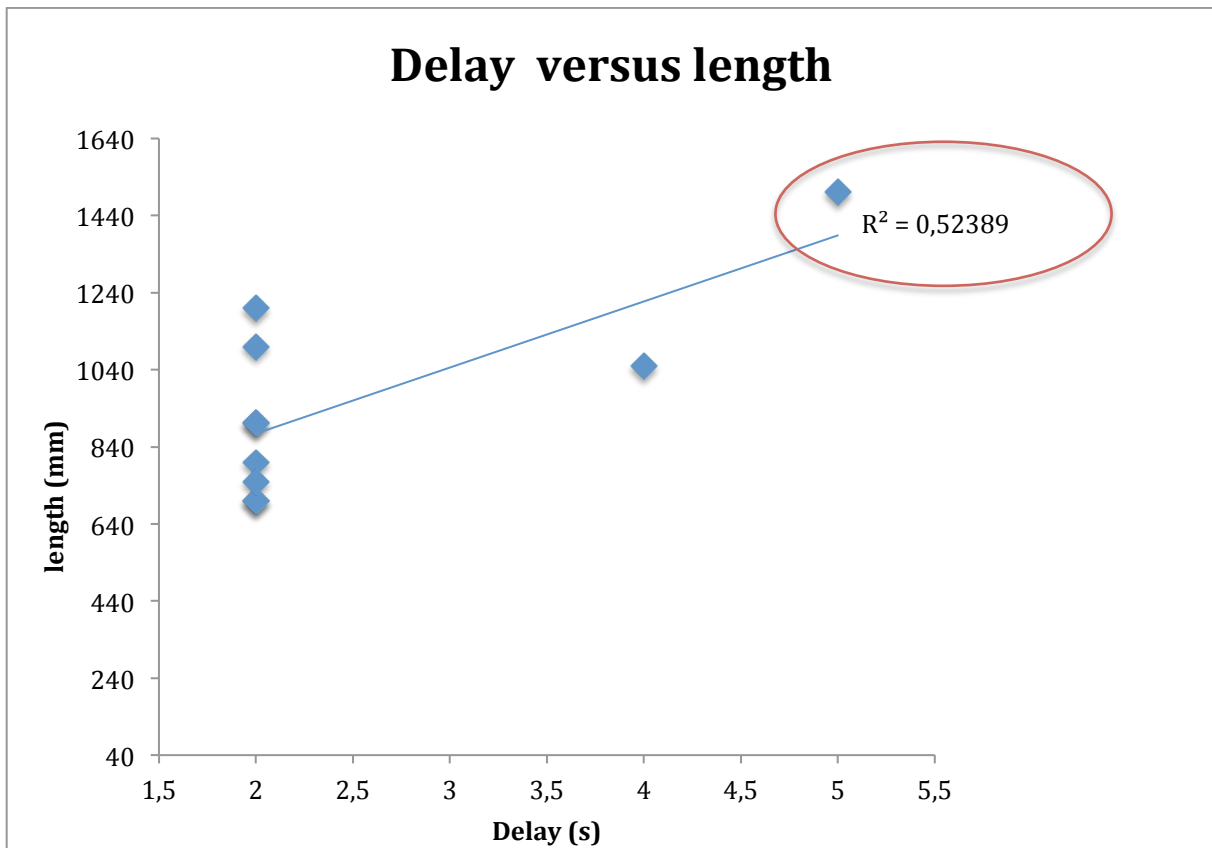


Figure 4.18: Tidal delay (s) versus bar length (mm).

Tidal excursion length

By combining maximum average velocity and tidal period the tidal excursion length could be calculated. Tidal excursion length is referred as the net horizontal distance over which water moves during one tidal cycle of ebb and flood. Tidal excursion length (mm) is here presented as the maximum velocity (mm/s) times half the tidal period (s). No significant correlations were present between tidal excursion length and bar width and height (plot not included). A strong and significant correlation existed between tidal excursion length and the length of the bars (fig 4.19 & table 4.2). The increase in tidal excursion length was accompanied by an increase in bar length. The numbers of bars in the system were not significantly correlated to the tidal excursion length (table 4.2).

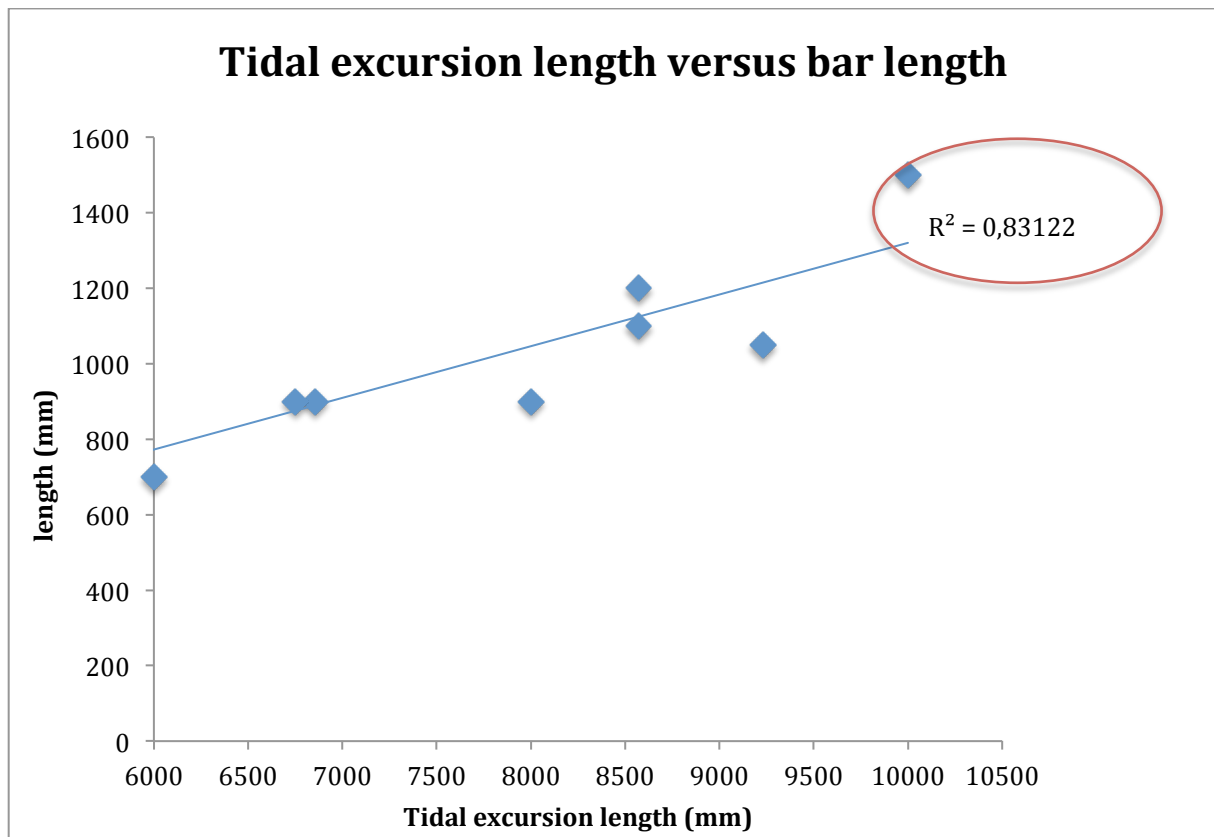


Figure 4.19: Tidal excursion length (mm) versus bar length (mm) and number of bars.

Table 4.2: Correlation factor is given to indicate the strength of the relationship between the two parameters (x and y). Strong and significant correlation factors are indicated in green. The relation, either positive or negative is given (P/N) in the correlation column.

Type	X-as	Y-as	Correlation R ²
Characteristics	Mean bar width	Bar height	0.84 P
	Number of bars	Width	0.61 N
		Height	0.52 N
		Width/height	0.0006 P
		Length	0.28 N
	Length	Width	0.17 N
		Height	0.02 N
		Width/height	0.22 P
	Conditions	Tilting speed	Width
Height			0.006 N
Width/height			0.24 N
Length			0.76 N
Number of bars			0.07 P
Amplitude		Width	0.33 P
		Height	0.30 P
		Width/height	0.0124 P
		Length	0.73 P
		Number of bars	0.39 N
Tidal excursion		Width	0.19 N
		Height	0.06 N
		Width/height	0.05 P
		Length	0.83 P
		Number of bars	0.18 P
Delay		Width	0.01 N
		Height	0.05 N
		Width/height	0.07 P
		Length	0.52 P
		Number of bars	0.008 P

4.2.3 Visual analysis of bar and channel shapes

Bars

The shape of tidal bars was based on visual interpretation due to movies from the photographs. When looking at the shape of tidal bars it could be seen that there was a division in round/diamond-shaped tidal bars or tidal bars with sharper edges (table 4.3). Figure 4.20 shows sketches of round/diamond-shaped bars or sharp-edged bars at the end of the experiments.

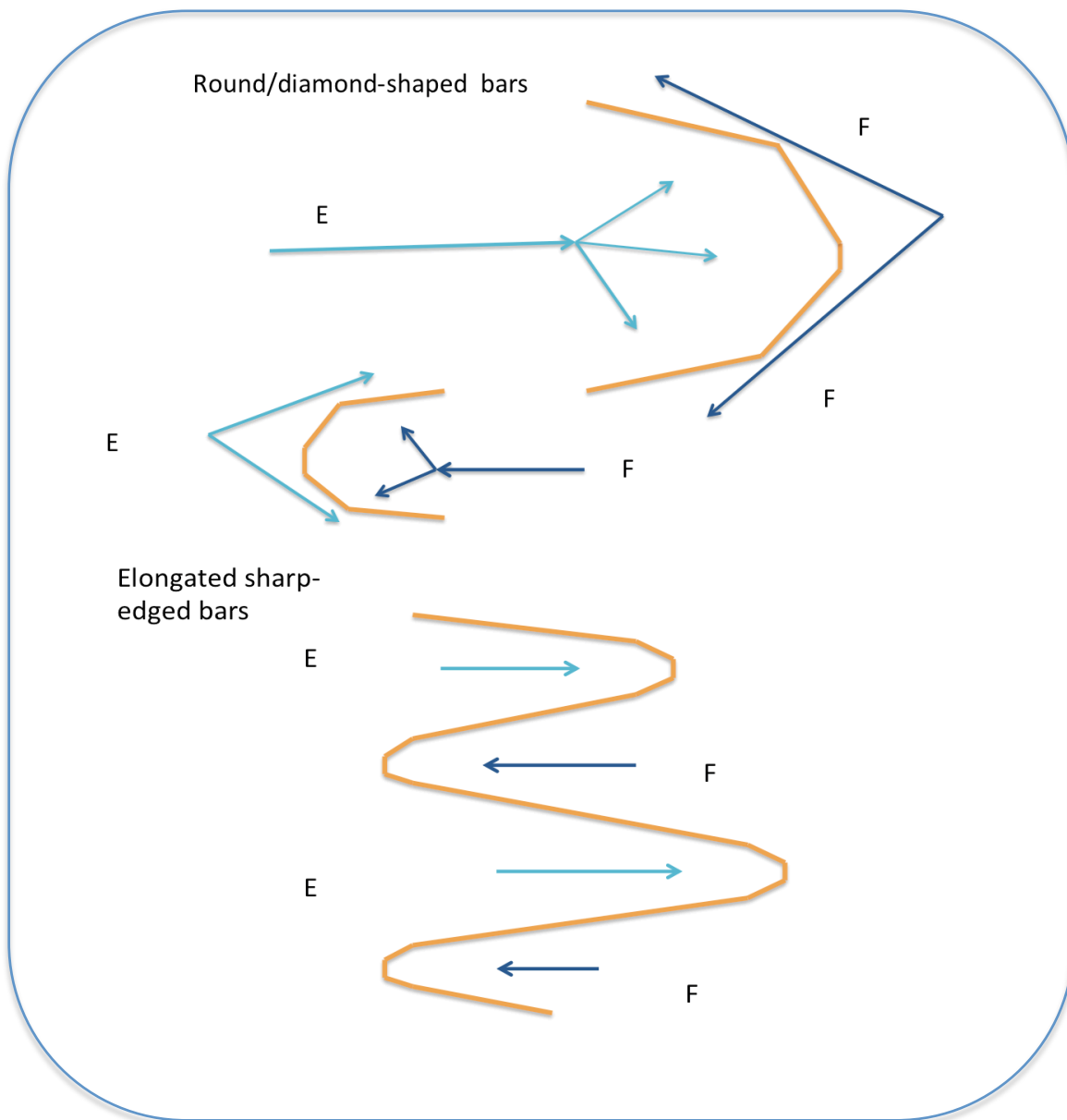


Figure 4.20: Sketch of different bar shapes: elongated sharp-edged bars (LA-case / Low tidal excursion length) and round/diamond shaped bars (HA-case / High tidal excursion length). E=ebb-dominated channel with a bar at the end and F=flood-dominated channel with a bar at the end.

The transitions however, are not hard transitions due to the fact that round bars can be present in all experiments and vice versa, but an overall average trend can be found in the tidal experiments. Here, experiment 1 is taken into account, because visual observation is done with the photographs and the characteristics of the photographs are the same for all experiments.

Table 4.3: Relative shape of tidal bars in experimental setting with tidal excursion length. Initiation indicates either few bars (one or two) or multiple bars (more bars below each other). Arrows → or ← a very specific dominant grow direction in the system.

Experiment	Initiation	Beginning	End	Tidal excursion length (mm)
1	Few bars	-	Wide, round (massive) and long	2.5
2	Few bars	Thin, long	Wide, round and long →	1
3	Few bars	Thin, long	Wide round and long→	0.86
4	Few bars	Long, somewhat wider	Wide, round and long (massive) ←	0.46
5	One bar	Thin, long	Less wide, round, less long	0.46
7	Multiple	Thin, less long (small)	Wide round bars, long	0.53
8	Multiple	Thin, small	Thin, intermediate in length, sharp	0.53
9	Multiple	Thin, small	Thin, intermediate in length, sharp	0.6
10	Multiple	Thin, small	Thin, longer, sharp/round	0.56
11	Few	Very small and thin	Wider, small, sharper ←	0.56
13	Few bars	Thin, long	Wide, round and long ←	0.46

The first morphological change in the experiment was visible as either few existing bars of multiple bars below each other (table 4.3). This division in initiation of bars resulted eventually in different end-stages of the system. When few (1 or 2) bars developed, these were after initiation relatively seen thin and long bars (elongated). In the end stage of the system it seemed that those bars had grown towards big round-shaped tidal bars, sometimes referred as massive bars (fig 4.2, fig 4.20). Four of those experiments showed that tidal bar development favored specifically one direction (table 4.3). When multiple bars (>2) developed (fig 4.6), it seemed that those first initiated bars were very small in width and in their length (small elongated bars). These bars were also much shaper (fig 4.20), indicating that the shape was not that large and round as in the other experiments (fig 4.2 & fig 4.6). No specific grow direction was present in these experiments. At the end stage, the elongated (very small in width but intermediate in length) shaper-bars were found in experiments with smaller tidal excursion length (*LA-case*). The large and round/diamond-shaped bars were found in experiments with high tidal excursion length (*HA-case*). When also involve the length of the bars it showed that the wide, round-shaped bars were in general larger than the length of the smaller and sharper-shaped bars.

When looking at along-profiles for a large tidal bar for the *HA-case*, it showed that bars exhibited a gentle slope towards the bars crest and a steep slope downwards at the end of the bar crest (fig 4.21). This was often the case for large tidal bars and this up-slope influenced tidal currents during ebb and flood flow. The bar exhibit a steep down-slope that hinders the flow.

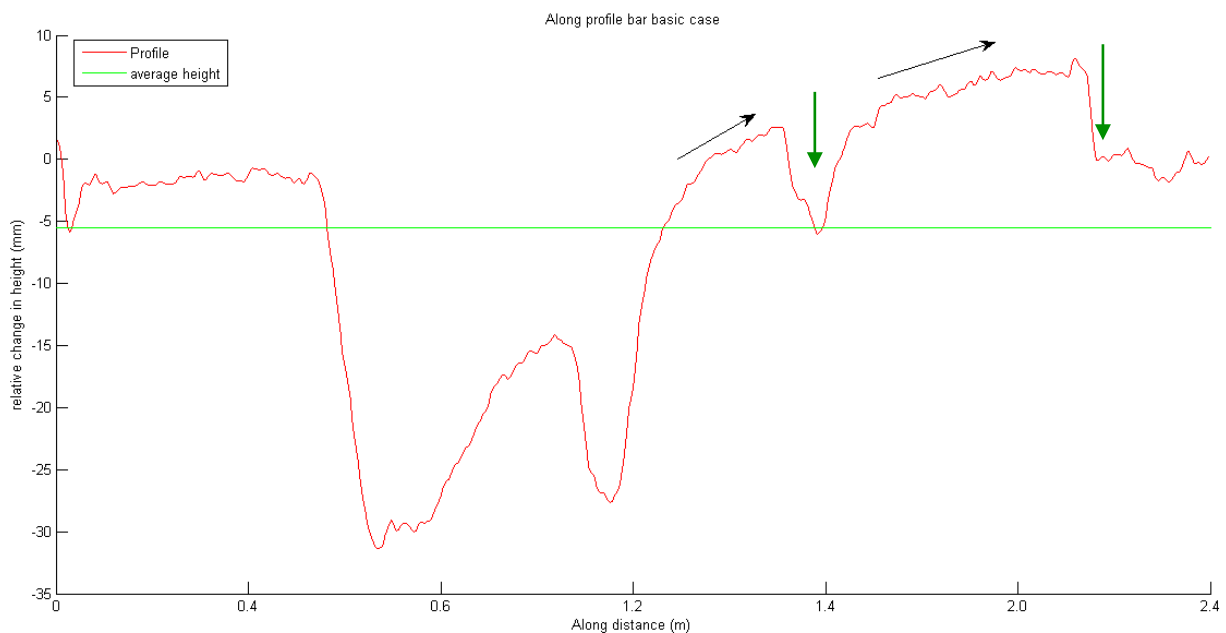


Figure 4.21: Along profile for the HA-case at the large bar-channel couple (fig 4.2). Bars are present above the average height line and channels are present below the average height line. Black arrows indicate slope upwards and green arrow indicate steep slope downwards.

Channels

As mentioned earlier in the chapter, channels were either ebb- or flood-dominated depending on the tidal phase. Visual observations from the movies and tidal experiments showed that tidal channel shapes differ depending on the case (table 4.4). Systems with narrow, long and intermediate/deep channels developed (fig 4.22, *top*), wide, long and deep channels developed (fig 4.22, *middle*), or intermediate in width, shallow in depth but small in length (fig 4.22, *bottom*). Remind that this is also not a hard transition but an average shape that represents the tidal experiments.

Tidal excursion length seemed to determine the shape of the channels. Wide, long and deep tidal channels and narrow, long and intermediate/deep tidal channels occurred in systems with high tidal excursion length (*HA-cases*, table 4A). Tidal channels that were intermediate in width, small in length and shallow in depth occurred in systems with low tidal excursion length (*La-cases*, table 4A).

Table 4.4: Relative shape of tidal channels (either flood-or ebb-dominated) in the experiments.

<i>Case</i>	<i>Width (mm)</i>	<i>Length (mm)</i>	<i>Length</i>	<i>Depth (mm)</i>
<i>High-amplitude cases</i>	<i>Wide</i>	<i>Long</i>	$\frac{3}{4}$ <i>tilting basin</i>	<i>Intermediate-deep</i>
	<i>Narrow</i>		$\frac{1}{2}$ <i>tilting basin</i>	
<i>Low-amplitude cases</i>	<i>Intermediate</i>	<i>Intermediate</i>	$< \frac{1}{4}$ <i>tilting basin</i>	<i>Intermediate-shallow</i>

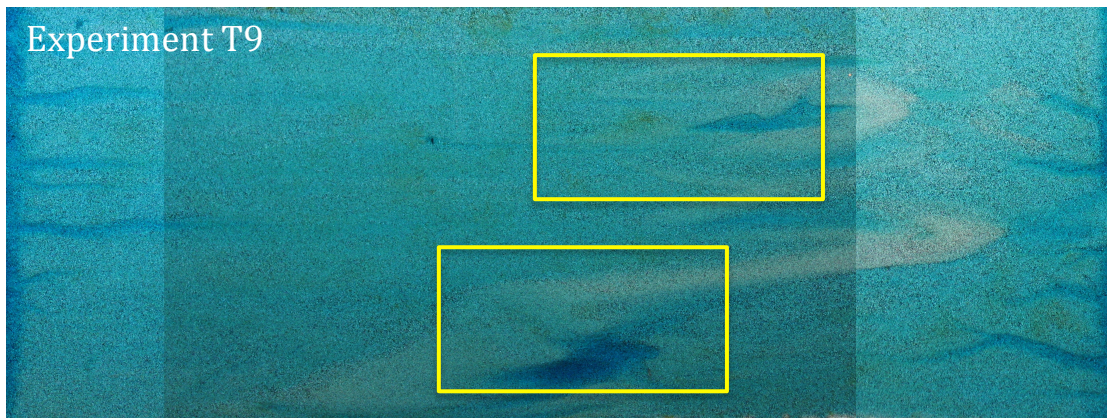
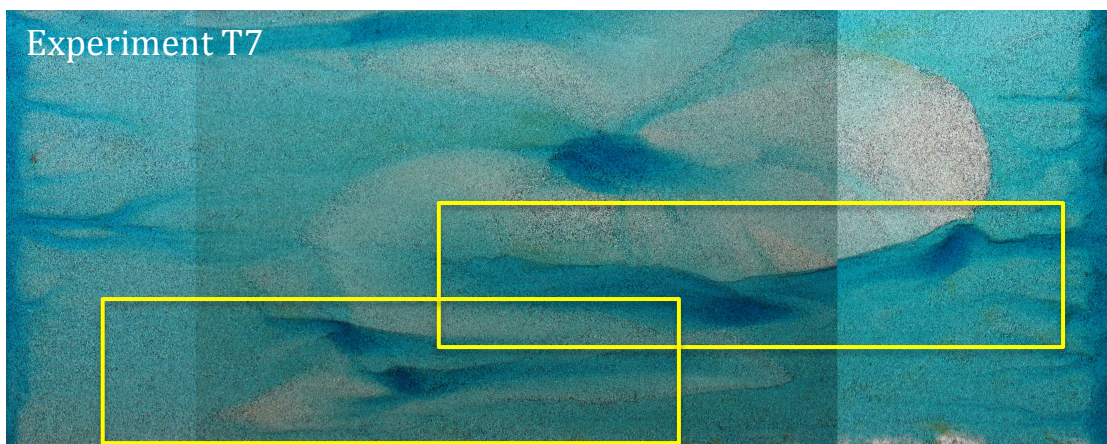
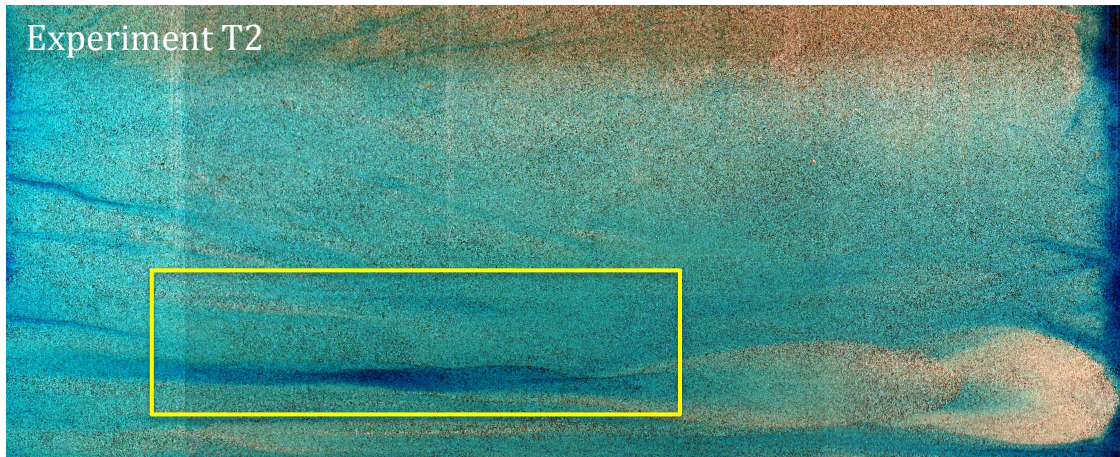


Figure 4.22: **(Top)** Narrow, long and intermediate/deep channels in experiment T2, **(Middle)** Wide, long and deep channels in experiment T7, **(Bottom)** Intermediate in width, small in length and shallow in depth in experiment T9. Experiment T2 and T7 are high-amplitude cases and T9 is a low-amplitude case (table 4A).

4.2.4 Tidal symmetry versus tidal asymmetry

The symmetrical tide case was compared with the asymmetrical tide case to see if there were differences in tidal bar development between both cases (table 4A). The evolution of the symmetrical tide case is given in figure 4.23 and evolution of asymmetrical tide case in figure 4.24.

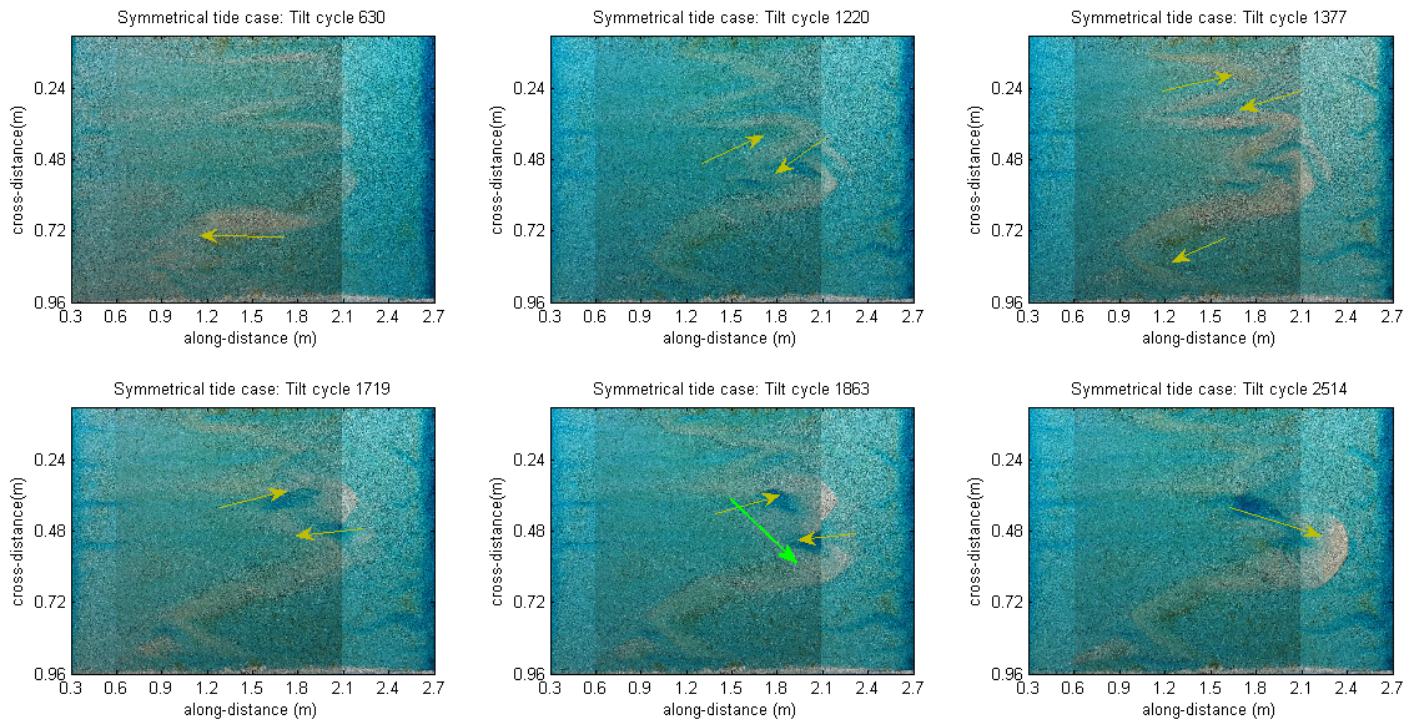


Figure 4.23: Morphological evolution of the tidal system in the symmetrical experiment T10 (Table 4A). Yellow arrows indicate dominant flow direction. Green arrow indicates disappearance of the bar.

Evolution of bars in symmetrical currents

Within the first 30 tilt cycles, the system showed no morphological changes and the sediment bed remained flat. Just after those 30 tidal cycles the first multiple tidal banks developed in the middle of the tilting basing (fig 4.24). The tidal bars were small and narrow (fig 4.23, *tilt cycle 630*). The tidal bars in the upper side of the tilting basing were narrow and small, while the bar at 0.9 meter cross-distance was somewhat thicker. This bar however, seemed to be the dominant bar, indicating that this bar expanded in size, while the other bars remained constant in shape. Flow pattern is indicated with yellow arrows (fig 4.23) and demonstrate that the bar head was present at the end of the tidal channel where tidal flow reduced and sediment settled down. When the tilt cycles increased, dominant bar development switched to the bars in the middle of the tilting basin (fig 4.23, *tilt cycle 1220*).

The tidal bars in the most upper side of the tilting basin became the dominant bar system after 1220 tilt cycles, which later on switched again towards the bars in the middle of the system (fig 4.23, *1377 tilt cycles*). The bar system in the middle of the tiling basin remained the dominant bar system towards the end of the experiment. The channels eroded further and more sediment was deposited on the tidal bar.

During further development, the flow towards the left lost strength and the flow towards the right became dominant (fig 4.23, *tilt cycle 1719*). The bar at the end of the channel eroded, due to strengthening of the flow (fig 4.23, *tilt cycle 1719-2514*). The tidal bar disappeared and sediment was deposited at the bar below, which developed into one large sharp/round-shaped dominant bar (fig 4.23, *tilt cycle 2514*).

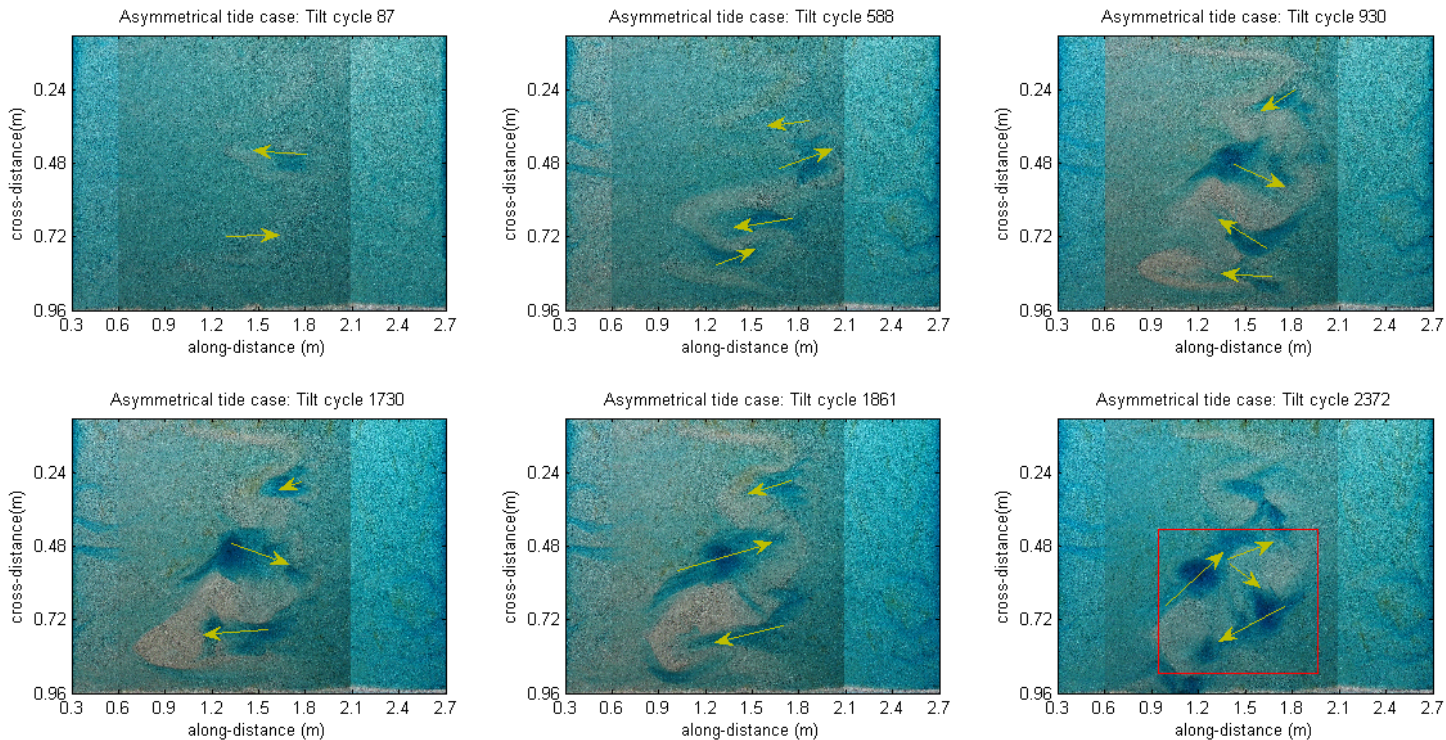


Figure 4.24: Morphological evolution of the asymmetrical experiment T11 (Table 4A). Orange box indicates dominant system.

Evolution of bars in asymmetrical currents

The system showed morphological changes after 25 tilt cycles. The first two dominant flow directions are indicated in figure 4.24 (*tilt cycle 87*), where two small bars and channels developed. The most striking observation is that the first initiated bars were narrow and small in length, with small and shallow tidal channels (fig 4.24, *tilt cycle 87-588*). The initiated bars formed due to perturbations in the sediment bed, but no long and narrow bars seemed to be visible after bar initiation, as was the case for bars in symmetrical currents. A bar-channel couple developed (*around 0.72 meters cross-distance*, fig 4.24, *tilt cycle 588-930*), but the bars and channels stayed relatively small. No sharp or large round bars or large and deep tidal channels formed. Tidal channels switched from location and therefore bars decayed or grew. During further evolution ebb- and flood-dominated channels seemed to evade each other (fig 4.24, *tilt cycle 930-2372*).

Really characterizing for the asymmetrical tide case is that flow seemed to turn around the tidal bar (fig 4.24, *orange box*) and no net migration was visible. No large round/diamond-shaped bars (fig 4.1 & 4.2) formed. Tidal channels were intermediate/deep and only present in the middle of the sediment bed.

Symmetry versus asymmetry

The evolution of mean bar width and height is presented in figure 4.25. Within the first 70 hours bar height of the symmetrical tide experiment increased from 80 mm towards 86 mm. In this period the height of the bars increased from 80 mm towards 94 mm for the asymmetrical tide experiment. For both experiments bar height decreased towards 85 mm (symmetrical tide) and 89 mm (asymmetrical tide). Bar height for the symmetrical tide experiment remains relatively constant after 50 hours, and could indicate that the an equilibrium bar height was reached. Bar width increased strong from 70 mm towards 97 mm within the first 70 hours for the asymmetrical tide experiment. Within this period of time bar width increased from 65 mm towards 84 mm for the symmetrical experiment, but in this period of time width also decreased between 25 and 45 hours. For both experiments bar width decreased after 70 hours towards 87 mm (asymmetrical tide) and 77 mm (symmetrical tide).

The number of bars in the system is highest for the symmetrical tide experiment (fig 4.26). After 80 hours however, the number of bars is highest for the asymmetrical experiment. The number of bars decreased from 12 (after 20 hours) towards 8 (after 95 hours) for the symmetrical tide experiment. In this period of time the number of bars decreased from 11 towards 8 for the asymmetrical tide experiment. Figure 4.25 seems to demonstrate that the total number of bars in the systems seemed to reach equilibrium.

The different end-stages for both systems are also visible with digital elevation maps (fig 4.27). This figure demonstrates that elongated, shaper-edged bars formed under symmetrical currents, while smaller and rounder bars formed under asymmetrical tide currents. Deep tidal channels formed under asymmetrical currents, while under symmetrical currents longer and shallower tidal channels formed (fig 4.27).

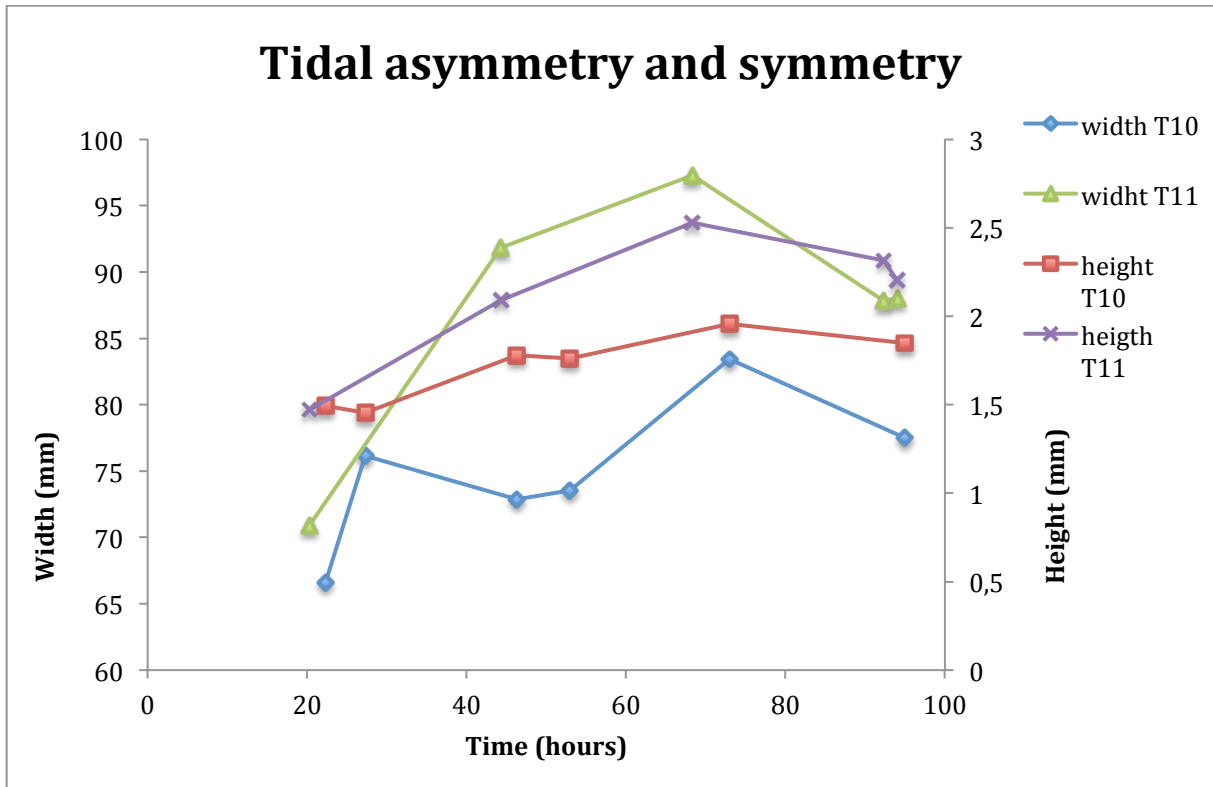


Figure 4.25: Evolution of bar width and height through time for the asymmetrical and symmetrical tide case.

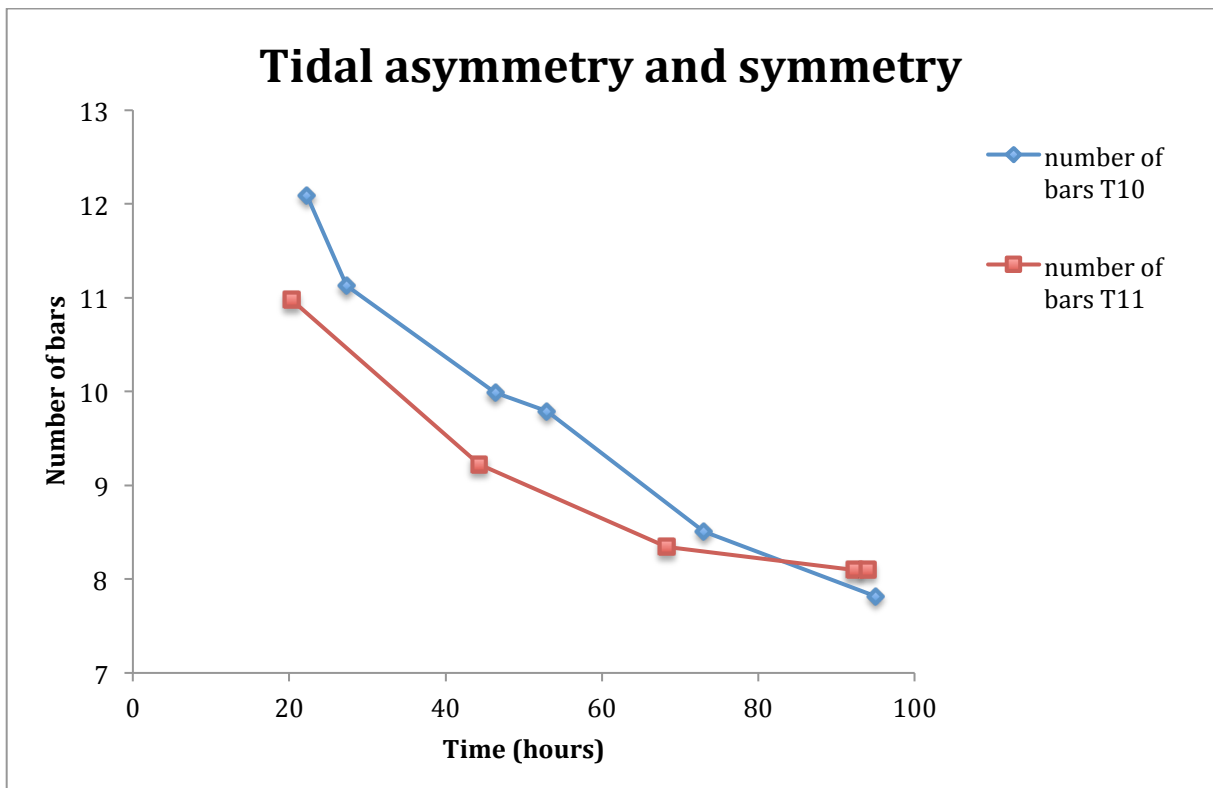


Figure 4.26: Evolution of number of bars through time for the asymmetrical and symmetrical tide case.

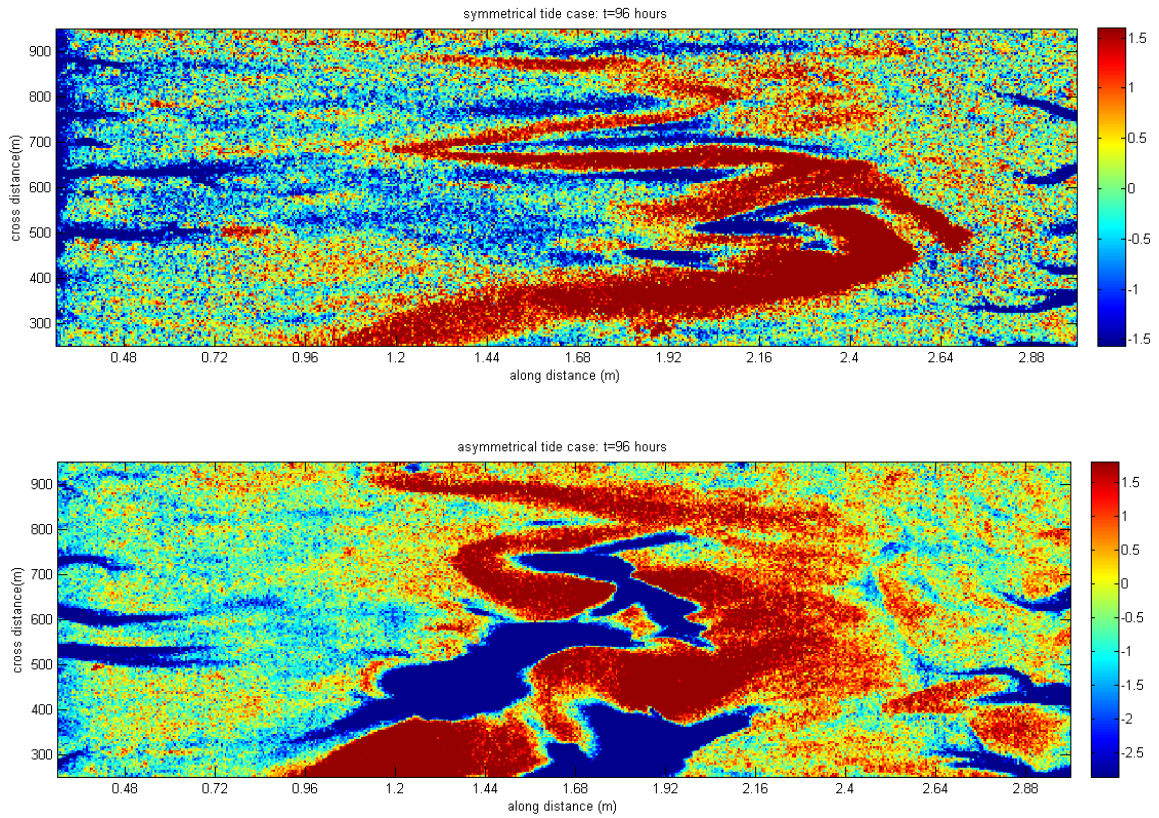


Figure 4.27: Digital elevation maps for symmetrical tide case (top) and asymmetrical tide case (bottom) after 96 hours. The DEM demonstrates the difference in bar and channel development under symmetrical or asymmetrical currents.

4.2.5 Braided rivers bars

Three braiding experiments were performed. All braiding experiments exhibited unidirectional flow and equal slope (table 4B). The evolution of braiding bars is given in figure 4.13.

The braided river formed in experimental setting was characterized by multiple channel systems, irregular bar pattern and bars that varied in their shape and size (fig 4.28). This braiding pattern developed relatively soon (fig 4.28, $t=1$ minute). The system started with two main channels each flowing towards the sides of the tilting basin with a large bar in-between the two channels. The two main channels converged after the main bar and formed lobate bars further downstream that increased in size and width during the evolution of the system (fig 4.28, $t=3$ minutes). The current flowed around bars or cut through bars to form smaller bars. During further development more bars were formed due to cutting of bars through the current. The channel at the end of the system, where the flow converged, deepened strongly through time. The braided bars migrated downstream with the flow (fig 4.28).

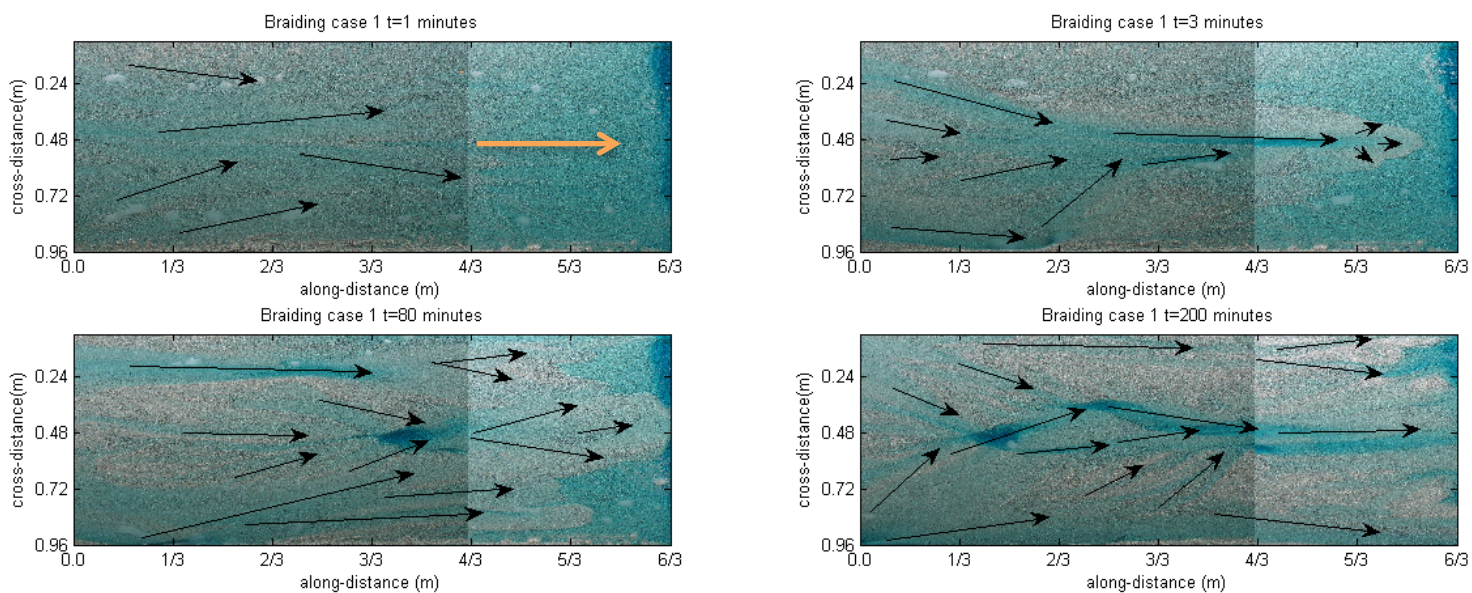


Figure 4.28: Bars and channels in braiding river experimental setting. Black arrows indicate flow pattern and the orange arrow indicates unidirectional flow.

The relation between mean bar width and mean bar height and length is presented in figure 4.29). Bar width and height differs in the three braiding experiments. This could indicate that the developed braiding pattern was highly dynamical and the initiated bars and channels were different each time the experiments were performed. There is no significant correlation between bar width and bar height and length (with $\alpha=0.02$ and $\alpha=0.1$). Although number of bars seemed to have a strong relation with bar width and length, there is no significant correlation between the variables (fig 4.30).

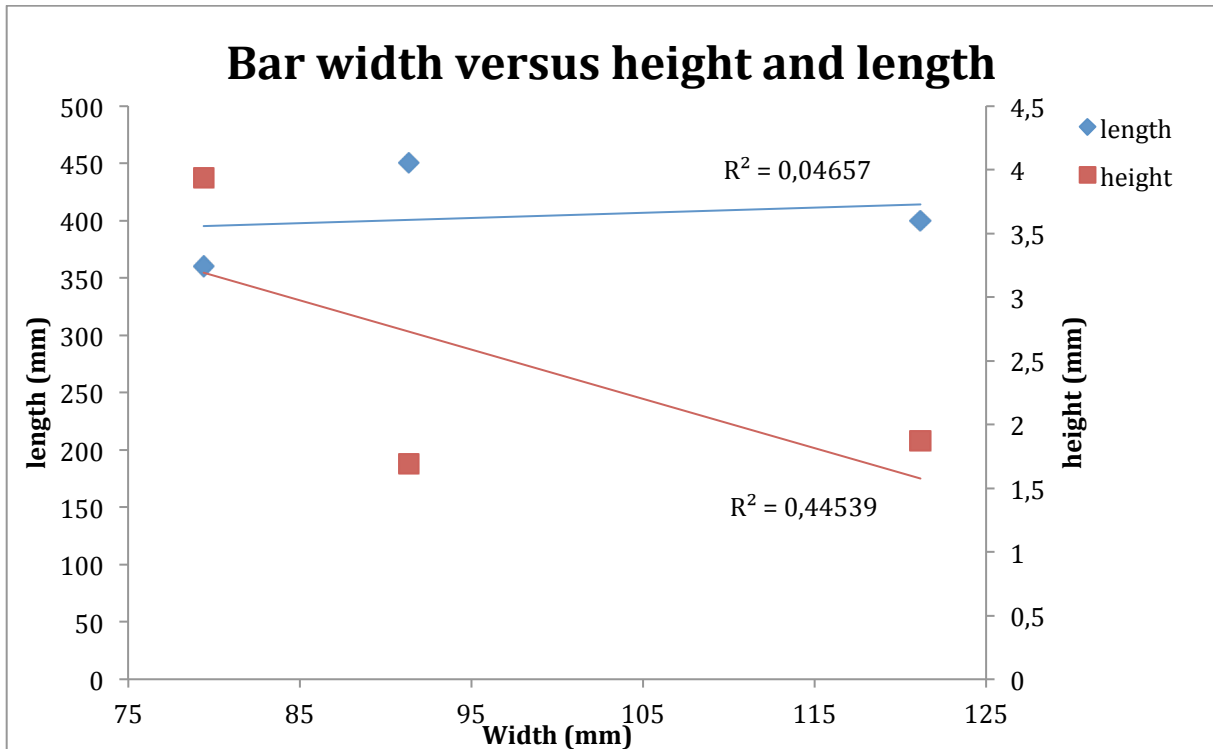


Figure 4.29: Relation between bar width (mm) and bar length (mm) and height (mm).

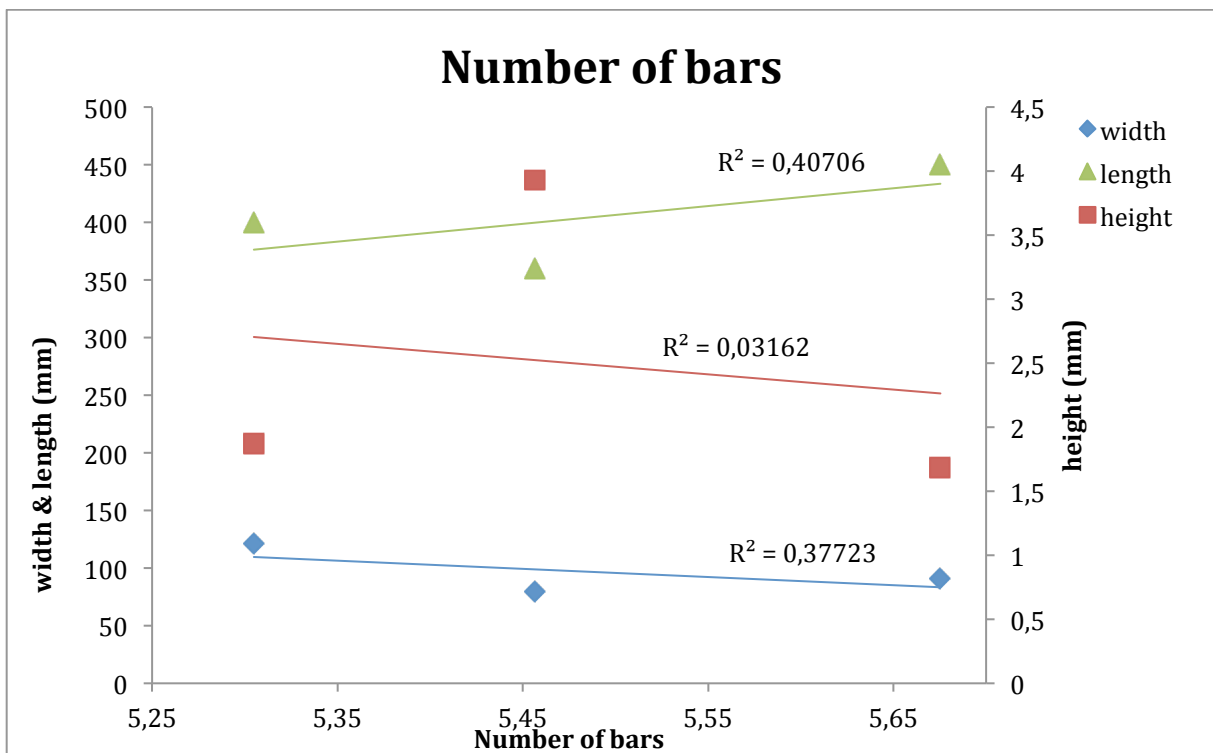


Figure 4.30: Relation between number of bars and bar width (mm) and length (mm) and bar height (mm).

Table 4.5: Mean values for width, height and width/height-ratio and mean number of bars for the braiding cases. Tides represent the mean average values for the tidal experiments with tidal amplitude of 8 mm. Braiding represents the mean average values for braiding case 1 and 2. Braiding case 3 is not taken into account due to the fact that no initial DEM was made.

Experiment	Mean width (mm)	Mean height (mm)	Mean width/height-ratio	Mean number of bars	Mean number of channels	Bar length (mm)
Braiding case 1	121.17	1.87	64.01	5	6	400
Braiding case 2	91.36	1.69	54.19	6	6	450
Braiding case 3	79.40	3.93	29.00	5	5	360
Tides	73.6	1,55	51,1	11	11	775
Braiding	106.3	1,78	59,1	5	6	425

The difference between values for the tidal experiment and braiding experiments is listed in table 4.5. This table shows that on average, mean bar width and height were higher in the braiding experiments than in the tidal experiment (with the same slope). The number of bars is on the other hand higher in the tidal experiments, as well as the total bar length (table 4.5). In terms of bar shapes it showed that tidal bar shape differed much from braided river bar shape. Due to the braiding pattern, multiple bars were present in-between the braiding channels (fig 4.28). These bars were also much smaller in terms of mean bar length. Braided bar length varied between 20 – 90 cm, whilst tidal bars varied in length between 60 – 200 cm. The number of bars was lower according to the statistics, but that is probably due to the way the number of bars were calculated (chapter 3). Due to visual comparison it was obvious that more bars and channels were present in the braiding experiments. Bifurcations and flow convergence were present.

The braiding pattern and braiding bars were also clearly visible on the DEMs (fig 4.31). The main flow was first around a big bar in the middle (around 0.48 m along-distance) and flow converged between 1.44 and 1.68 m along-distance. The channel was indeed very deep where flow converged. The braiding pattern was highly dynamical, due to the fact that both DEMs were different in morphological change with the initial flat bed. Both DEMs showed the characteristics of the braiding pattern, such as bifurcations, flow convergence and braiding bars.

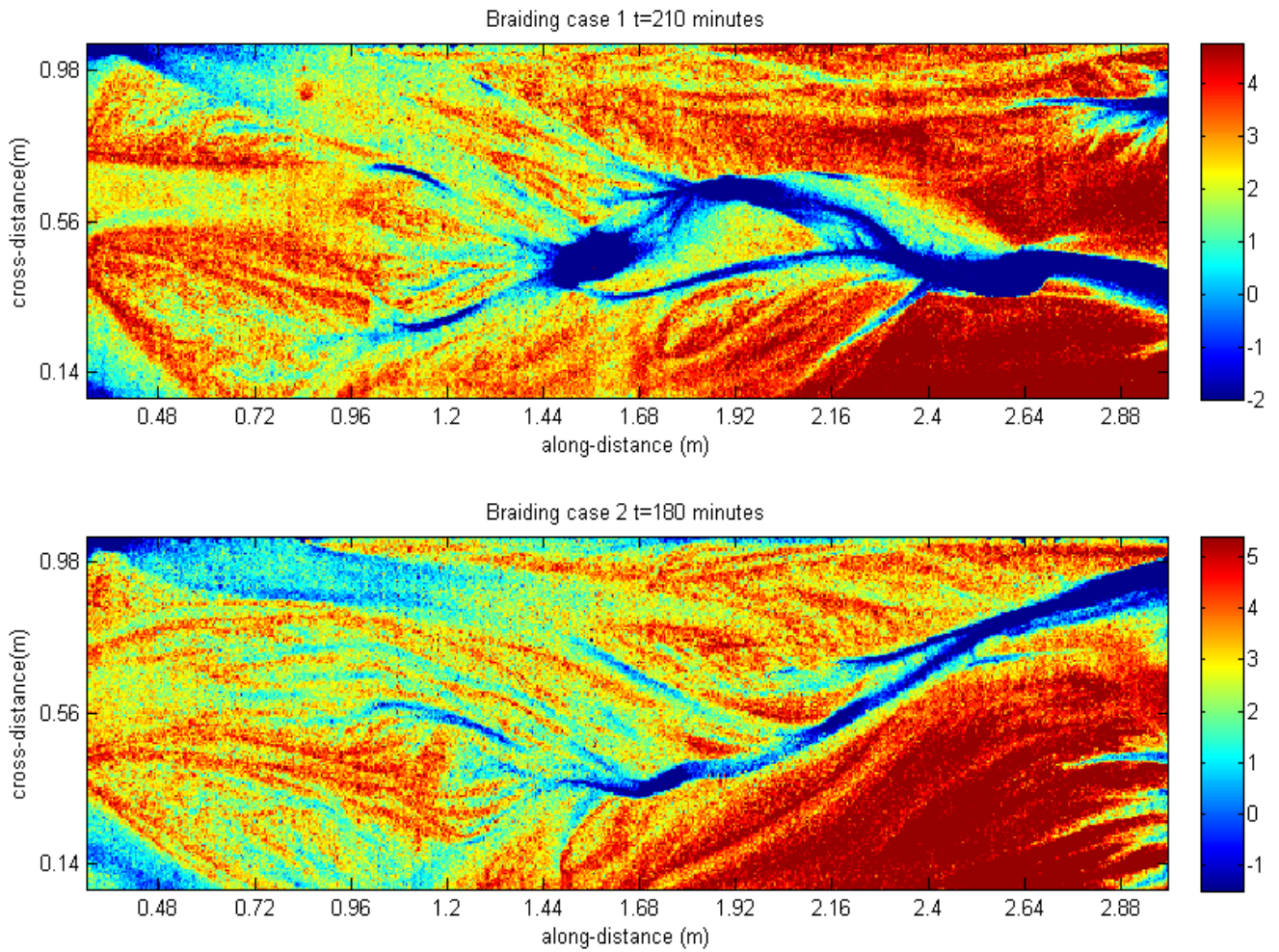


Figure 4.31: Digital elevation maps of the braiding experiments. High values indicate deposition (red) and low values indicate erosion (dark blue).

5. Discussion

In this section experimental tidal bars and channels are compared to tidal bars and channels in natural systems and compared with results from previous model studies. Initiation and formation of tidal bars and channels were investigated by the use of an experimental tilting basin, wherein the tilting speed, amplitude and tidal delay were varied. In the experiments, tidal bars and ebb- and flood dominated channels were formed. Unrealistic deep scour holes were also formed in the tidal experiments. The results are discussed for the case of short tidal systems, where basin length is small compared to tidal wavelength, as is the case in nature-systems (Kleinhans et al, 2012a). Tidal wavelength can be calculated with the wave celerity ($c=(g*h)^{0.5}$), whereas g represents the gravitational acceleration ($g=9.81 \text{ m/s}^2$) and h represents the waterdepth. Calculated wavelength equaled 3-6 meters. In order for the wavelength to decrease to fall within the length of the tilting basin, the tilting speed has to increase significant (*tilting speed of 30-40 mm/min*).

5.1 Experimental tidal bars and tidal channels

5.1.1 Bar and Channel initiation

A relatively small perturbation in the sediment bed appeared to be the main trigger for initiation of bars in the system. Small irregularities in the sediment bed ultimately led to the spontaneous development of free tidal bars in the middle of the tilting basin, due to positive feedback between the water motion, sediment transport and the sediment bed. It is well known from the fluvial literature that free fluvial bars form due to irregularities in the sediment bed (Kleinhans, 2010; Tubino et al., 2013, Seminara et al., 2012). The results of the tidal experiments revealed that free tidal bars exhibited the same initiation pattern as for fluvial bars. The spontaneous development of free tidal bars is in agreement with model results obtained by Schramkowski et al., (2002) and Seminara and Tubino (2001). Both their stability analyses showed that from an initially flat sediment bed bars emerged from small perturbations.

Similar to tidal bars, tidal channels initiated and grew due to inherent feedback between tidal currents and the erodible sediment bed. These results from the tidal experiments are also in agreement with the results of Schuttelaars and de Swart (1999), who investigated the initial formation of channels in short tidal embayments.

Initiation of bedforms in tidal systems is related to the combined effect of bottom friction and sediment transport processes. Above tidal bars, tidal currents are more retarded due to the combination of low waterlevel and high resistance from the bottom over the larger area of the tidal bars. A lower tidal current above the tidal bars diminishes sediment transport and this results in a net transverse sediment concentration gradient. The resulted sediment transport induces net sediment transport fluxes towards the bars from the deeper tidal channels (de Swart and Zimmerman, 2009; Schramkowski et al., 2002).

5.1.2 Further development of the system

After initiation two types of bars emerged: either few (1-2) elongated bars developed (fig 4.1 & fig 4.20) or multiple small elongated bar developed (bar rows) (fig 4.5 & fig 4.20). After initialization bars developed parallel to the flow and expanded in height, width and length. Dalrymple (1977) and Dalrymple et al., (1975) also observed this pattern of bars being present parallel to the flow in the Cobequid Bay, Fundy. Tidal bars and channels were only active during one phase of the tidal cycle. This resulted in separate flood- and ebb-dominated channels, which were responsible for the asymmetric pattern of bar development. Tidal bars created localized areas of ebb- and flood-directed residual movement of sediment. Flow during one phase of the tides was dominant over the steep side of the bar, while the reversing flow was dominant at the flanks and gentle side of the bars. It seemed therefore that the bar crest was able to resist the reversing flow. This possibly resulted from the steep slope at the bar crest (fig 4.21), that hindered the opposite flow (fig 4.2, *yellow arrows*) and forced the flow around the flanks of the tidal bars. At the steep side of the bar (fig 4.2, *red arrows*), flow diverged. Here, flow velocities decreased and hence sediment was deposited at the bar crest. The pattern of flow during one phase being dominant over the steep side of the bar, and reversing flow dominant at the flanks and gentle side of the bars is also observed in the Cobequid bay and Minas Basin in Fundy (Dalrymple et al, 1970; Dalrymple, 1977; de Vries, 1970).

Tidal bars developed at the end of the tidal channel due to dominant ebb or flood tidal currents. Higher tidal currents were present in the channels due to higher waterdepth and lower resistance from the bottom. The amount of bed material that can be moved with the currents is a power function of the current speed and therefore tidal channels can transport more sediment. The currents in the tidal channels displayed characteristics of a tidal jet current due to the fact that sediment and flow were concentrated in the tidal channels. At the mouth of the channel, the jet emerged freely where the flow diverged and sediment was deposited and lobate bars formed due to decreased flow velocities. This asymmetric (either flood or ebb dominated) channel-bar pattern is characteristic for the tidal systems in the tidal experiments. This asymmetric channel-bar development pattern is also observed in the Cobequid bay and Minas Basin in Fundy (Dalrymple et al, 1970; Dalrymple, 1977; de Vries, 1970).

Observations from the experimental movies show that development of bar height and width and length from initial bed is relatively fast. Then bars seemed to develop slower, especially for bars in the LA-case experiments. It seemed here that the system reached equilibrium due the fact that bar width and height remained more or less equal during further evolution of the system (fig 4.8 & 4.9). Bars in the HA-case remained dynamically active during the whole evolution of the system and developed further due to bar merging and overtaking. However, the experiments should be performed longer, in order to see if bars in the LA-case remain at equilibrium and if the HA-case reaches equilibrium. Bars in fluvial systems develop relatively fast in bar length when starting from initial flat bed, but then they develop slower until they reach a quasi-steady equilibrium (Tubino et al., 2013).

Tidal experimental bars also developed further due to the deposition of sediment transport. Sediment at the bars was being spread out over the bar due to flow divergence (fig 4.2). According to figure 4.21 bars exhibited a steep slope towards the bars crest (*black arrow*). This steep slope at the bar crest reduced in divergence of the flow, which in turn resulted in decreased flow velocities and hence deposition of sediment. Due to deposition, waterdepth decreased and this resulted in even more deposition as flow velocities were reduced due to the combination of lower waterdepth and higher bottom friction. Bars grew not infinite high due to the fact that gravity dampened the bars. Gravity pulls the sediment particles downward, which result in reduction of bar height (Tubino et al., 2013). Bars could also increase in width and length due to bar merging and overtaking. Characterizing is that mean bar width and height are significant correlated; indicating that when bar grew in width this was accompanied by an increase in height (fig 4.11). That was also noted when looking at the evolution of the system with the use of the movies. Divergence of sediment at the bars due to the combination of lower waterlevels and higher bottom friction results in both increased bar width and height. The length of bars is not significantly correlated to bar width or height (fig 4.13). This implies that when bars grew in length, this was not accompanied by an increase in bar width or height. The number of bars is significantly correlated to the width of the bars (fig 4.12). When the number of bars increased, bars decreased in their width. This is probably the result of bar merging and overtaking.

Wavelength in the experiments seemed to scale with channel width. The tidal bars in the experiments had wavelengths in the order of 3-6 times channel width. These results are in agreement with field and laboratory data (Tambroni et al, 2005; Seminara and Tubino, 2001; de Swart and Zimmerman, 2009). The wavelengths of free river bars fall in the range of 5-12 times channel width according to observations (Tubino et al, 2013). The length of the experimental tidal bars (table 4.1) is 3-6 times smaller than the length of the tidal basin. It turns out that these results are in agreement with observations of Seminara and Tubino (2001).

5.1.3 Bar migration

Visual observations from the tidal experiments showed that tidal bars formed under the symmetrical tidal forcing and show no net migration over a tidal cycle. The bars were migrating back and forth over a tidal cycle in a symmetrical way. These results are in agreement with the results of Seminara and Tubino (2001), who showed by the use of a three-dimensional model that bars exhibited no net migration over a tidal cycle. This differs significantly from fluvial bars due to the fact that fluvial river bar theory suggests that unstable rivers bars migrate downstream with migration speed being much smaller than the flow velocity (Tubino et al, 2013).

By forcing the system with an asymmetric tide, it showed from visual observations in the tidal asymmetry experiment that bars still exhibited no net migration over a tidal cycle. The bars seemed to move forward and backward in a symmetric way. One side of the tilting basin exhibited stronger flood flow, while the opposite side exhibited stronger ebb flow. One might expect that bars migrated in the system due to the stronger flood flow to one side of the tilting basin, but migration seemed not to be present under asymmetrical currents. This may be due to the fact that asymmetry is too small to show significant different patterns from the symmetrical tide experiments. Another problem arises due to the fact that some previous symmetrical tide experiments prefer a specific side of the tilting basin to develop extensively towards that side (table 4.3), even while no asymmetry was present.

5.1.4 Ebb- and flood-dominated channels and recirculating sediment transport

Ebb- and flood-dominated channels formed in the tidal experiments show similarities with that being observed in the Westerschelde and Wadden Sea (Van Veen, 1950; Swinkels et al, 2009). In Van Veen (1950) definitions, the flood-tidal channel is open to the flood-current and exhibits a sill at the end of the flood-channel, while the ebb-tidal channel is open to the ebb-current and exhibits a sill at the end of the ebb-channel. This observed pattern is visible in the tidal experiments (fig 4.20). At the end of an ebb- or flood-dominated channel a bar (or sill in Van Veen (1950)) was present.

Also small connecting channels were present at the bars that connected the main ebb- and flood-dominated channels (fig 4.3). The swatchways (connecting channels), as being observed as channels between the main ebb- and flood-dominated channels in the Cobequid bay, are also present in the Westerschelde, as they are referred as connecting channels (Swinkels et al., 2009). Those channels are the link between the ebb- and flood-dominated channels. The main driving force for the development of the connecting channels are the water level differences between the ebb- and flood-dominated channels according to several studies in Swinkels et al., (2009). The connecting channels are often present where the strongest pressure gradient between the channels occurred.

A recirculating sediment transport pattern was observed in the tidal experiments. Sediment was being transported during one phase of the tides in the ebb-tidal channels, while sediment was transported backwards during reversed flow in the flood-channels. Due to symmetrical tides the flood and ebb channels had the same dimensions and dynamics. This pattern of recirculating sediment transport pattern was also observed in the Westerschelde (Swinkels et al, 2009), where the circulating pattern is the result of the asymmetric water motion during ebb and flood. A residual sediment-circulating pattern was also observed in the Cobequid bay, Fundy according to the investigation of Dalrymple (1977). There, deep major channels that were located at the north and south shores of the bay were flood dominated as was shown from their data. Channels in the middle of the bay were shallower and were ebb-dominated channels (Dalrymple, 1977). This result eventually in two large-scale flow cells and sediment transport cells in the bay.

5.2 Dominant forcing parameter: tidal excursion length

The crucial parameter that controlled the formation of free tidal bars seemed to be tidal excursion length. In the first experiments (failure case, table 4A), tidal excursion length was too low for bars to develop in the system. Probably no sufficient feedback between the flow and sediment caused perturbations to develop towards significant bars. The results show that only bar length is significantly correlated to tilting speed (fig 4.14), amplitude (fig 4.17) and tidal delay (fig 4.18).

5.2.1 Tidal excursion length and bar length

High tidal excursion length is the combination of higher amplitudes and lower tilting speed and low tidal excursion length is the combination of lower amplitudes and higher tilting speeds. Bar length that scaled with tilting speed (fig 4.15) can be explained by the fact that when tilting speed increased, tidal period decreased and there is less time for the tidal currents to accelerate. This may result in less sediment being transported with the tidal currents and hence tidal bars remained smaller in length. Bar length scaled also with tilting amplitude (4.17). When tilting amplitude increased, the slope increased which resulted in a stronger pressure gradient. Flow could accelerate more easily and therefore sediment transport increased which resulted in increased bar length. Bar length was also significantly correlated to tidal delay (fig 4.18). When delay increased, bars increased in their average length. This may be due to the fact that the flow had more time to transport sediment before the flow reversed which enhanced sediment transport and bars increase in their length. It must be noted that the effect of the delay is difficult to investigate while most experiments exhibited the same value for the delay. Strange is the fact then that tidal delay does not correlate well to bar width and height, as one might expect increasing bar height and width as delay increased, as more time is present for the flow to transport sediment before the currents reversed again.

The combination of the parameters demonstrates the fact that tidal excursion length is significantly correlated to the length of the bars (fig 4.19). This is the most important relation between parameters as this result is in agreement with previous modelling studies. Schramkowski et al., (2002) modelled the excitation of bars with stability analyses. Their results showed that the growth rate of bars do not only depend on wavenumber of the channel and perturbations, but also on tidal excursion length. The results of the tidal experiments are in agreement with the results obtained by Schramkowski et al., (2002) (fig 4.19). The results of Schramkowski et al., (2004), who extended their stability analyses with non-linear effects to study finite-amplitude tidal bars (chapter 2.3), showed that finite-amplitude bars initiated when they scaled with tidal excursion length. It seems logical for bar length to scale with tidal excursion length, as net horizontal distance over which water moves during one tidal phase increases (high tidal excursion length). Sediment could be transported further upstream or downstream to form longer bars. Despite the fact that the net horizontal distance over which water moves increased, no correlation was present between tidal excursion length and bar height.

According to fluvial bar theory the width/depth ratio of the channel is the crucial parameter that controls the formation of free fluvial bars (Tubino et al., 2013; Kleinhans, 2010; Kleinhans and van den Berg, 2010). Fluvial bars only initiate when the ratio is above a certain threshold value. However, the effect of the width/depth ratio for the bars in the tidal experiments is not investigated by varying channel width. The width/depth ratio for the tidal experiments is more than 100, which falls in the range of highly braiding rivers (high braiding index) according to Kleinhans and van den Berg (2010) for both sand and gravel-bed rivers (fig 2.7). However, no braiding pattern occurred in the tidal experiments and no braiding bars developed. Width/depth ratios for tidal systems is therefore probably different related to the development of overdamped, underdamped and exciting bar regimes that influence channel pattern.

5.2.1 Tidal excursion length and bar shape

Visual observations showed that wide, round/diamond-shaped and long tidal bars (fig 4.20) were found in tidal experiments with high tidal excursion length. High tidal excursion lengths (higher amplitudes and lower tilting speeds) caused few bars at initiation, which developed towards large round/diamonds-shaped tidal bars. This may be due to the fact that the high amplitudes enhanced sediment transport because the high amplitude resulted in higher slope values for the tilting basin (table 3.1). Due to increased slope flow strength is enhanced and this increased sediment transport. The high tidal excursion length resulted in a longer period for flood and ebb flow, which implied that there is more time for the sediment to be transported with the tidal currents. When more sediment could be transported, bars grew more extensively, which results in wider, rounder and longer bars (fig 4.2). Another trend for experiments with high tidal excursion length is that those experiments exhibited less tidal bars. This may be due to the fact that due to the much wider and rounder-shaped bars, bars were more easily merged or being overtaken by other bars, which eventually leads to less bars in the system (but higher and wider).

The high and round tidal bars formed in the tidal experimental setting are also found in natural tidal systems. For example, large round tidal bars are found in the Dutch Wadden Sea and Aberdovey estuary (fig 2.2). In those natural tidal systems bars seems also round-shaped. Round-shaped tidal bars are also found in the Cobequid bay, Fundy. Here, bars are asymmetric in form where length is being longer than bar width.

Elongated and sharper-edged bars (fig 4.20) were found in systems with low tidal excursion length. Low tidal excursion length resulted in multiple bar rows below each other, which eventually developed towards thin, small and shaper bars. When tidal period is lower, there is less time for the sediment to be transported in the tidal channels. Less sediment is deposited at the end of the channel to increase bar height, width and length. Also due to the low tidal period, bars grew less fast and change to be merged together or overtaking by other bars is therefore relatively much smaller. However, tidal period is small, but there are relatively seen more tidal cycles for bars to develop. Sharper-edged tidal bars can also be found in natural tidal systems, such as in the Western Scheldt in the Netherlands (fig 2.1).

5.3 Braided rivers bars

This chapter will describe the experimental braided rivers bars itself compared to previous braided river studies and will describe differences between the tidal and braided rivers bars in experimental setting.

5.3.1 Experimental braided bars

The braided river that was formed in the experimental setting was characterized by multiple channel systems, irregular bar pattern and bars that varied in their shape and size (fig 4.28). An important feature of braiding bars in the experiments is the interaction between their bars and channels. Visual observations it showed that the braided rivers bars were eroded by migration of the channels and bars itself induced channel avulsions within the experimental river system. These characterizations are in agreement with the results of the modelling study of Schuurman et al, (*in prep*). They modelled self-formed braided rivers with a physics-based model to quantify bar pattern dynamics that are compared with field observations, flume experiments and linear stability analyses. The bars were dynamically active which implies that the bars were still modified in their dimensions through the evolution of the system. In full-scale nature systems bars can be stable, as is the case in the Brahmaputra where their bars are stable due to vegetation or topographic forcings or resistant rivers banks.

The braided rivers bars formed probably as a response due to a perturbation of the initial flat bedlevel, whereas positive feedback between the flow and sediment resulted in the formation of channels and bars. This is probably the main reason why upstream bars formed. Downstream bars however, could also be formed as a response of perturbations of the flow upstream due to bars. These results are in agreement with Schuurman et al, (*in press*). The braided rivers bars formed in the experimental setting were relatively formed very fast. In the first stage bar formation, the bars grew rapidly in their horizontal direction. The first formed bars grew due to bar merging and migrated relatively fast downstream.

The channels were eroded deeper (fig 4.28) and sediment transport was more concentrated in the channels. The system remained active during the end of the experiment, as bars grew due to merging or eroded due to erosive force of the tidal channels.

Braided rivers bars are found in rivers with relatively large width-to-depth ratio, as been explained by linear stability analyses (several studies in Schuurman et al, *in press*; Kleinhans, 2010; Kleinhans and van den Berg, 2010). River pattern can be predicted by the use of potential specific stream power, as a function of valley slope, channel width and mean annual discharge as was illustrated by Kleinhans and Van den Berg (2010). For a braiding pattern to develop a sufficient high potential specific stream power and a large enough width-to-depth ratio are necessary (Schuurman et al, *in press*). The braided river bars in the experimental setting were formed under the same width-ratio as the tidal bars, but then sufficient sediment supply upstream was necessary. The sediment feeder was necessary upstream to feed enough sediment to the system to prevent erosion upstream that would prevent the braiding pattern to develop (as was seen by visual observation).

Other necessary conditions for the formation of braided bars were a sufficient slope for the tilting basin in order to initiate bedload and suspended load transport and configuration forcing.

The bars that formed in experimental setting were irregular bars inbetween the multiple channels (fig 4.28). The bars migrated relatively fast downstream through the braiding river. Some bars merged together to form larger braided river bars, which migrated downstream. These observations in the experimental setting are in agreement with Schuurman et al, (*in press*). Field observations (Schuurman et al, *in press*) have showed that braided bars have different sizes and shapes and can be classified into three types of bars: unit bars, compound bars and islands (several studies in Schuurman et al, *in press*). The unit bars are the key element in braiding rivers as they migrate fast through the river. When unit bars merge together, they form large, irregular compound bars. Those bars can be either mid-channel bars or bank-attached bars. Islands are often covered by vegetation and are more stable. Those three types of bars are often found in braiding rivers, such as the Brahmaputra in India. It seems that unit bars and compound bars were found in experimental settings. No islands were visible due to the fact that the bars were not stable (no vegetation or strong banks).

5.3.2 Braided river bars versus tidal bars

Braided river bars and tidal bars differ much in their shape. Bars formed under uniform flow were higher in both bar width and height, but smaller in their length (table 4.5). The smaller length was probably due to the fact that the multiple channel system cuts the bars more often, which led to a reduction of bar length. The bars were higher in width and height. This may be due to the fact that more sediment was available for the growth of bars due to sediment supply upstream and reversing flow did not influence the bars.

No significant correlates were present between bar width and height and length (fig 4.29) and between number of bars and bar width, length and height (fig 4.30). Probably more experiments should be performed, as now only three braided river experiments were performed. This is different from the tidal experiments, as there is a strong significant correlation between bar width and height (fig 4.11). Also in the tidal experiments number of bars is significantly correlated to bar width, as is not the case for the braided river experiments.

5.3 Recommendations

The first recommendation is to remove the '*carpet*' in the tilting basin, as the carpet released a lot of unwanted fluff in the tidal system. The fluff in the system influenced the tidal currents in such way that they were obstacles for the flow and hence those perturbations may lead to the development of bars or tidal channels in the system. Then, bars and channels developed due to unwanted external forcings instead of spontaneous forcings.

In the present configuration the water flowed in- and out of the system through an opening of 10 centimeters. However, this small opening influenced in- and outflow and also initiation and further development of bars and channels in the system. It is therefore recommended that inflow and outflow of water is through a larger opening such that the opening does not influence inflow and outflow. Bars and channels were also influenced by the edge of the tilting basin. Deep channels formed along the edges of the basin. Adding roughness to the edges may prevent this.

Tidal delay is not varied as much as the other two variables. It is suggested that more experiments are performed with varying tidal delay in order to investigate the effect of tidal delay on bars and channels. Also unrealistic large scour holes were present in the system. It is suggested that coarser sediment is used to prevent such unrealistic scour holes.

In order to experiment further on tidal bars more elements on the tidal system can be added. Now, only a sediment bed was present for the investigation of bar and channel initiation and development. To improve the investigation on bars fluvial input can be added to the system, or adding mud (silica flour) and adding vegetation (alfalfa). Also bars in estuaries are influenced by waves and sea level rise, therefore experiments on waves and sea level rise are necessary. Humans also influence many estuaries all around the world by dredging and dumping. The effect of these influences can be investigated by further research.

6. Conclusions

The conclusion answers the main research questions of this thesis that are listed in chapter 2.5:

Do tidal bars develop spontaneously in tidal experiments or only results from forcings (forcing such as channel curvature, variations in width)?

Free tidal bars and ebb- and flood-dominated channels were produced in a tilting basin in all tidal experiments. Both tidal bars and ebb- and flood-dominated channels initiated spontaneously due to small perturbations in the sediment bed that ultimately lead to the formation of bedforms in the tidal system. No forcings, such as channel curvature or variation in width were necessary for free bars and channels to develop.

Which elements characterize formed tidal bars in experimental setting?

In the tidal system two type of bars emerged:

- (1) Large round/diamond-shaped bars
- (2) Elongated sharper-edged bars

The main forcing behind the significant differences in the tidal systems is tidal excursion length. The experiments demonstrated that bar length is significantly correlated to tidal excursion length. This observation is in agreement with modelling studies by Schramkowski et al., (2002) and Schramkowski et al., (2004). In the experiments bar width scaled with bar height. Another striking observation is that bars were only morphological active during one phase. Bars exhibited no net migration, which is in agreement with model studies by Seminara and Tubino (2001).

Is the tidal channel network created in experimental setting similar to nature (i.e. ebb- and flood-tidal channels according to van Veen (1950) and how are the ebb- and flood-tidal characterized?

The experiment exited ebb- and flood-dominated channels that were active during one tidal phase. The flood channel was open to the flood current and exhibited a bar at the end, while the ebb channel was open to the ebb current and exhibited a bar at the end. This is in similar to nature (Westerschelde and the Wadden Sea, Van Veen (1950)). The presence of ebb- and flood-dominated channels indicated a recirculating sediment transport pattern.

How is the braiding pattern characterized?

The braided river formed in the experimental setting was characterized by multiple channel systems, irregular bar pattern and bars that varied in their shape and size. The bars that formed in experimental setting were irregular bars inbetween the multiple channels. The bars migrated relatively fast downstream through the braiding river.

How do tidal bars differ from (experimental) fluvial bars?

Under symmetrical and asymmetrical currents tidal bars showed no net migration over a tidal cycle, whereas unstable fluvial bars migrate downstream. The forcing behind fluvial and tidal bars is also different. Fluvial bars are strongly determined by the width/depth ratio, whereas tidal bars are controlled by tidal excursion length. Tidal bar and fluvial bar wavelength scales both with channel width. Tidal bars in the experiments had wavelengths in the order of 3-6 times the channel width. The wavelengths of free river bars fall in the range of 5-12 times channel width.

Braided river bars formed in experimental setting and tidal bars differ significantly much in their shape. Bars formed under uniform flow were higher in both bar width and height, but smaller in their length.

7. Acknowledgements

First I would like to thank the first supervisor of this report Maarten G. Kleinhans for his contribution for this thesis. His enthusiasm and ideas were very helpful for the experiments and writing this thesis. Secondly I would like to thank the second supervisor Maarten van der Vegt for helping to understand the mathematic side of the tidal bars and the interpretation. The experiments were performed in the tilting basin at the Department of Physical Geography. Many thanks for the technicians Henk Markies, Chris Roosendaal and Marcel van Maarseveen for the set-up of the improved tilting basin and for the use of the software. Also I am grateful for the improvement they performed during the experiments in the tilting basin to improve the results of the tidal experiments. Also I am grateful for the help of Wouter Marra and Tjalling the Haas (PhD candidates at the department of Physical Geography). They were very helpful when analyzing the results with Matlab, for providing scripts and helping me to write my own scripts.

8. References

- Alpaos, A., Lanzoni, S., Marani, M., Fagherazzi, S., Rinaldo, A. (2005) Tidal network ontogeny: Channel initiation and early development. *Journal of geophysical research*. **Vol.** 110
- Cleveringa, J., Oost, A.P. (1999) The fractal geometry of tidal channel systems in the Dutch Wadden Sea. *Geologie en Mijnbouw* **Vol.** 78, pp. 21–30.
- Dalrymple, R.W., Knight, R.J., Middleton, G.V. (1975) Intertidal sand bars in Cobequid Bay (Bay of Fundy). Reprinted from: *Estuarine research* **Vol.** 2, geology and engineering.
- Dalrymple, R.W. (1977) *Sediment Dynamics of Macrotidal Sand Bars, Bay of Fundy*. Master thesis
- Dalrymple, R.W., Choi, K. (2007) Morphological and facies trends through the fluvial-marine transition in tide-dominated depositional systems: A schematic framework for environmental and sequence- stratigraphic interpretation. *Earth science reviews* **Vol.** 81, pp. 135-174.
- De Swart, H.E. and Zimmerman, J.T.F. (2009) Morphodynamics of tidal inlet systems. Review article. *Annual review of fluid mechanics*, 2009. **Vol.** 41, pp. 203-29.
- De Vries Klein, G. (1970). Depositional and dispersal dynamics of intertidal sand bar. *Journal of sedimentary petrology* **Vol.** 40 (4), pp. 1095-1127.
- Dronkers, J. (1986). Tidal asymmetry and estuarine morphology, *Neth. J. Sea Res.* **Vol.** 20, pp. 117–131.
- Garotta, V., Bolla Pittaluga, M., Seminara, G. (2006) On the migration of tidal free bars. *Physics of fluids* **Vol.** 18.
- Garotta, V., Rummel, A.C. & Seminara, G., 2008. Long-term morphodynamics and hydrodynamics of tidal meandering channels. In: Dohmen-Janssen, C.M. & Hulscher, S.J.M.H. (eds.): *River, Coastal and Estuarine Morphodynamics conference (Enschede)*, Taylor and Francis/Balkema.
- Hibma, A., Stive, M.J.F., Wang, Z.B. (2004). Estuarine morphodynamics. *Coastal engineering*. **Vol.** 51, pp. 765-778
- Kleinans, M.G., Ferguson, R.I., Lane, S.N., Hardy, R.J. (2012). Splitting rivers at their seams: bifurcations and avulsion. *Earth surface processes and landforms*.

Kleinhans, M.G., M. van der Vegt, R. Terwisscha van Scheltinga, A.W. Baar and Markies, H. (2012b), Turning the tide: experimental creation of tidal channel networks and ebb deltas, Netherlands J. of Geoscience **Vol.** 91(3), pp. 311-323

Kleinhans, M.G. and Van den Berg, J.H. (2010) River channel and bar patterns explained and predicted by an empirical and a physics-based method, Earth Surf. Process. Landforms , pp. 287-326.

Kleinhans, M.G. (2010). Sorting out river channel patterns. A review. Progress in Physical Geography.

Kleinhans, M.G., van Dijk, W.M., van de Lageweg, W.I., Hoendervoogt, R., Markies, H., Schuurman, F. (2010a). From nature to lab: scaling self-formed meandering and braided rivers. University of Utrecht.

Kleinhans, M.G., Bierkens, M.F.P., van der Perk, M. (2010b). On the use of laboratory experimentation: 'Hydrologist, bring out shovels and garden hoses and hit the dirt'. Hydrol. Earth Syst. Sci., **Vol.** 14, pp. 369–382.

Kleinhans, M.G., Schuurman, F., Bakx, W. & Markies, H., 2009. Meandering channel dynamics in highly cohesive sediment on an intertidal mud flat in the Westerschelde estuary, the Netherlands. Geomorphology 105: 261-276.

Masselink, G., Hughes, M.G. (2003). Introduction to coastal processes and geomorphology. Great Britain: Hodder Education.

Schramkowski, G.P., Schuttelaar, H.M., de Swart, H.E., (2002). The effect of geometry and bottom friction on local bed forms in tidal embayment. Continental shelf research, pp. 1821-1833.

Schramkowski, G.P., Schuttelaars, H.M., de Swart, H.E., (2004). Ocean Dynamics, **Vol.** 53, pp. 399-407.

Seminara, G., Tubino, M., (2001) Sand bars in tidal channels. Part 1. Free bars. Journal of fluid mechanics. **Vol.** 440, pp. 49-74.

Seminara, G., Lanzoni, S., Bolla Pittaluga, M., Solari, L., (2012). Estuarine patterns: an introduction to their morphology and mechanics.

Schuttelaars HM, de Swart HE. (1999) Initial formation of channels and shoals in a short tidal embayment. Journal of Fluid Mechanics. **Vol.** 386, pp. 15–42

Schuurman, F., Kleinhans, M.G., Marra, W.A., (in press) Morphodynamic modeling of large braided sand-bed rivers. Journal of geophysical research.

- Solari L, Seminara G, Lanzoni S, Marani M, Rinaldo A. (2002) Sand bars in tidal channels. Part 2: tidal meanders. *J. Fluid Mech.* **Vol.** 451, pp. 203–38
- Stefanon, L., Carniello, L., D'Alpaos, A. & Lanzoni, S., 2010. Experimental analysis of tidal network growth and development. *Continental Shelf Research* 30: 950–962.
- Struiksma, N., K. W. Olesen, C. Flokstra, and H. J. De Vriend (1985) Bed deformation in curved alluvial channels, *J. Hydraul. Res.*, **Vol.** 23, pp. 57 – 79.
- Swinkels, C.M., Jeuken, C.M.C.J.L., Wang, Z.B., Nicholls, R.J. (2009) Presence of connecting channels in the Western Scheldt Estuary. *Journal of Coastal Research* **Vol.** 25(3), pp. 627-640.
- Tambroni, N., Bolla Pittaluga, M., & Seminara, G., 2005. Laboratory observations of the morphodynamic evolution of tidal channels and tidal inlets. *Journal of Geophysical Research* 110: F04009.
- Todeschini, I. (2006) Long-term morphological response of tide-dominated estuaries. Doctoral thesis in Environmental Engineering. Faculty of Engineering, University of Trento.
- Tubino, M., Repetto, R., Zolezzi, G., (2013) Free bars in rivers. *Journal of Hydraulic Research.* **Vol.** 37(6), pp. 759-775.
- Van der Wal, D., van Kessel, T., Eleveld, M.A., Vanlede, J., (2010) Spatial heterogeneity in estuarine mud dynamics. *Ocean dynamics* **Vol.** 60, pp. 519-533.
- Van Dijk, W.M., van de Lageweg, W.I., Hoendervoogt, R., Kleinhans, M.G., (2012) Experimental meandering river with chute cutoffs. *Journal of geophysical research.*
- Van Leeuwen, S.M. (2002) Tidal inlet systems: bottom pattern formation and outer delta development. Doctoral thesis at Utrecht University.
- Van Rijn, L.C., (1993) Principles of sediment transport in rivers, estuaries and coastal seas. Aqua Publications. ISBN 90-800356-2-9
- Van Scheltinga, R.W. (2012) Turning the tide: creation of tidal inlet systems and estuaries in experimental scale models. MSc research thesis. Utrecht University, Faculty of Geosciences, Department of Physical Geography.
- Van Veen, J. (1950) Ebb and Flood-Channel Systems in the Netherlands Tidal Waters (in Dutch with English summary), KNAG 2e Ser., part 67, Delft Univ. of Technol., Netherlands. New version (2005).

Vlaswinkel, BM, Cantelli A. (2010) Geometric characteristics and evolution of a tidal channel network in experimental setting. *Earth Surface Processes and Landforms*. **Vol.** 36(6), pp. 739-752

Wonnacott, T.H., Wonnacott, R.J. (1990) *Introductory statistics*, 5th edition. 736p.